THE FINITE ELEMENT ANALYSIS OF

CONVECTION HEAT TRANSFER

B.P. BURNESS

B.Sc.(Mech.Eng.)(U.C.T.)

Cape Town

DECEMBER 1987

Submitted to the University of
Cape Town in partial fulfillment
for the degree of Master of
Science in Engineering

I, Bruce Peter Burness, submit this thesis in partial fulfillment of the requirements for the degree of Master of Science in Engineering. I claim that this is my original work and that it has not been submitted in this or similar form for a degree at any other University.

Signed...  ....

Date.....4 - 12 - 1987

ABSTRACT

This thesis reviews the development and current methods of numerical convection heat transfer from available literature, encompassing an analysis of the various finite element formulations available for investigating convection.

It further describes the finite element formulation for the primitive variable convection heat transfer equations via a Galerkin weighted residual scheme and using mixed interpolation, and it demonstrates the capability of this method by means of five practical examples, namely natural convection in a thermally driven square cavity, a thermally driven vertical slot, a thermally driven triangular cavity, and a liquid convective diode, and forced convection in a cooling pond.

This study also provides the background and framework for the problem of transient convection heat transfer, and for further steady-state studies using parameters outside those considered herein.

ACKNOWLEDGEMENTS

I thank my supervisor, Dr. H.T. Pearce whose encouragement and thoughtful guidance was of great assistance throughout the project.

I am grateful to the Council for Scientific and Industrial Research for providing the necessary funding, without which this project would not have been possible.

TABLE OF CONTENTS

LIST OF ILLUSTRATIONS

CHAPTER 3 :

CHAPTER 4 :

CHAPTER 5 :

CHAPTER 6 :

NOMENCLATURE

S.1 : UPPER CASE CHARACTERS :

B.....body force

Gr.....Grashof number

M_i .....shape function (4-noded element)

N_i .....trial or shape function (8-noded element)

P.....pressure variable

Pr.....Prandtl number

Q.....energy source

Ra.....Rayleigh number

Re.....Reynolds number

T.....temperature variable

T_e .....mapping of master elt. onto typical mesh elt.

V.....space of admissible functions

V_h .....finite-dimensional subspace of V

S.2 : LOWER CASE CHARACTERS :

d.....partial derivative

l_x , l_y .....unit outward normal components at the boundary

n.....number of nodes per element

t.....time variable

u_i .....velocity variable

u_h , v_h .....Galerkin approximations

w_i .....weighting factors of numerical integration

x_i .....spatial variable

S.3 : **GREEK CHARACTERS** :

α.....thermal diffusivity

β.....coefficient of thermal expansion

Φ_i .....basis functions

ρ.....density variable

ξ, η.....master element coordinates

μ.....dynamic viscosity constant

ν.....kinematic viscosity constant

θ.....temperature variable

Γ.....domain boundary

Ω.....solution domain

Ω_h .....finite element solution domain

S.4 : **VECTORS** :

(F).....load or force vector

$\underset{\sim}{g}$.....gravity vector

$l(v)$.....linear term of second order variational boundary value problem

$\underline{u}$.....primitive variables array

S.5 : **MATRICES** :

$B(u,v)$.....bilinear term of second order variational boundary value problem

[J].....Jacobian matrix

[K].....coefficient stiffness matrix

S.6 : **SUPERSCRIPTS AND SUBSCRIPTS :**

$( )^{*}$ .....dimensionless variable/function

$( )^{e}$ .....element designation

$( )^{-1}$ .....inverse

$( )_{i}$ .....numerical integration counter

CHAPTER 1

INTRODUCTION

1.1 AN INTRODUCTION TO THE PROBLEM

Convection heat transfer takes place when a temperature difference exists between a fluid and a solid boundary. The redistribution of energy via this mode of heat transfer is partly due to conduction and partly due to the motion of the fluid itself. Thus, as in conduction heat transfer, Fourier's law of heat conduction is applicable to convection heat transfer, but in convection it is also essential to consider the fluid motion.

The mathematical description, and the geometry and boundary conditions, of practical convection heat transfer situations are sufficiently complicated that an analytical solution can seldom be obtained, or, if the solution has been developed, it involves a series solution that demands laborious and slowly converging numerical evaluation. For this reason, a large amount of research has been devoted to the development of approximate solution methods using other computational techniques. These techniques have frequently been used to advantage, especially with the development of high-speed computers which have been used to solve problems heretofore considered intractable.

1.1.1 FLUID FLOW

In the mechanical sense, fluids differ from solids in that they are unable to sustain shearing stresses without continuously deforming. In other words, a fluid can be defined as a class of idealized materials which, when in rigid body motion (including the state of rest), cannot sustain any shearing stress. The flow of a real fluid is usually very complex and, as a result, complete solutions of problems can seldom be obtained without resorting to experimentation. In general, the parameters such as velocity, pressure and density which describe the behaviour of a fluid, are not constant in a particular set of circumstances. They may vary from one point to another, or from one instant to the next, or they may vary with both position and time.

Mathematical analysis of problems of fluid flow is generally possible only if certain simplifying assumptions are made. One of the chief of these is that the shearing stress associated with the fluid motion depends linearly on the instantaneous value of the rate of deformation. This type of fluid is known as a Newtonian fluid, and it has been found to describe adequately the mechanical behaviour of many real fluids over a wide range of situations. Fluid flow can also be simplified by assuming the fluid to be incompressible i.e. the density of every particle in the fluid remains the same regardless of the state of stress. Incompressible Newtonian fluids are governed by a set of equations known as the Navier-Stokes equations of motion, Lai et al [1].

By making the further assumptions that the flow is steady and frictionless i.e. the time dependent term and the density become known constants, these equations can be reduced to Bernoulli's equation. Using this equation, problems such as flow from a reservoir through a sharp-edged orifice and flow over a weir are greatly simplified, Massey [2].

However, a large number of practical problems encountered in the field of fluid motion cannot be simplified in this way, and it is for this reason that a numerical solution of the Navier-Stokes equations is sought.

1.1.2 CONVECTION HEAT TRANSFER

The mathematical modelling of convection heat transfer requires the development of an energy balance along with an analysis of the fluid motion of the problem concerned. There are two types of convection heat transfer: (1) forced convection, where fluid is forced over or through the heat transfer surface (or any other surface), and (2) natural, or free, convection, in which motion of the fluid occurs as a result of density changes arising from the temperature gradients.

As implied by the term forced convection, the fluid motion is due to the application of pressure or tangential frictional forces on the fluid boundary. This type of convection occurs in a wide variety of engineering problems including : a cooling tower exhausting into the atmosphere, Kinsman [3], flow of effluent into lakes and estuaries, Gallagher et al [4], flow of fluid in a heat

exchanger, Holman [5], and air flow due to a local ground hot spot such as a fire, Milthorpe and Steven [6].

The movement of the fluid in free convection, whether it is a liquid or a gas, results from the buoyancy forces which are imposed on the fluid when its density in the region surrounding the heat transfer is decreased as a result of the heating process. In other words, the fluid becomes less viscous as it is heated at the surface.The buoyancy forces, commonly referred to as body forces, would not be present if the fluid were not acted upon by some external force field, such as gravity.

Free convection is commonly encountered in engineering problems such as : the thermal insulation of buildings, Batchelor [7], heat transfer through solar collectors, Gartling and Nickel [8], and through double-glazed windows, Elder [9] and Gill [10], cooling fluids in channels surrounding a nuclear reactor core, Petuklov [11], thermal convection flow in a furnace, Kawahara [12], and convectively cooled underground electric cable systems, Chato and Abdulhadi [13].

1.2 FORMULATION OF THE PROBLEM

In order to simplify the analysis, the fluid is assumed to be incompressible and linearly viscous, and driven only by buoyancy forces, while any applied pressures or tangential tractions are given as boundary conditions. The fluid motion is assumed to be steady and two-dimensional.

Another assumption is that the buoyancy forces can be sufficiently accurately described by the Boussinesq approximation. In this approximation, the density changes are expressed directly in terms of changes in temperature only, and the resulting buoyancy forces are then introduced into the momentum equations in the form of body forces. However, the density changes are ignored in the inertia terms of the momentum equations and the continuity equation. It is also assumed that the dissipation due to viscous forces in the momentum equations does not contribute significantly to the energy transport equation. Further, it should be noted that only essential boundary conditions, where the variable is prescribed, have been used in the practical examples, although the method can readily be applied to problems involving natural boundary conditions, where the derivative of the variable is prescribed.

Under these assumptions, the conservation of mass, momentum, and energy form the governing equations for the boundary value problem and may be expressed as (see Gartling and Nickell [8]),

$$du/dx + dv/dy = 0 \tag{1.1}$$

$$udu/dx + vdu/dy = -(1/\rho)\,dP/dx + \nu\nabla^2 u \tag{1.2}$$

$$udv/dx + vdv/dy = -(1/\rho)\,dP/dy - g\beta(T-T_0) + \nu\nabla^2 v \tag{1.3}$$

$$udT/dx + vdT/dy = \alpha\nabla^2 T \tag{1.4}$$

with the boundary conditions given by,

$u = u_o$, $v = v_o$, $T = T_o$, $P = P_o$.

The various symbols in the above equations have their conventional meanings, except the partial derivative which is represented throughout this analysis by d (see NOMENCLATURE, pg. xi).

1.2.1 AVAILABLE FINITE ELEMENT FORMULATIONS

The equations above can be restated in two other forms by the definition of a stream function and a vorticity function. Each of these three formulations provides the basis for a finite element analysis of the heat convection boundary value problem. In the first case, the primitive variable formulation (as given above), the discretised equations are obtained directly in terms of the velocities, temperature and pressure. This procedure has been successfully employed for investigating fluid flow by Heinrich and Marshall [14], Allaire et al [15], Taylor and Hughes [16], Huyakorn et al [17], Reddy [18], and Yoshida and Nomura [19], and for analysing natural convection by Gartling and Nickell [8], Kawahara et al [20], Chen et al [21,22], Reddy and Satake [23], Reddy [24], Bertin and Ozoe [25], Prakash and Patankar [26], Schnipke and Rice [27,28], and Dalman et al [29].

The second alternative, the stream function-vorticity formulation, satisfies the continuity equation identically by the introduction of the stream function, Ψ, defined as,

$$u = d\Psi/dy \ , \ v = -d\Psi/dx. \qquad (1.5)$$

Further, the pressure is eliminated from the momentum equations by appropriate differentiation and subtraction. The introduction of the vorticity function, w, defined as,

$$w = dv/dx - du/dy \tag{1.6}$$

then allows the flow problem to be described in terms of the two variables, stream function and vorticity function. This formulation was used by Kawahara [12], Campion-Renson and Crochet [30], Dhatt et al [31], Peeters et al [32], and Olson [33] to evaluate fluid flow problems, and by Tabarrok and Lin [34], Reddy and Satake [23], Ozoe et al [35], and Miyauchi et al [36] to solve examples of natural convection.

A third alternative requires the elimination of the vorticity function from the stream function-vorticity formulation as described above. This procedure, which leads to a fourth order equation in terms of the stream function, was utilised by Kawahara and Okamoto [37] for the analysis of flow problems.

As can be deduced, the number of variables in this last procedure is least, which may be considered as an advantage. However, this reduction in the number of variables is achieved at the expense of admitting higher order derivatives in the system equations. The existence of these higher derivatives is disadvantageous for two reasons. Firstly, the continuity requirement of the variables, from one element to the next, becomes stringent and difficult to satisfy. Second, while the accuracy of the computed values of the stream function may be

acceptable, those of the velocities will generally be inferior as a consequence of differentiations of an appropriate field of the stream function. These features of the stream function formulation make the use of high degree polynomials as shape functions, mandatory. A further drawback of this formulation is that it requires the definition of complicated boundary conditions.

The stream function-vorticity formulation also suffers from a loss of accuracy that results when the velocities are derived from the stream function. However, the major difficulty encountered when implementing this formulation, is that the no-slip boundary conditions need to be dealt with in an iterative manner.

2.2 THE PRIMITIVE VARIABLE FORMULATION

The primitive variable formulation has often been employed by researchers because (1) it represents directly the variables of most interest, (2) it is directly applicable to three-dimensional problems, (3) it is the most convenient method for defining appropriate boundary conditions, and (4) the continuity equation is imposed exactly.

The main disadvantage of the direct formulation is the fact that the manner in which the continuity equation is incorporated into the discretised equations gives rise to some zero elements along the diagonals of the system matrix and this prevents the use of standard solver routines. However, the matrix can be easily adjusted by pivoting the rows of the matrix in such a way that the

equations gives rise to some zero elements along the diagonals of the system matrix and this prevents the use of standard solver routines. However, the matrix can be easily adjusted in such a way that the zero diagonals are replaced by non-zero elements of the matrix.

The system matrix is not positive definite, and thus the eigenvalues of the matrix are both positive and negative. Experience has shown that, for the incompressible case, certain combinations of orders of interpolation cause so-called spurious zero eigenvalues. These are referred to as pressure modes in the literature (see Prakash and Patankar [26]).

Equal-order interpolation generally creates these pressure modes, but it can occur in other elements as well. It is not always obvious when such singularities can occur in an element. This situation, also known as 'checkerboarding', results in a square mesh when an even number of those elements displaying a pressure mode, is used along each side.

The 'checkerboard' mode has been effectively removed when the penalty formulation has been employed, or when the pressure variable has been interpolated using bi-linear shape functions instead of the bi-quadratic shape functions used for the velocity variables (see Prakash and Patankar [26]).

The latter procedure, known as mixed interpolation, has been used to investigate fluid flow by Huyakorn et al [17], and also convection heat transfer by Gartling and

Nickell [8], Kawahara et al [20], Chen et al [21], and Dalman et al [29].

Other authors, namely Heinrich and Marshall [14], Allaire et al [15], Reddy [18,24], Reddy and Satake [23], and Bertin and Ozoe [25], have successfully used the penalty function method with reduced integration to obtain stable solutions. In this method, the incompressibility constraint is imposed through the addition of a penalized constraint error term to the equations of motion. The pressure is the Lagrange multiplier associated with the incompressibility constraint, which is satisfied only in a weak sense in the penalty method i.e.

$$P = - \lambda (du/dx + dv/dy)$$

A large value of λ enforces the continuity equation to approach zero because the pressure is bounded and this satisfies the mass balance approximately. This method is also advantageous in that the pressure is eliminated as a dependent variable.

On balance, the primitive variable formulation thus seems to be the most suitable formulation for investigating natural convection, and hence its adoption for use in this study. Mixed interpolation is used, with eight node 'serendipity' elements being employed for the velocities and temperature, and four node quadrilateral elements being used for the pressure.

1.3 OBJECTIVES OF THIS STUDY

The objectives of this study are fourfold :

1. To outline the development and current methods of numerical convection heat transfer from available literature.

This study reviews the relevant available literature on fluid flow and convection heat transfer. The review encompasses an analysis of the various finite element formulations available for investigating convection heat transfer, listing both their advantages and the disadvantages, and it highlights the difficulties encountered by the various researchers. The parameters for which a solution is obtainable, and the size and type of mesh used, are also defined. Where similar examples have been investigated, the results of the various authors are compared and reasons for any discrepancies are given.

2. To describe the finite element formulation for the primitive variable equations via a Galerkin weighted residual scheme and using mixed interpolation.

3. To demonstrate the capability of the method by means of a number of practical examples. In order to verify the accuracy of the method, the first example investigated is natural convection in a square cavity, the results of which are widely documented in the literature. A large range of parameters is considered, and the solutions to the problem are compared with those obtained by previous

authors. A slight variation of this example, that of natural convection in a rectangular cavity, is also considered. The purpose of this example is to determine the effect various aspect ratios, and non-rectangular elements, have on the flow, and the temperature and pressure distributions.

The third problem analysed, free convection in a triangular cavity, is investigated to establish the effectiveness of 8-node serendipity elements in analysing triangular shapes, and to determine the effect heating the upper side of the cavity has on the variables. The example of natural convection in a liquid diode was chosen to demonstrate the usefulness of the method in optimising the design of passive solar heating of buildings, thereby showing the direct applicability of the method to actual situations.

The purpose of the final example, the cooling pond of the nuclear power plant at Chernobyl, U.S.S.R., is (1) to show that the method can also be applied to forced convection, and (2) to show the ease with which complicated geometric shapes can be modelled. This example is also undertaken to demonstrate the applicability of the method to an existing physical problem, and thereby show its usefulness in enabling predictions to be made as to the impact thermal pollution will have on the environment.

4. To provide, via the review and the development of the computer code used for the above examples, the background and framework for the problem of transient convection heat transfer, and also for further steady-state studies using

parameters outside the ranges considered in the current study.

1.4 ORGANISATION OF THE STUDY

In Chapter 2, the relevant available literature is summarised and reviewed. The various numerical methods and finite element formulations available for investigating convection heat transfer are discussed and evaluated. Also, any difficulties encountered by the researchers, are noted, and possible reasons as to their existence are given.

Chapter 3 contains the primitive variable finite element formulation, developed from the equations of conservation of mass, momentum and energy. Initially, the analysis is simplified by making a number of assumptions. The governing equations are then normalized, using sets of dimensionless variables, in order to facilitate generalization to enable a large range of problems to be investigated. Before they can be manipulated for use in the finite element method, their variational, or weak, formulations are derived.

Chapter 4 concerns the finite element modelling of the governing equations based on the primitive variable formulation, and Chapter 5 discusses the solution of steady-state non-linear problems, this being the type encountered in convection heat transfer.

In Chapter 6, the capability of the method is then demonstrated on five practical examples, namely (1) natural convection in a square cavity, (2) natural convection in a rectangular cavity, (3) natural convection in a triangular cavity, (4) natural convection in a liquid diode, and (5) forced convection in the cooling pond of the nuclear power plant at Chernobyl, U.S.S.R. Wherever possible, the results are compared with those obtained by other authors by either experimental or numerical methods.

Finally, conclusions are drawn from the results, and recommendations for further studies are made.

CHAPTER 2

LITERATURE SURVEY

2.1 NUMERICAL SOLUTION OF FLUID FLOW PROBLEMS

Convection heat transfer involves the interaction of conduction heat transfer and fluid flow, and for this reason, a brief review of the relevant literature concerning fluid flow is followed by research conducted specifically in the field of convection heat transfer. Equations such as those governing fluid flow and convection heat transfer are parabolic in nature, and can be solved using several numerical methods such as finite difference methods, the method of lines, the Galerkin method, and finite element methods.

The finite difference method remains popular in fluid problems (see Cebeci and Bradshaw [38]), and was used by Dennis and Chang [39] to obtain solutions for the equations of motion for steady incompressible flow around a circular cylinder for Reynolds numbers between 5 and 10^2. The purpose of their research was to numerically obtain reliable data on steady flow for a wide range of Reynolds numbers, particularly with regard to the growth of the wake.

They observed that the wake length increased almost

linearly with Reynolds number over the whole range from the value, just below Re=7, at which it first appeared. Their results for wake length and drag coefficient compared very well with both previous numerical and experimental studies. They also presented calculated values of the angle of separation, and the pressure and vorticity distributions over the cylinder surface. These results were in agreement with those published by previous authors, but they were unable to predict, with any certainty, the tendency of the fluid properties as the Reynolds number became very large. This was because they attempted to obtain their results by integrating the time-dependent equations of motion, but they found that the approach to steady flow was so slow that they abandoned the method.

In another study, Dennis and Walker [40] investigated steady axially symmetric incompressible flow past a sphere for Reynolds numbers between 10^{-1} and 40. They utilised a semi-analytical formulation to reduce the equations of motion to ordinary differential equations, which they solved using a series truncation method. This they found to be advantageous over the finite difference method as it removed the necessity of approximating derivatives in the angular direction. They also did not encounter the difficulties imposed by computer core limitations when the methods based on finite differences are used. Their calculated drag coefficients compared very well with those of previous authors and with experimental data.

With the rapid advance of electronic computers, it has become feasible to investigate different finite-difference

formulations of the steady-state, three-dimensional Navier-Stokes equations. All of these formulations followed one of the two basic approaches of incompressible fluid flow, namely the primitive variable (velocity-pressure) formulation, or the vector potential and vorticity formulation.

Williams [41] numerically integrated the primitive variable formulation of the Navier-Stokes equations for certain three-dimensional flows using a finite difference technique. He presented some features of a solution for steady wave flow in an annulus, noting the resemblance of his results to that of the classical Eady wave.

Aziz and Hellums [42] analyzed the Navier-Stokes equations in terms of the vector potential and the vorticity components. They found that it was possible to solve three-dimensional unstable laminar flow problems of a very general type by finite-difference methods, and that the computer time required was relatively small. They also concluded that their solution technique was stable even for large time steps, and would readily extend to problems with complications such as variable properties or non-Newtonian behaviour.

Studies have shown that the numerical solution of the Navier-Stokes equations using the finite difference technique presents serious difficulties when the Reynolds number is large and the convection terms are much larger than the diffusion terms. Such situations generate a system of equations which is no longer diagonally dominant and hence cannot be solved by standard relaxation methods.

Another major difficulty occurs when solving these equations for flow over non-rectangular boundaries. Although attempts were made to overcome this problem by constructing curvilinear meshes in finite-difference methods (see Ghosh et al [43]), early progress in the finite element method enabled any complicated geometry to be suitably represented and allowed appropriate boundary conditions of the model to be imposed in a natural way.

2.2 FINITE ELEMENT ANALYSIS OF FLUID FLOW

In order to use the finite element method to analyse fluid flow, the equations of motion of viscous incompressible fluids first have to be transformed into a global integral form via an approximate method such as the Galerkin weighted residual method. The flow domain is then divided into a number of subdomains called elements. Each element is associated with a number of discrete points or nodes located within or on the element boundary. The spatial variation in the flow variables within the element is then defined in terms of the values at the node points.

Thereafter, the global equations are integrated over each element, usually by some form of numerical integration leading to an element contribution in matrix form, and the contributions from each element are summated, to give the final equation, which is also usually in matrix form. This equation is then solved, after the introduction of appropriate boundary conditions, for the nodal values of the variables. For non-linear problems, such as most fluid

flow problems of practical interest, an iterative technique has to be used to solve the final matrix equation.

The solution of the fluid flow equations by a finite-difference method requires the derivatives of the variables in these equations to be approximated by some difference approximations at discrete points of a grid i.e. the derivative of a variable at a particular grid point is expressed directly in terms of the derivatives of the same variable at the surrounding grid points. It differs from the finite element method in that (1) each equation appears immediately in its assembled form in the system of equations to be solved, and (2) unsymmetric matrices of coefficients often appear due to boundary condition approximation.

Whereas the first difference may be a point in favour of the finite difference method, the second is a distinct disadvantage. Further advantages of the finite element method over the finite difference method are : (1) in non-homogenous problems, direct assembly of elements with different properties presents no difficulties, and (2) discontinuous interfaces do not require any special treatment. Another factor which has contributed to the success of the finite element method is the repetitive nature of the computations of the element matrices.

According to Zienkiewicz [44], the success of the finite element method can be attributed to three factors, namely (1) the analogy with discrete engineering-type assembly (and the consequent use of both computer programs and

intuition already established), (2) the capability of dealing with complex geometrical shapes by the use of arbitrarily-shaped simple elements, and (3) the 'banded' nature of the simultaneous equations which are used to solve the problem once assembled. While the first 'advantage' may appear psychological and idiosyncratic, the second two are real and stem from the piecewise-continuous definition of the shape functions of the finite element method.

Numerous texts, such as Hinton and Owen [45,46], Dhatt and Touzot [47], and Bathe [48] deal with finite element interpolation and discretization, and the application of the method to engineering problems.

2.2.1 Driven Cavity Flow

An early investigation of the two-dimensional steady flow of a viscous fluid by Kawahara and Okamato [37] using the finite element method, was based on the stream function formulation, considering the conditions for surface force as a natural boundary condition. Kawahara et al [20] studied both steady and unsteady viscous flow. They combined the Newton-Raphson and the perturbation methods to solve the steady flow problem and found that this procedure was much more adaptable to solving the non-linear equations involved, than using the perturbation method on its own. The limitation on combining the two methods is that the initial guess should be selected as close as possible to the exact solution. In a later study, Kawahara [12] employed the stream function formulation to

investigate the steady flow in a driven cavity at $Re=6x10^3$. He concluded that the use of the stream function as the variable enabled him to obtain a numerically stable finite element method for the example.

Usuki [49] investigated the problem of the two-dimensional steady flow around a box girder in uniform flow using the local potential principle. This functional was derived by first multiplying the continuity equation by a small pressure variation, and the primitive variable formulation of the equations of motion by a small velocity variation. These resultant expressions were then added, and integrated over the finite element region.

He wished to determine whether the approximate solutions generated by this method gave either upper or lower bounds of the solution. He found however, that, due to the convective term, a classical variational principle could not be found, and thus the local potential principle did not give clear bounds to the solution. He also obtained the coefficient of drag, lift and pitching moment of the girder and concluded that their values seemed acceptable.

Campion-Renson and Crochet [30] used the stream function-vorticity method for solving the Navier-Stokes equations with finite elements. The use of this method previously necessitated the use of an iterative procedure to satisfy the boundary conditions, which was seen as a major disadvantage. The authors showed that such iterations were unnecessary by first evaluating the governing equations for a Reynolds number of zero, and then using an 'incremental loading' process for increasing the value of

Re. When the desired value of Re was reached, the calculation was achieved by applying the modified Newton-Raphson algorithm. They corroborated their method with two examples, namely a driven cavity, and flow in a channel with a step. Both examples showed excellent agreement with existing solutions.

A least squares approach was applied by Milthorpe and Steven [6] to a modified form of the governing equations in the stream function-vorticity format. They showed that the finite element method could be successfully applied to a large range of problems in fluid mechanics by performing several numerical examples, including flow in a driven cavity, and flow around a cylinder.

In the former case, the problem was run for several Reynolds numbers, and it was found that, as the Reynolds number increased, the intensity of rotation within the cavity increased, as did the position of the zero streamline near the bottom of the cavity. This agrees with other studies done on this problem. The analysis of flow past a cylinder produced results in reasonable agreement with previous work. However, some spurious vorticity was detected in the field far from the cylinder. This can probably be attributed to the arbitrary location of the boundary conditions remote from the cylinder.

Moult et al [50] derived the finite element equivalents of the stream function-vorticity formulation of the Navier-Stokes equations, and transformed these to upwind forms suitable for the solution of problems involving Rayleigh numbers larger than 10^6, and Reynolds numbers greater than

10^4 . Upwind difference techniques become necessary at these values as the large Rayleigh or Reynolds numbers result in the convection terms of the governing equations being much larger than the diffusion terms. Such situations lead to a system of equations which is no longer diagonally dominant, and hence cannot be solved by standard relaxation methods. The authors illustrated the use of these equivalents by means of a comparison between their results and published works for a driven cavity. It was shown that the results compared favourably.

A new finite element technique for two-dimensional viscous incompressible flow was developed by Ikegawa [51]. He applied the finite element method to the conservation law of vorticity together with the continuity equation, and solved the resulting sets of algebraic equations by the use of a kind of relaxation method. He too, computed results for viscous flow past a cavity and found them to be in good agreement with experimentally determined results. The computations were relatively stable and the new technique saved considerable computing time. He concluded that this technique can also be effectively employed for other two-dimensional viscous flow problems governed by the Navier-Stokes equations.

Dhatt et al [31] also used the driven cavity example to illustrate a new method of solving the Navier-Stokes equations using the finite element method. They proposed that the flow be represented by the stream function-vorticity formulation and that the no-slip boundary conditions be explicitly introduced in the non-linear equations. This formulation, coupled with the Newton-

Raphson method, enabled the study of steady flows with high Reynolds numbers without any convergence problems. Their results compared favourably with those obtained by Campion-Renson and Crochet [30]. The advantage was that the new method required relatively smaller mesh configurations and fewer iterations to achieve accurate and convergent solutions.

Using the primitive-variable formulation, Heinrich and Marshall [14] developed a penalty function finite element method to analyse two-dimensional viscous incompressible flow. This procedure was shown to be an accurate and efficient method for the numerical solution of flow problems governed by the Navier-stokes equations. They also concluded that the penalty method effectively imposed the continuity constraint. The example they utilised to demonstrate their method, was that of driven cavity flow, and they considered Reynolds numbers up to 400. Their results for this problem were in excellent agreement with the available solutions in the literature.

Allaire et al [15] employed the penalty function approach to analyse steady viscous flow, and used a simplex element with a linear velocity and constant pressure, as opposed to previous authors who used higher order elements. The simplex element yields analytical expressions for the element matrices which, in turn, lead to efficient solutions. They overcame such problems as 'overconstrainment' and 'lock-up', which previously hampered the use of this type of element.

They prevented 'overconstrainment' by using linear

triangular elements in a special criss-cross triangulation pattern. These elements were not 'overconstrained' because the ratio of the number of degrees of freedom available to solve the problem, to the number of constraints due to incompressibility, is aided by the additional geometric relations.

Using this criss-cross triangulation pattern, locking was avoided by placing the centre node at the exact location of the intersection of the diagonals. If this node is placed anywhere else, continuity errors occur. Mass is not conserved over each element, and a locking phenomenon results, where nodal velocities are independent of the value of the penalty parameter for very large ranges.

The method was tested on examples of Couette flow, Poiseuille flow, and driven cavity flow. The results obtained for the first examples matched the analytical solutions very well. Those obtained for the driven cavity predicted the shape and location of the centre of the primary vortex, and the streamlines through the channel, fairly well. These results are also in reasonable agreement with those obtained by Campion-Renson and Crochet [30] as far as the shape and location of the primary vortex are concerned.

However, some discrepancy existed between the numerically-determined flow fields and those found experimentally. This was especially evident at the interface between the driving channel and the cavity. The authors postulated that these discrepancies may have been caused by the fact that, in this region, the local element Reynolds numbers

are high.

One of the most recent papers investigating driven cavity flow, was written by Peeters et al [32], who used the stream function-vorticity formulation to solve the incompressible, two-dimensional Navier-Stokes equations. The no-slip solid walls boundary condition was applied by taking advantage of the simple implementation of natural boundary conditions in the finite element method, eliminating the need for an iterative evaluation of wall vorticity formulae. In addition, with the proper choice of elements, they constructed a stable scheme which allowed convergence to be achieved for all Reynolds numbers, from creeping to inviscid flow, without the traditional need for upwinding and its associated false diffusion. Peeters et al [32] computed results for Re=400, and found that their results compared very well with previously published material.

2.2.2 Flow Over Cylinders And Steps

Although no example on the finite element analysis of flow or forced convection over cylinders and steps is presented in this study, the literature involving these problems has been included so as to present an overall view of the state of the research that has been undertaken in the fields of fluid flow and convection heat transfer up to the present time.

Olson [33] used the stream function-vorticity formulation to study steady incompressible flow in both the two-dimensional and the axisymmetric geometries. He employed

the Newton-Raphson method to solve the non-linear algebraic equations and tested the formulations on both flow over a circular cylinder and flow in a constricted cylindrical tube, for Reynolds numbers between 10^{-2} and 10^{2}.

He noted that flow over a circular cylinder is of special interest as, above a certain critical Reynolds number, the flow separates from the downstream side of the cylinder and forms a recirculating vortex. Thus it is easily comparable to previous work in this area. Comparing his results to those obtained by Dennis and Chang [39] and Dennis and Walker [40], who used the finite difference method, it can be seen that the separated flow patterns compare extremely well, especially as to the point of separation. However, the numerical results for quantities on the cylinder surface, such as drag and pressure coefficient, do not compare as well. This can be attributed to the approximations of the boundary conditions that he used.

The analysis of axisymmetric flow in a tube with a step change in diameter showed slight discrepancies with previous work but these were due to the coarseness of the finite element grid, especially in the recirculating vortex after the step.

He concluded that the two-dimensional program consistently exhibited good stability, fast convergence and good accuracy, even for the higher Reynolds numbers. However, the axisymmetric one, in some cases, did not converge for the higher Reynolds numbers or for more refined grids.

Unfortunately, this behaviour was somewhat erratic so that no consistent pattern emerged.

In a later study, Taylor and Hughes [16] used the primitive-variable formulation to analyse two-dimensional fluid flow, and they tested their method using the same, or similar, examples as Olson [33], namely flow over a circular cylinder, and flow over a backward step. They included a development of the necessary computer programming and solution techniques, in which they showed that the non-linearity of the convection term in the Navier-Stokes equations leads to non-symmetry of the coefficient stiffness matrix. The non-linearity necessitates the use of an iterative procedure to solve for the primitive variables.

The results obtained for the cylinder in crossflow were in good agreement with those obtained by Olson [33], and the dimensionless velocity distributions obtained for flow over a backward step compared favourably with previously published material in Denham and Patrick [52] and Atkins et al [53]. Taylor and Hughes [16] also included a section in which they showed that the steady-state Navier-Stokes equations can be extended quite readily to accommodate simple models of turbulence.

Huyakorn et al [17] compared various mixed-interpolation finite elements in the velocity-pressure formulation of the Navier-Stokes equations. They considered four types of elements, namely the four node quadrilateral element, the six node triangular element, the eight node serendipity element, and the nine node Lagrangian element. They compared the elements via the results obtained from two

examples, one of which was steady flow through a sudden expansion.

The Lagrangian elements gave the most accurate pressure and velocity distributions, while the triangular elements were found to be of intermediate accuracy and dependent on the triangular pattern used. Their results also showed that the serendipity elements sometimes generated spurious pressure distributions.

Allaire et al [15] also applied their simplex element to flow over a backward step. The results at various Reynolds numbers were in good agreement with those obtained by Taylor and Hughes [16] and Denham and Patrick [52]. Of note is the fairly reasonable prediction of the recirculation region considering the coarse mesh used.

Chen et al [21] used the finite element method to solve the full Navier-Stokes equations for the problem of laminar flow of air around three horizontal cylinders in a staggered tube bank, and around four horizontal cylinders in an in-line tube bank. They employed the same finite element model as Taylor and Hughes [16] to solve the primitive variable formulation of the governing equations.

The authors noted that the Reynolds number caused significant variations in the total drag, friction drag, and pressure drag, as well as the shift of location of the separation flow. They also found that their results for the upper region of the upstream cylinder compared favourably with those obtained by Dennis and Walker [40], and Badr [54] for a single cylinder. A further conclusion

was that the greater the spacing between the cylinders, the closer the results resembled those of a single cylinder.

2.2.3 Lake Circulation And Tidal Flow

Another field of flow problem which has been studied in recent years using the finite element method, is that of lake circulation and tidal flow. Hamblin [55] obtained solutions of the linearized steady state equations for the lake circulation and wind set-up under a uniform wind stress. He also investigated some types of oscillatory flows, namely surface seiches, internal Kelvin waves and astronomical tides, and the time-dependent response of a body of water to a varying wind stress and barometric pressure gradients.

He concluded that his numerical hydrodynamical models were in reasonable agreement with field data, thus demonstrating that the finite element method is flexible enough to treat both a variety of steady-state and dynamical problems in lakes as well as a wide range of lake geometries.

Kawahara [12] analysed unsteady tidal flow by applying the perturbation method to the periodic motion. The numerical results he obtained were similar to those obtained from the finite difference method and observed field data. He concluded that the numerical procedures used were suitable, and of practical use, in analysing tidal flow problems from the viewpoint of computing time, computer core storage and numerical stability.

A numerical method, which can be used to formulate a model of both tidal propagation and dispersion in estuaries, rivers and seas, was developed by Taylor and Davis [56]. The model simulated the current velocity, water-depth and effluent dispersion, both spatially and temporally, during a tidal cycle, and any required biological, chemical and decay processes were coupled to the physical dispersive mechanism. The authors presented a number of examples to illustrate their method including tidal propagation in the southern North Sea, which illustrated fully two-dimensional flow, and an estuary subjected to a continuous point effluent discharge. The results obtained for the former example compared favourably with material published previously.

Gallagher et al [4] presented a paper which analysed wind-induced steady-state circulation of variable-depth shallow homogenous lakes. They used a finite element formulation of the governing equation derived by Ligget and Hadjitheodorou [57]. This development assumed homogeneity, hydrostatic pressure, specified wind shears, and a small Rossby number. The last assumption, together with a boundary condition of zero velocity normal to the lake free surface and the bottom, enabled construction of a linear equation in two dimensions whose coefficients were a function of all three dimensions.

They computed results for rectangular basins which compared favourably to those obtained previously by authors using the finite difference method. Also, in order to demonstrate the advantages of geometric representation using the finite element method, they analysed the wind-

driven circulation of Lake Ontario, North America, but they were unable to make comparisons of these results due to lack of available data.

In a later study, Gallagher [58] reviewed the finite element procedures available for the analysis of wind-driven lake circulation. Various features of practical importance are neglected in the basic two-dimensional representation of this type of steady-state fluid flow. These include the presence of islands, the existence of thermal stratification, and the three-dimensional character of a real lake. Once again, the author illustrated his method by analysing circulation in both simple test problems and Lake Ontario, North America. As stated above, no field data of this lake is available, and thus a comparison could not be made. The author did, however, study the convergence of the solution by using higher order elements.

2.2.4 Three-Dimensional Fluid Flow

All fluid flows in nature are three-dimensional, but, due to the non-linearity of the Navier-Stokes governing equations, and the limitations imposed by both experimental as well as numerical techniques, researchers have been forced to analyse only those motions that are believed to be independent of the third dimension. However, many important fluid flow problems of practical interest are not capable of approximation by a two-dimensional model, and they have remained beyond the realms of a detailed investigation until recently.Thus the finite element analysis of the three-dimensional Navier-

Stokes equations has to date only been investigated by a few authors.

Reddy [18] presented results for the problem of wall driven cavity flow in a cubical box, which he obtained using a penalty finite element method. He concludes from his computations for the Reynolds numbers of 10^2 and $4x10^2$, that the fixed wall has the kinematic effect of reducing the strength of the flow field. On comparing his results with recent finite difference solutions for the same problem, the author found the agreement to be good.

2.2.5 Transient Fluid Flow

Although the problems considered in the current study were assumed to be steady-state, this section and section 2.5.3 on transient natural convection were included to show the state of the research that has been conducted in finite element analysis of time-dependent flow and convection.

Gresho et al [59,60] used a modified finite element to solve the time-dependent incompressible Navier-Stokes equations. Beginning with the Galerkin finite element method and the simplest appropriate isoparametric element, they modified the spatial approximation to improve the cost-effectiveness of the method. This they achieved in two ways, namely the mass matrix was lumped, and all the coefficient matrices were generated by means of 1-point quadrature. For the time integration, they used the explicit Euler method in such a way that it compensated for that portion of the time truncation error which is intolerable for advection-dominated flows.

The authors demonstrated the method on three sample problems, namely steady flow in a lid-driven cavity at $Re \leqslant 10^4$, flow past a cylinder at $Re \leqslant 400$, and the simulation of a heavy gas release over complex topography. They concluded from their results that their techniques provided a means for obtaining accurate and affordable, truly time-dependent solutions to the incompressible Navier-Stokes equations, and that they could also be utilised for finding steady solutions, when the solution existed. They also found that 1-point quadrature, mass lumping and explicit Euler time integration increased the cost-effectiveness, although, in time simulations, a loss in accuracy could be directly attributed to the mass lumping, and, to a lesser extent, to the 1-point quadrature. Finally, they showed that steady laminar flow in a two-dimensional lid-driven cavity was stable for Reynolds numbers less than 10^4.

Yoshida and Nomura [19] used the finite element method to solve the primitive variable formulation of the time-dependent, incompressible Navier-Stokes equations. The imposition of the continuity and boundary conditions led to a set of non-linear recurrence equations which represented the evolution of the velocities and pressures under the incompressibility constraint. An iteration process, necessitated by the non-linear convective terms, was performed in every integration step until convergence was achieved.

They verified their method by comparing their results of flows around a rectangular-section cylinder with experimental data available in the literature. Thus, the

authors were able to conclude that (a) their solutions satisfied the incompressibility conditions, (b) the time-dependent solutions agreed fairly well with experimentally visualised flow fields, and (c) the fluid forces acting on the obstacles could be successfully predicted using their procedure.

2.3 EARLY INVESTIGATIONS OF CONVECTION HEAT TRANSFER

2.3.1 The Window Cavity

One of the earliest and simplest models involving free convection was the window cavity, and some of the more well-known papers reporting on experimental work performed on this example, are reviewed below.

Air layers enclosed between two vertical plates with different temperatures are used in many engineering applications as a means to decrease the heat flux and the corresponding heat losses. Natural convection arising in such layers limits the insulating effect. In other applications, the convection in the enclosed fluid is utilised to transport heat. Accordingly, the problem of predicting the amount of heat transported through such a layer has found considerable attention in the past.

Eckert and Carlson [61] investigated the temperature field in an air layer enclosed between two isothermal vertical plates with different temperatures using a Mach-Zehnder interferometer. They found that, below a certain Grashof

number and above a certain aspect ratio, heat is transferred from the hot to the cold boundary by conduction in the central part of the layer. Convection contributed only in the corner regions.

For large Grashof numbers and below a certain aspect ratio, the results showed that the boundary layers existed along the surfaces of the enclosure, whereas in the central core the temperature was uniform in horizontal planes. The temperature increased, however, in the vertical direction.

In one of the most oft-quoted reports, Elder [62] conducted an experimental study of laminar free convection in a vertical slot. He made the height of the cavity larger than the width, and the length of the cavity was sufficiently long in the third dimension for the mean flow to be two-dimensional nearly everywhere.

For Rayleigh numbers less than 10^3, he found that the temperature distribution closely resembled the solution to Laplace's equation, but a weak stable unicellular circulation was generated. The flow was vertical throughout the slot except near the ends. Large temperature gradients developed near the walls for $10^3 \leqslant Ra \leqslant 10^5$, and in the interior region, a uniform temperature gradient was established. For Rayleigh numbers near 10^5, the interior region generated a steady secondary flow.

2.3.2 Cooling Ponds and Lakes

Industrial development is increasingly confronted with the

demand for environmental impact studies prior to the approval of construction. In the case of power plants, especially difficult problems are posed with the dissipation of heat, since high temperatures are critical to the efficiency of the plant. For this reason, the other example modelled in the present study is a cooling pond or lake, and some of the investigations conducted by previous authors are described below.

Kinsman [3] investigated a number of alternative schemes available for the dissipation of heat from the cooling system of a power plant. He stated that local heat dissipation to open water is an obvious and attractive method as long as compliance with water standards is maintained. Although the supply of sea water is practically unlimited, ocean sites are accessible only in a few cases due to increasing restrictions. Very large lakes, bays and estuaries can be utilised, but hydraulic and ecological factors restrict their use. It is also possible to use rivers, but few have sufficient flow to supply the water quantities required.

According to Kinsman [3], lakes and reservoirs are more viable propositions because of natural stratification, where cool water can be taken from the deep areas, and warm water returned to the surface. From here, the heat is dissipated via evaporation, radiation, conduction and convection. However, these cooling ponds require large land areas, which are not always available, and they cause increased water consumption through natural evaporation.

Because of the increasing size of power plants and the

scarcity of large sites, closed systems, such as cooling towers, are receiving more and more consideration. However, they are more expensive, and are more difficult to design, than cooling ponds, and they reduce the net power available from the plant.

Stefan [63] discussed the modelling of warm water surface discharge into a lake. He stated that, at the time of writing, a prediction of the dispersion of a thermal plume for any particular lake and outfall could not be made by analytical methods. Instead, physical models were commonly used, while mathematical models were being developed and tested. Only once these mathematical models had achieved a certain accuracy when compared with measurements, were they able to be used for forecasting further results.

He concluded that physical modelling had to include three phenomena, namely mixing at the outlet, stratification, and surface heat transfer. On theoretical grounds, he found modelling to be justified even though it could not be achieved in a rigorous way. Assumptions had to be made, but as long as these were made judiciously, overall flow and temperature patterns would most likely be obtained with an accuracy adequate for many purposes.

To minimise short circuiting and to utilise effectively the entire free surface of a cooling pond, a system of internal dikes is usually constructed. These dikes are quite expensive, and thus some rational approach for designing their layout is required. Tatinclaux et al [64] developed a dye injection method, for use in hydraulic models, to investigate the flow behaviour in a shallow

cooling pond, and to predict its performance for various dike arrangements.

Their investigation was restricted to shallow lakes in which there was almost complete vertical mixing, and in which the density currents were relatively small compared to the primary pumping currents. Using their method, they were able to design an efficient and economical dike system, and predict the resulting intake temperature for any particular lake.

2.4 NUMERICAL SOLUTION OF CONVECTION PROBLEMS

De Vahl Davis [65] studied steady laminar two-dimensional flow of a fluid in an enclosed rectangular cavity, where the motion was generated by a temperature gradient normal to the direction of the body force. The governing vorticity transport and energy equations were solved by means of the finite difference method. The author assumed that the Boussinesq approximation held i.e. he neglected the density variation in the inertial terms of the equation of motion but retained it in the buoyancy term of the vertical equation. Calculations were made for Rayleigh numbers up to 2×10^5 and Prandtl numbers in the range between 10^{-1} and 10^3, for various aspect ratio's, and for both linear and adiabatic boundary conditions on the temperature.

He found that his results for the linear thermal boundary condition were in excellent agreement with previous

authors, whereas a comparison of those obtained for the insulated thermal boundary condition was less favourable. However, this he attributed to an error in the vorticity boundary condition adopted by the other authors. An interesting outcome of his calculations was the lack of effect of the Prandtl number of the fluid on the motion. It did, however, have a vital effect on the stability of his solution procedure, especially at higher Rayleigh numbers.

In a later paper, Mallinson and De Vahl Davis [66] solved the three-dimensional steady-state Navier-Stokes and energy equations for the problem of natural convection in an enclosure resulting from differential side heating.

Their results showed the three-dimensional motion generated by the presence of no-slip adiabatic end walls. For $Ra=10^4$, they found the three-dimensional motion to be caused by the inertial interaction of the rotating flow with the stationary walls together with a contribution arising from buoyancy forces generated by longitudinal temperature gradients. For small values of the Prandtl number, the inertial effect dominated, whereas when the Prandtl number was large, the inertial mechanism diminished and the weaker thermal effect dominated.

Due to the fairly limited amount of work which has been done on natural convection in cavities with large aspect ratios (width/height>10), Shiralkar and Tien [67] conducted a recent study of the problem using a finite difference technique. Comparing their results with existing analytical and experimental results, they found

the agreement to be good at the moderate and high Prandtl numbers to which most previous works had been restricted. They extended their study to low Prandtl numbers using both an analytical model and a numerical solution of the full equations. A comparison between the two showed the agreement to be very good.

Schmidt et al [68] studied laminar natural convection in a water-filled enclosure, with an aspect ratio of two, using both an experimental and a numerical model. Two opposing vertical walls were held at different uniform temperatures, and the remaining four walls of the enclosure were insulated. The study was conducted at a relatively high Rayleigh number near the upper limit of the laminar flow region. A multilevel-multigrid algorithm was used to predict the flow for the experimental conditions studied, and the mean velocity profiles obtained from this algorithm were in excellent agreement with the experimental profiles.

A comprehensive finite difference investigation into laminar two-dimensional forced convection in cavities was conducted by Bhatti and Aung [69]. The walls of the cavity were held at a uniform temperature and calculations were carried out at various aspect ratios and Reynolds numbers. The numerical technique was based on a hybrid upwind/ central differencing of the governing differential equations that were first integrated over control volumes surrounding the node points in a rectilineal, non-uniform grid system.

Their results showed that while the average Nusselt number

in the cavity was related to the Reynolds number raised to a power, the latter depended on the aspect ratio and varied between the cavity floor and the side walls. The influence of the upstream boundary layer thickness was found to be negligible.

Their results clearly show that the downstream wall had the largest influence on the overall heat transfer. They also found that the overall heat transfer could not be given any simple relation derived from a similarity analysis of the shear layer.

Chen and Yoon [70] also considered forced convection across a cavity. They presented numerical solutions for flow pattern and temperature distribution which they obtained using the finite analytic numerical method. This technique, introduced recently by Chen and Li [71], differs from other numerical methods in that it utilises a local analytic solution in an element of the problem to construct the total numerical solution.

They concluded that while the finite difference method has had some success (see Bhatti and Aung [69]), difficulties such as proper finite difference approximation of the convection terms, and false numerical diffusion for high Reynolds number flow, remain. They found the derivatives of the finite element solution to be less accurate and sometimes discontinuous, unless a higher degree approximating function was used. Instability in solving the system of equations from this method at high Reynolds number flow also sometimes occurs.

Their finite analytic method was effective in eliminating instability and false numerical diffusion for flow at high Reynolds numbers. They checked the accuracy of the method against vorticity, conservation of mass, and conservation of energy relations, and found their results to be agreeable to within 5% for every Reynolds number considered.

2.5 FINITE ELEMENT ANALYSIS OF CONVECTION HEAT TRANSFER

2.5.1 Natural Convection In A Window Cavity

Some of the earliest authors to investigate free convection in a window cavity using the finite element method, were Kawahara et al [20]. They employed the primitive variable formulation and mixed interpolation. As stated in section 2.2.1, they combined the Newton-Raphson and perturbation methods to solve the discretized non-linear simultaneous equation system. Although they only quote an example for $Ra=6.06x10^3$, it is in reasonable agreement with the examples published by De Vahl Davis [65]. They also studied another example, namely pottery heated from the bottom, and the computed results were consistent with their predictions.

Tabarrok and Lin [34] studied two-dimensional natural convection problems using the stream function-vorticity formulation of the governing equations, which they simplified by using the Boussinesq approximation for the buoyancy forces. They used a simple triangular finite

element model to analyse a rectangular window cavity, and found that their results compared very well with those obtained experimentally by Ozoe et al [72].

Another example examined by Huyakorn et al [17] in their comparison of various mixed-interpolation finite elements, was thermally driven flow in a window cavity with $Ra=6x10^3$. In their paper, the authors are not specific as to how the temperature variable was included in their method. However, as with their other example of steady flow through a sudden expansion, they found that the nine-node Lagrangian elements gave the most accurate results. The triangular and serendipity elements produced results of approximately the same order as each other, but they were less accurate than the nine-node Lagrangian elements' results. In all of these cases, convergence was achieved to within a tolerance of 5%.

However, in the four node case, convergence was achieved only for the velocity and temperature solution, but not for the pressure solution. They found that, unless certain boundary conditions were used, large oscillations, which took the form of a 'checkerboard' pattern, occurred in the pressure field. In such instances, although the pressure solution was completely erroneous, the velocities and temperatures remained accurate. They finally concluded that the temperature was the least sensitive to the type of element used, whereas the pressure was the most sensitive.

A paper presented by Reddy and Satake [23] compared the penalty function and stream function formulations of the

governing equations of free convection in enclosures, for Rayleigh numbers less than 10^6. Although the penalty finite element models seemed to be computationally simpler than the stream function-vorticity ones, the results obtained from both methods applied to the window cavity problem were in good agreement with those presented by Tabarrok and Lin [34] and Ozoe et al [72]. However, those obtained from the penalty method were on the lower side of those obtained using the stream function method, and those presented in the prior works. Reddy and Satake [23] also used the penalty finite element model for the vertical slot problem, and compared their results with those of Elder [62]. The correlation was very good.

In conclusion, they found that the stream function-vorticity formulation presented convergence problems for Rayleigh numbers higher than 10^4. However, for very high Rayleigh numbers, the penalty parameter of the penalty method was, of necessity, very large, causing the equations to be ill-conditioned.

In a later study, Reddy [24] again used the penalty function method to solve the governing equations of natural convection. However, in this paper, he analysed both the two-dimensional and the three-dimensional window cavity problems. For the two-dimensional example, his results were in good agreement with those reported earlier by De Vahl Davis [73]. He concluded that the fixed wall of the three-dimensional cavity has the kinematic as well as the thermal effect of reducing the strength of the flow field. However, due to lack of literature available for this problem, comparison of his results to judge their

quality is not possible.

Bertin and Ozoe [25] developed an efficient scheme for the convergence of natural convection calculations using the penalty finite element method with a modified Galerkin scheme. They demonstrated the method on two examples, namely laminar natural convection in a window cavity and in a horizontal layer of fluid. Rapid convergence was achieved by initially setting the penalty parameter at a small value, and then increasing it to larger values in discrete steps. This procedure decreased the computing time to 5% or less of that required for a single large value of the penalty parameter, while producing less than a 2% difference in the final average Nusselt number.

Prakash and Patankar [26] presented a finite element method for solving the Navier-Stokes equations using equal order velocity-pressure interpolation. Their method consisted of developing a discretization equation for pressure from the continuity equation and the semi-discretized momentum equations. They were thus able to compute both velocity and pressure at all grid points in the domain, while preventing the appearance of any spurious 'checkerboard' pressure fields. An added advantage of their method was that the discretization equation for pressure was similar to the discretization equation for any other variable, and hence, the same equation solver routine could be used for all the variables. Their results for natural convection in a square cavity compared excellently to those obtained by previous authors.

In two similar papers, Schnipke and Rice [27,28] presented a new finite element method for two-dimensional convection heat transfer. It was designed in particular to be competitive with finite difference methods in terms of storage requirements, solution times, and range of applicability.

The majority of finite element codes currently available is based on direct solution methods such as Gaussian elimination rather than a segregated solution approach, where the velocities and pressures are solved in a sequential manner rather than simultaneously. The use of direct solution methods requires a considerable increase in the amount of storage compared to segregated solution methods. In addition, for large two-dimensional problems and in particular for three-dimensional problems, direct solution methods require more solution time compared to iterative methods.

There are basically two reasons why researchers have been reluctant to use segregated solution methods. Firstly, the basic design of most finite element fluid mechanics codes closely follows earlier solid mechanics codes, where a direct solution is generally the optimum approach. The second reason involves the pressure solution techniques commonly used in finite element methods. Penalty methods require the use of simultaneous solution techniques, and the primitive variable formulation using mixed interpolation is not amenable to iterative solution methods.

The method used by Schnipke and Rice [27,28] included a

streamline upwind formulation for the advection terms of the governing equations, and equal interpolation for all variables. They were able to achieve the latter without any 'checkerboarding' of the pressure solutions by using the pressure equation developed by Prakash and Patankar [26]. Their method also used an iterative solution procedure which greatly reduces the computer execution times and storage requirements.

One of the examples they tested the method on, was thermally driven cavity flow. Even though a relatively coarse mesh was used, their results were found to be in excellent agreement with those published by De Vahl Davis [73] in his benchmark numerical solution of the same problem. Although the agreement at the lower Rayleigh numbers was within 5%, the error at the high Rayleigh numbers was 10%. This comparatively large error can be attributed to the coarse mesh, and also to the fact that the temperature difference across the cavity in this case, was large, causing steep gradients in some elements.

The authors concluded that their method was flexible in terms of geometry and boundary conditions, and it was able to solve difficult problems completely. The savings in computer time and storage allowed the formulation to be competitive with existing finite difference methods while maintaining the flexibility of finite elements.

2.5.2 Natural Convection In Other Examples

Using the primitive-variable formulation, Gartling and Nickell [8] investigated two free convection examples,

namely an annular receiver tube for a solar collector and an isothermal horizontal cylinder enclosed by a rectangular isothermal box at a lower temperature. In the case of the former example, they examined the effect the annular gap size had on convective losses from the receiver tube and found that their computations agreed well with the experimentally obtained correlation of Eckert and Drake [74]. They concluded that these losses were minimised by sizing the gap to produce a Rayleigh number less than 10^3.

The isotherm plot from the cylinder enclosed by the rectangular box was compared with the fringe pattern obtained experimentally by holographic interferometry. The plotted contour values were chosen to correspond with the temperature of the fringes, and the correlation between the two was found to be excellent.

Reddy [24] used the penalty function model to analyse the concentric cylindrical annulus problem. For $Ra=10^3$, the streamlines obtained from the annulus analysis compared well visually with those of Kuehn and Goldstein [75]; however, the isotherms showed some plume behaviour compared with the essentially conduction patterns obtained by the latter authors. For $Ra=4,7x10^4$, the streamlines obtained were somewhat different to those of Kuehn and Goldstein [75], although the vorticity centre compared very well.

However, the isostreams compared favourably to the study performed by Gartling and Nickell [8], who used the primitive-variable formulation with $Ra=4,1x10^4$. The

isotherms obtained by Reddy [24] have the same form as those of both Kuehn and Goldstein [75] and Gartling and Nickell [8], except that in the latter two studies, the corners were more rounded.

Ozoe et al [35] investigated natural convection between horizontal plates heated from below using the stream function-vorticity formulation. The average Nusselt number was extrapolated to zero element size, which they found to be necessary to obtain agreement with experimental data for the same problem. They, therefore, concluded from their computations for several element sizes, that extrapolation or the equivalent was essential to eliminate numerical error and thereby obtain reliable results, even with higher-order finite element formulations.

2.5.3 Transient Natural Convection

Miyauchi et al [36] investigated two-dimensional transient natural convection using the stream function-vorticity formulation of the governing equations. In order to suppress spatial disorder of the temperature distribution and to accelerate the time integration of the non-linear natural convection problem, the authors employed upwind weighting functions. For the time integration, they used the explicit Euler and two-step Lax-Wendroff methods.

The motivation behind their analysis was the need to investigate the problem of free convection around a horizontal hot cylinder in order to determine the maximum allowable operation temperature, and to design the heat removing equipment, of a large vacuum vessel under

construction at the time. They successfully applied their method to this problem, and also justified the method by comparing almost stationary solutions for the thermally-driven window cavity with those of the time independent solution of Reddy and Satake [23]. The agreement was found to be very good.

2.5.4 Forced Convection

Gartling and Nickell [8] also investigated forced convection in a circular tube for a Reynolds number of 685. The tube had a finite wall thickness with a heat flux applied at the outside tube radius. They compared their results with an integral technique reported by Yang [76]. The agreement was excellent except in the vicinity of the inlet. They attributed this discrepancy to the fact that Yang [76] neglected several axial diffusion and convection terms in the integral solution technique.

Another example presented by Schnipke and Rice [27,28] to validate the results computed by their new finite element method, was that of a heated cylinder in cross-flow. They found that, for Re=10, some conductive heating of the fluid approaching the cylinder occurred. However, for $Re=10^2$, the fluid maintained the free stream temperature until very near the surface of the cylinder. The higher Reynolds number also had a noticeably larger wake region.

They compared their results to an empirical relation quoted by Holman [5], and found them to be accurate to within 12% of the relation. The authors also tried to obtain results for a Reynolds number of $5x10^2$, but they

encountered convergence problems caused by vortex formation.

Dalman et al [29] modelled the fluid and heat transfer for a row of spheres in a cylindrical tube by investigating the flow past two spheres in a long tube. They employed the velocity-pressure formulation of the Navier-Stokes results, and obtained results for Reynolds numbers up to 200, with Prandtl numbers of 0.72 and 7.0, for a range of sphere sizes and sphere separations. These results showed that as the gap between the spheres decreased, the flow past the spheres was confined to a region close to the tube wall, and a circulatory region of flow appeared between the spheres. This eddy led to poor heat transfer in this region. An increase in Re did not improve the situation, as the eddy grew in size with a consequent decrease in heat transfer. This was explicable since the improvement in convective heat transfer was offset by the formation of the circulatory flow from which the heat could only diffuse away.

More recently, Chen et al [21] also reported the finite element solutions of forced convection over a staggered and in-line tube bank. Comparing their isotherm plots to those Schnipke and Rice [28] obtained for the single cylinder, it can be seen that the behaviour of the upper region of the upstream cylinder is similar to that of a single cylinder. As with their analysis of the flow problem, they concluded that, as the gap between the cylinders increased, the results resembled those of a single cylinder.

Gallagher [58] identified the need for the finite element calculation of the temperature distribution caused by the discharge of heated effluent into a lake. This type of example is of obvious importance to the power generation industry as it will enable predictions to be made, prior to construction, as to the effect a power plant will have on the surrounding area.

He observed that physical modelling was, at the time, viewed as the most appropriate method of obtaining data for environmental impact studies. The data obtained from these studies indicated that satisfactory results were given by gross analytical models, such as those which dealt with overall heat and energy balances. Thus, he concluded, more field measurements of physical data and of their correlation with analytical procedures were necessary before it could be determined whether the finite element method was of value for the full range of thermal pollution analyses. He postulated that the physical circumstances might be too uncertain to justify the related computational expense.

Loziuk et al [77] applied the primitive variable formulation of the finite element method to the governing equations of hydrothermal analysis for the steady-state analysis of two-dimensional temperature distributions in flowing bodies of water.

They tested their method on two examples, namely a simplified one-dimensional cooling pond, and a two-dimensional river study. In the former case, they compared their results to an exact solution and found the agreement

to be very good. The river study gave results which compared favourably with those of a laboratory study, and they were thus able to conclude that, although three-dimensional effects are important, the two-dimensional analysis offered a suitable alternative for the purposes of design i.e. the usefulness in design applications of the inclusion of the third dimension was limited, as it caused a significant increase in computational time.

2.5.5 Combined Convection

Many engineering applications for either pure forced or pure free convection have been presented in the preceding sections. However, neglecting the effect of the buoyancy force on forced convection heat transfer is possibly not justified when the velocity is small and the temperature difference between the surface and the ambient fluid is large. Thus the predictions of the local heat transfer rate in combined convection are of practical interest, as are the conditions under which the buoyancy force effects first become significant.

Wong et al [78] employed the finite element method based on the primitive variable formulation, and using mixed interpolation to investigate the problem of laminar combined convection from a hot isothermal sphere. The authors obtained numerical results over the entire surface of the sphere, including the zone beyond the seperation point.

They found that their computations compared favourably with those of Dennis and Walker [40], and were also in

good agreement with those presented by Donea et al [79], who used the finite element method to analyse pure forced convection.

Chen et al [22] studied the flow and heat transfer characteristics of laminar combined convection from two isothermal spheres of the same diameter in tandem arrangement, the distance between the sphere centres being twice the value of the diameter. Their results for gases with a Prandtl number of 0.7 showed that the parameter Gr/Re^2 had a marked effect on the surface shear stress and average Nusselt number, especially for the downstream sphere. The behaviour of the upstream sphere was close to that of a single sphere.

2.6 SYNOPSIS

The literature of the finite element analysis of steady-state two-dimensional fluid flow and convection heat transfer for parameters in the ranges,

$$10^{-2} \leqslant Re \leqslant 10^{4}$$
$$10^{3} \leqslant Ra \leqslant 10^{6}$$

is now fairly extensive, and current research in this field is primarily concerned with applying one of the established procedures to practical situations.

Apart from assuming the flow or convection to be steady-state and two-dimensional, most authors up till now have

further assumed the fluid to be incompressible and linearly viscous, and the buoyancy forces to be sufficiently accurately described by the Boussinesq approximation. Another assumption generally used, is that the dissipation due to the viscous forces in the momentum equations does not contribute significantly to the energy transport equation.

Researchers use one of three finite element formulations to analyse the convection heat transfer (or fluid flow) boundary value problem. For the primitive variable formulation, the discretised equations governing the problem are obtained directly in terms of the velocities, temperature and pressure from the equations of conservation of mass, momentum and energy.

The stream function-vorticity formulation satisfies the equation of mass conservation identically by the introduction of the stream function. Also, the pressure is eliminated from the momentum equations by appropriate differentiation and subtraction. By introducing the vorticity function, the flow problem can be described in terms of two variables only, namely the stream and vorticity functions. For the stream function formulation, the vorticity function is eliminated from the stream function-vorticity formulation, which results in a fourth order equation in terms of stream function alone.

The number of variables in the stream function formulation is the least, which may be considered advantageous. However, this reduction in variables is achieved by admitting higher order derivatives in the system

equations. Higher order derivatives are undesirable as the continuity requirement of the variables between elements is stringent and difficult to satisfy, and the accuracy of the velocities will generally be reduced due to differentiations of an appropriate field of the stream function. Furthermore, this formulation necessitates the definition of complicated boundary conditions.

The stream function-vorticity formulation also produces less accurate velocities since they, too, are derived from the stream function. The main disadvantage of this formulation, however, is that the no-slip boundary conditions need to be dealt with iteratively.

The primitive variable formulation is advantageous because it represents the variables of most interest, it is directly applicable to three-dimensional problems, and it is the most convenient formulation for defining appropriate boundary conditions. The major drawback of this formulation is that the incorporation of the continuity equation into the discretised equations gives rise to some zero elements along the diagonals of the system matrix.

Most authors who used the primitive variable formulation encountered two main difficulties, namely (1) spurious pressure distributions, or 'checkerboarding', and (2) non-convergence of their solutions at Rayleigh numbers greater than 10^6, and Reynolds numbers greater than 10^4.

The system matrix is not positive definite, and thus the eigenvalues of the matrix are both positive and negative.

Experience has shown that, for the incompressible case, certain combinations of orders of interpolation cause so-called spurious zero eigenvalues. These are referred to as pressure modes.

Equal-order interpolation generally creates these pressure modes, but they can occur in other elements as well. It is not always obvious when such singularities can occur in an element. This situation, also known as 'checkerboarding', results in a square mesh when an even number of those elements displaying a pressure mode, is used along each side.

The 'checkerboard' mode has been effectively removed when the penalty formulation has been employed, or when the pressure variable has been interpolated using bi-linear shape functions instead of the bi-quadratic shape functions used for the velocity variables.

Most authors attributed the non-convergence of their solutions at high Rayleigh and Reynolds numbers to ill-conditioning of the equations, which is caused by the very large parameters (including the Rayleigh and Reynolds numbers) which exist under these conditions i.e. the convection terms of the governing equations are much larger than the diffusion terms, and thus the equations are no longer diagonally dominant. For this reason, standard relaxation methods cannot be used in solving the system of equations. This numerical difficulty can be overcome by employing upwind differences to approximate the convection terms.

According to Heinrich et al [80], the procedure, in essence, applies the finite element method using weighting functions of non-symmetric forms different from those originally used as shape functions. By suitable choice of such functions, stability can be established, although some accuracy loss that is inherent in the finite differences, occurs. The loss in accuracy can, however, be minimised by varying the necessary upwinding from element to element.

It can now be considered standard that using either the primitive variable formulation with mixed interpolation or the stream function-vorticity formulation, for Rayleigh numbers less than 10^6 and Reynolds numbers less than 10^4, will produce a stable solution.

Apart from utilising available methods to investigate practical examples, research is currently being conducted into problems such as turbulent flow, and transient and three-dimensional flow and convection, as the knowledge in these areas is far from complete.

CHAPTER 3

FORMULATION OF THE GOVERNING EQUATIONS OF CONVECTION HEAT TRANSFER

3.1 INTRODUCTION

The present analysis encompasses the convection transfer of thermal energy in regions containing both a moving fluid and a solid body, the solid body forming the boundary of the fluid region. Within this very general class of problems, a number of assumptions and restrictions are made during the course of this chapter to facilitate the ease of solution of the problem.

The primitive-variable analysis requires the development of three different sets of equations to solve for the unknowns, namely the velocities, the pressure and the temperature. The equations governing the motion of a viscous incompressible fluid are known as the Navier-Stokes equations. The condition of fluid incompressibility is enforced through a further equation known as the continuity equation, or equation of mass conservation.

Making a further assumption that the body forces acting on the fluid are not dependent on temperature, the previous two sets of equations can be used to evaluate the flow of any Newtonian incompressible fluid. Due to the existence

of a temperature difference across the fluid, a further variable, namely temperature, is introduced. For this reason, another equation, the heat conduction equation, is required, and the Boussinesq approximation is employed to introduce temperature into the Navier-Stokes equations.

The Navier-Stokes and the continuity equations, and the heat conduction equation will be dealt with separately. The development of both of these sets of equations will be sub-divided into two sections. Firstly, the equations will be normalized to facilitate generalisation, and then the variational, or weak, boundary-value formulations will be derived for use in the finite element method.

The application of boundary conditions, which is of particular importance when the order of the differential equations is reduced by developing the variational boundary-value problem, together with the introduction of initial conditions, will also be outlined in this chapter.

3.2 THE NAVIER-STOKES FLUID FLOW EQUATIONS AND THE CONTINUITY EQUATION

Fluid motion in nature is three-dimensional and, for an incompressible Newtonian fluid, can be described by the Navier-Stokes equations of motion, Lai et al [1],

$$\rho(du_i/dt) + \rho u_j (du_i/dx_j) = \rho B - dP/dx_i + \mu(d^2 u_i/dx_j dx_j) \qquad (3.1)$$

where ρ = density (constant, for an incompressible fluid),

μ = viscosity (constant),

B = body force,

u_i = velocities u,v,w (variables),

P = pressure (variable),

d = partial derivative (throughout this study).

The above set of equations can be divided into five distinct terms, namely (1) the time-dependent term, $\rho(du_i/dt)$, (2) the convective term, $\rho u_j (du_i/dx_j)$, (3) the body force term, ρB, (4) the pressure term, $-dP/dx_i$, and finally, (5) the diffusive term, $\mu(d^2 u_i/dx_j dx_j)$. Unlike the diffusive term, the convective term is non-linear, and for this reason, the stiffness matrix (formed in the following chapter) is non-symmetric. This, in turn, enforces the use of an iterative procedure to solve the overall matrix equation.

As can be seen in the above equations, there are four unknowns, namely u, v, w and P, and only three equations. The fourth equation is supplied by the continuity (conservation of mass) equation,

$$(du_i/dx_i) = 0 \qquad (3.2)$$

As was mentioned in chapter 1, the geometry of the fluid/solid region in this analysis will be confined to two dimensions (either plane or axisymmetric), although

the shape of the boundary is arbitrary. To simplify the derivation of the equations in the following sections, only the case of plane two-dimensional flow will be treated in detail. The derivation of the axisymmetric form of the equations follows in a straightforward manner. Thus the three variables of the two-dimensional (x,y) cartesian system are the velocities, u and v, and the pressure, P.

Under the standard assumption of convection heat transfer (i.e. the Boussinesq approximation is valid, see Chandrasekhar [81]), and further assuming steady flow, the Navier-Stokes equations (3.1) become (in the absence of all body forces except the gravity vector) :

$$u_j \, (du_i / dx_j) = -1/\rho \, (dP/dx_i) - \beta \, (T-T_0) \, g_i \delta_{i2} + \nu \, (d^2 u_i / dx_j \, dx_j) \qquad (3.3)$$

where β = coefficient of thermal expansion (constant),
T = temperature (variable),
T_0 = temperature (constant),
ν = kinematic viscosity.

It will be noted that a fourth variable, that of temperature, T, has been introduced. For this reason, a further equation is required and, for this purpose, the heat conduction equation, which describes the transport of thermal energy in a fluid, is employed (see section 3.3).

The gravity vector, $\underset{\sim}{g}$, consists of the acceleration due to gravity in the given coordinate system; in this case, the (x,y) plane. Assuming the positive y-direction corresponds

to the upward vertical, the gravitational acceleration in the x-direction, $g_x = 0.0$ m/s, and in the y-direction, $g_y = -g = -9.81$ m/s^2 .

It is convenient to write the generalised equations in a non-dimensional form to enable the investigation of a large range of problems. In this respect, the following dimensionless variables are introduced,

$$x_i^* = x_i / L \; ; \; u_i^* = u_i / u_0 \; ; \; P^* = P/\rho u_0^2 \; ; \; g_i^* = g_i / g_0$$

where L is a characteristic length,
u_0 is a datum velocity,
g_0 is a datum gravity force.

Incorporating these into the set of equations (3.3) by multiplying throughout by L/u_0^2 results in the following,

$$u_j^* (du_i^*/dx_j^*) = -(dP^*/dx_i^*) - (\beta g_0 L/u_0^2)(T-T_0) g_i^* \delta_{i2} + (\vartheta/u_0 L)(d^2 u_i^*/dx_j^* dx_j^*) \qquad (3.4)$$

At this juncture, it is necessary to introduce four well-known fluid and heat transfer constants, namely the Reynolds number, the Prandtl number, the Grashof number, and the Rayleigh number.

The Reynolds number is a fundamental characteristic of fluid flow, which may be used in situations where the inertia and the viscous forces are most significant, as it is proportional to the magnitude ratio between these two forces acting on any particle in the continuum. It is

defined as,

$$Re = \rho L u_0 / \mu = L u_0 / \nu$$

It must be remembered that the Reynolds number concerns only the forces due to viscosity and inertia, and thus, when forces arising from other causes (e.g. gravity or fluid compressibility) play an important part in the flow, its general character may be determined by other criteria.

The Prandtl number, Pr, has been found to be the parameter which relates the relative thicknesses of the hydrodynamic and the thermal boundary layers. It can be defined as the ratio between the kinematic viscosity, ν and the thermal diffusivity, α of a fluid, i.e.

$$Pr = \nu/\alpha$$

The kinematic viscosity of a fluid conveys information about the rate at which momentum may diffuse through the fluid as a result of molecular motion. The thermal diffusivity is a measure of the diffusion of heat in the fluid. Thus the ratio of these two quantities expresses the relative magnitudes of diffusion of momentum and heat in the fluid.

But these diffusion rates are precisely the quantities that determine the thickness of the boundary layer for a given external flow field; large diffusivities imply that the viscous or temperature influence is felt farther out in the field. The Prandtl number is thus the connecting link between the velocity and the temperature field.

Physically, the Grashof number, Gr, may be interpreted as a dimensionless group representing the ratio of the buoyancy forces to the viscous forces in the free convection flow system. It has a role similar to that accomplished by the Reynolds number in forced convection systems and is the primary variable used as a criterion for transition from laminar to turbulent boundary-layer flow. The definition of the Grashof number is as follows,

$$Gr = g_0 \beta (T_1 - T_0) L^3 / \nu^2$$

where T_1 and T_0 are reference temperatures.

The final dimensionless group to be introduced is the Rayleigh number, Ra, which is defined as the product of the Grashof and Prandtl numbers, i.e.

$$Ra = GrPr = g_0 \beta (T_1 - T_0) L^3 / \nu \alpha$$

Thus the Rayleigh number represents the ratio between the buoyancy forces and the product of the viscous forces and the thermal diffusivity of the fluid.

Substituting the Reynolds and Rayleigh numbers into the dimensionless Navier-Stokes equations (3.4),

$$u_j^* (du_i^* / dx_j^*) = -(dP^* / dx_i^*) + 1/Re (d^2 u_i^* / dx_j^* dx_j^*) - Ra (T - T_0) / (T_1 - T_0) g_i^* \delta_{i2} \qquad (3.5)$$

Since the gravity term is merely a function of temperature, these equations can be simplified further by

introducing,

$$\theta^* = f(T) = (T - T_0)/(T_1 - T_0) \qquad (3.6)$$

which, as can be seen, is dimensionless.

Thus the final dimensionless form of the Navier-Stokes equations of motion is as follows, having substituted equation (3.6) into equation (3.5),

$$u_j^* (du_i^*/dx_j^*) + (dP^*/dx_i^*) - 1/Re\,(d^2 u_i^*/dx_j^* dx_j^*)$$

$$= - Ra\theta^* g_i^* \delta_{i2} \qquad (3.7)$$

The corresponding dimensionless continuity equation is,

$$(du_i^*/dx_i^*) = 0 \qquad (3.8)$$

For convenience of presentation, the asterisk is omitted from the above equations such that from this point onwards the quantities in equations (3.7) and (3.8) are assumed to be dimensionless even when no asterisk is present.

The above equations can also be written in invariant form as follows,

Navier-Stokes equations of motion :

$$(\nabla \underline{u})\,\underline{u} + \nabla P - 1/Re\,(\nabla^2 \underline{u}) = -Ra\theta \underline{g} \qquad (3.9)$$

continuity equation :

$$\text{div } \underline{u} = 0 \qquad (3.10)$$

3.3 THE HEAT CONDUCTION EQUATION

The equation which governs the energy transfer occurring between material bodies as a result of a temperature difference, is the heat conduction or conservation of energy equation,

$$dT/dt + u_j\,(dT/dx_j) = \alpha(d^2T/dx_j\,dx_j) + Q \qquad (3.11)$$

where T = temperature (variable),

u_j = velocities u,v (variables),

α = thermal diffusivity (constant),

Q = energy source.

It should be noted that, since only the derivatives of temperature occur in equation (3.11), the temperature variables T and θ can be interchanged without losing generality or changing the form of the energy equation.

The above equation is similar to the Navier-Stokes equations in that it contains (1) a time-dependent term, dT/dt, (2) a non-linear convective term, $u_j\,dT/dx_j$, and (3) a linear diffusive term, $\alpha(d^2T/dx_j\,dx_j)$. The heat source term, Q, can be compared to the body force term of the equations of motion.

As in section 3.2, the heat conduction equation is normalised by introducing a set of dimensionless

variables, namely,

$$\theta^* = (T - T_0)/(T_1 - T_0) \; ; \; u_i^* = u_i/u_0 \; ; \; x_i^* = x_i/L \; ;$$
$$Q^* = QL^2/\nu\theta_0 \; ;$$

where L is a characteristic length,

u_0 is a datum velocity,

θ_0 is a reference temperature.

Assuming steady-state conduction, incorporating these variables into equation (3.11), and multiplying throughout by $(L^2/\nu\theta_0)$, results in the following equation,

$$(Lu_0/\nu)(u_j^* \, d\theta^*/dx_j^*) = (\alpha/\nu)(d^2\theta^*/dx_j^* dx_j^*) + Q^* \qquad (3.12)$$

Once again, the dimensionless group, (Lu_0/ν) has occurred. As defined in the previous section, this is known as the Reynolds number, Re. Also, the dimensionless group, (ν/α), was defined as the Prandtl number, Pr. Utilizing both these numbers, equation (3.12) can be simplified to read,

$$Re\,(u_j^* \, d\theta^*/dx_j^*) = 1/Pr\,(d^2\theta^*/dx_j^* dx_j^*) + Q^* \qquad (3.13)$$

As indicated for the Navier-Stokes and continuity equations, the asterisk for the above equation will also be omitted from this point onwards, such that the quantities in equation (3.13) are assumed to be dimensionless even when no asterisk is present.

Equation (3.13) can also be written in invariant form as,

$$Re\,(\nabla\theta)\,\underline{u} - 1/Pr\,(\nabla^2\theta) = Q \qquad (3.14)$$

3.4 METHOD OF WEIGHTED RESIDUALS

Having defined the governing equations, the method chosen for solution depends largely on the physical problem being analysed. If the convection domain and boundary conditions are well posed then an analytical solution could well be possible. However, for the majority of convection problems of practical interest, the convection domain is geometrically complex and recourse has to be made to an approximate method which may then be amenable to direct analysis. The approximate method employed for this study is the method of weighted residuals which has been used extensively in the fields of fluid mechanics and convection heat transfer.

Weighted residual methods are numerical techniques which can be used to solve a single or set of partial differential equations. For a set, say representative of equations (3.9), (3.10) and (3.14),

$$L(\mathbf{u}) = (F) \qquad (3.15)$$

in the domain, Ω (see fig. 3.1), where **u** is the exact solution and may represent a single variable or a column vector of variables. Two possible types of boundary conditions exist, namely,

(1) essential (Dirichlet) : $G(\mathbf{u}) = u_0$ on Γ_{u0},
where the value of the variable is prescribed, and

(2) natural (Neumann) : $S(\mathbf{u}) = q$ on Γ_q,
where at least the first order gradient in the

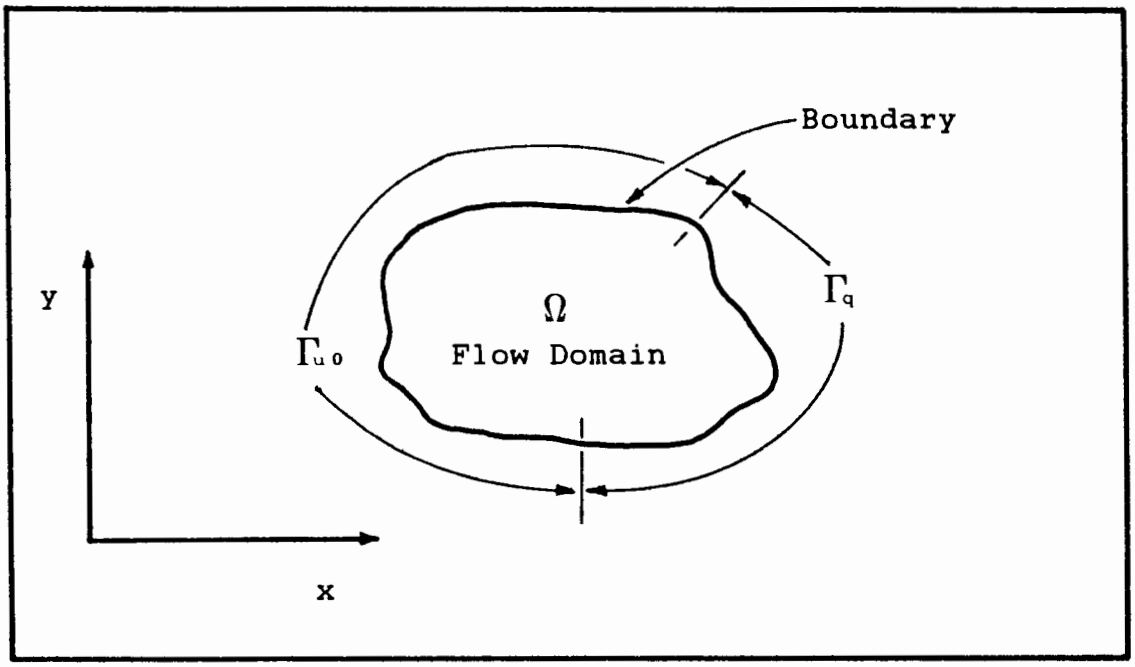

Fig. 3.1 FLOW DOMAIN AND BOUNDARY TYPE

variable is prescribed.

The relevance and full explanation of each type of boundary condition will become apparent when considering the governing equations of convection in section 3.6. The initial step in the application of the weighted residual procedure is to assume that u can be approximated over the whole domain by,

$$u = \sum_{1}^{n} a_i b_i \qquad (3.16)$$

where $\underline{a}$ are functions described in terms of independent variables, such as spatial coordinates (x,y), and $\underline{b}$ are undetermined parameters.

Using this approximation and combining (3.15) and (3.16) results in an error or residual, **E**, such that

$$\mathbf{E} = L(\hat{u}) - (F) \neq 0 \qquad (3.17)$$

where **E** is exactly zero when $\hat{u} = u$ i.e. an exact solution is possible.

In order to make **E** identically zero, a set of weighting functions, W, are employed such that over the whole domain, Ω,

$$\int_{\Omega} W\mathbf{E}\, d\Omega = 0 \qquad (3.18)$$

If the number of unknown parameters is **s**, and there are **s** linearly independent weighting functions, equation (3.18) can be rewritten as,

$$\int_{\Omega} W_k \mathbf{E}\, d\Omega = \int_{\Omega} W_k [L(u) - (F)]\, d\Omega = 0 \quad k = 1,2,3\ldots\mathbf{s} \qquad (3.19)$$

The only limitations placed on W_k at this stage, are that it must be positive, single-valued, and finite. The Galerkin weighted residual method utilises the above concepts to transform the differential equations into a form where finite element techniques can be effectively adopted.

3.5 THE GALERKIN WEIGHTED RESIDUAL METHOD

Refining the concept of defining approximated values of the required variable via a direct summation (see equation (3.16)), and subdividing the domain into elements (see fig. 3.2), the variable value within that subregion can now be defined in terms of discrete values on the boundary of or within that region,

$$u = \sum_{1}^{n} (N_i b_i)$$

where $\underline{N}$ are a set of trial functions written in terms of the local coordinates with n discrete values within or on

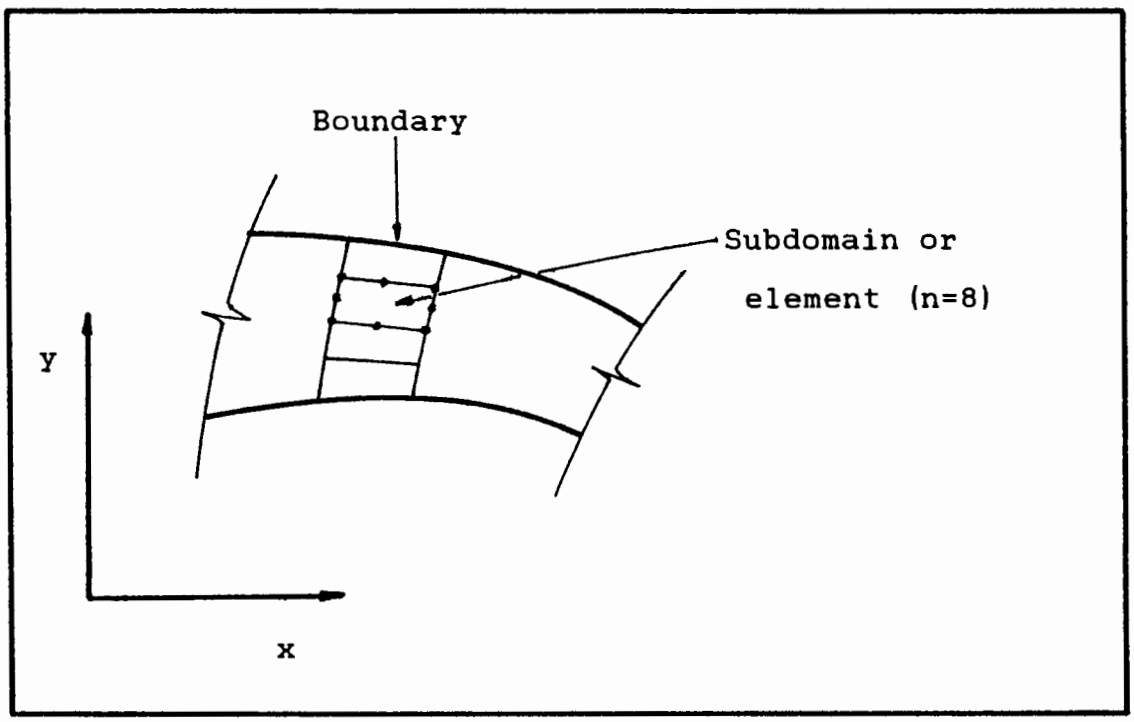

Fig 3.2 DEFINITION OF A SUBDOMAIN OR ELEMENT

the boundary of an element, and $\underline{b}$ are undetermined parameters. Each element will, normally, possess a unique set of equations and $\underline{b}$ are now confined to each element.

The residual now becomes,

$$\mathbf{E} = L\left(\sum_{1}^{n} (N_i\, b_i)\right) - (F) \qquad (3.21)$$

Substituting equation (3.21) into equation (3.19), and noting that, in the Galerkin method, the same approximating functions are used for the weighting and trial functions, i.e. $W_k = N_k$, results in the following generalised equation,

$$\int_{\Omega} N_k \left[L\left(\sum_{1}^{n} N_i\, b_i\right) - (F)\right] d\Omega = 0 \qquad (3.22)$$

where orthogonalisation has been effected with the same functions.

3.6 VARIATIONAL FORMULATION OF THE NAVIER-STOKES AND CONTINUITY EQUATIONS

To convert the normalized Navier-Stokes fluid flow equations (3.9), to the variational formulation, both sides of the equations are multiplied by an arbitrary

function, $\underline{u}'$, and integrating over the whole domain, Ω, results in the following,

$$\int_{\Omega} \left((\nabla \underline{u})\,\underline{u} - 1/Re\,(\nabla^2 \underline{u}) + \nabla P \right) . \underline{u}'\ d\Omega = -Ra \int_{\Omega} \theta \underset{\sim}{g} . \underline{u}'\ d\Omega \qquad (3.23)$$

Invoking Green's theorem, the diffusion term of the above equations can be reduced to,

$$1/Re \int_{\Omega} (\nabla^2 \underline{u})\,\underline{u}'\ d\Omega = 1/Re \int_{\Gamma} \underline{u}' . d\underline{u}/dn\ d\Gamma - 1/Re \int_{\Omega} \nabla \underline{u} . \nabla \underline{u}'\ d\Omega$$

(3.24)

where Γ represents the complete boundary.

The boundary integral of equations (3.24) can be rewritten as,

$$1/Re \int_{\Gamma} \underline{u}' . d\underline{u}/dn\ d\Gamma = 1/Re \int_{\Gamma_q} \underline{u}' . d\underline{u}/dn\ d\Gamma + 1/Re \int_{\Gamma_u} \underline{u}' . d\underline{u}/dn\ d\Gamma$$

(3.25)

In the above equations,

$$d\underline{u}/dn \equiv l_x\, d\underline{u}/dx + l_y\, d\underline{u}/dy \qquad (3.26)$$

where l_x and l_y are components of the unit outward normal

vector at the boundary.

The boundary integral terms, as shown in equations (3.25), require some explanation before proceeding with the development of the variational formulation of equations (3.24). The physical significance of $d\underline{u}/dn$ can be interpreted as an outward flux. On common faces between two elements, the nett flux will, if the distribution of $\underline{u}$ is correct, be zero. Therefore, for elements within the domain under consideration, the nett effect of the boundary integral term in equations (3.25) is zero and can effectively be ignored. On that part of the boundary where the values of $\underline{u}$ are defined,

$$\underline{u} = \tilde{\underline{u}}$$

then the second term in equations (3.25), namely the term integrated over the boundary $\Gamma_{\underline{u}}$, disappears from the variational formulation, and the prescribed values are set prior to the solution.

Therefore, without loss of generality, equations (3.24) become,

$$1/Re \int_{\Omega} (\nabla^2 \underline{u}) . \underline{u}' \, d\Omega = 1/Re \int_{\Gamma_q} \underline{u}' d\underline{u}/dn \, d\Gamma - 1/Re \int_{\Omega} (\nabla \underline{u} . \nabla \underline{u}') \, d\Omega \qquad (3.27)$$

Substituting equation (3.27) into equation (3.23) results in the following,

$$\int_\Omega ((\nabla \underline{u})\,\underline{u}).\underline{u}'\ d\Omega + 1/Re \int_\Omega \nabla \underline{u}.\nabla \underline{u}'\ d\Omega + \int_\Omega \underline{u}'\nabla P\ d\Omega$$

$$= -Ra \int_\Omega \theta \underline{u}'.\underline{g}\ d\Omega + 1/Re \int_{\Gamma_q} \underline{u}'.d\underline{u}/dn\ d\Gamma \qquad (3.28)$$

which are the variational, or weak, formulations of the Navier-Stokes equations of motion. Note that the boundary integral is only retained on boundaries where a flux type boundary condition is imposed.

Applying the same method to the continuity equation (3.10), both sides of the equation are multiplied by the arbitrary function $\underline{u}'$, and integrating over the domain, Ω, gives,

$$\int_\Omega u'(\text{div } \underline{u})\ d\Omega = 0 \qquad (3.29)$$

which is the variational formulation of the continuity equation.

3.7 VARIATIONAL FORMULATIONAL OF THE HEAT CONDUCTION EQUATION

The development of the dimensionless heat conduction

equation (3.14), to the variational formulation, is similar to that of the Navier-Stokes equations. Both sides of the equation are multiplied by an arbitrary function θ', and integrated over the whole domain. Equation (3.14) becomes,

$$\int_{\Omega} (Re\,(\nabla\theta)\,\underline{u} - 1/Pr\,(\nabla^2\theta))\,.\,\theta'\;d\Omega = \int_{\Omega} Q.\theta'\;d\Omega \qquad (3.30)$$

Once again, using Green's theorem, the diffusion term can be reduced as follows,

$$-1/Pr\int_{\Omega}(\nabla^2\theta)\,\theta'\;d\Omega = -1/Pr\int_{\Gamma_q}\theta'\,d\theta/dn\;d\Gamma + \int_{\Omega}\nabla\theta.\nabla\theta'\;d\Omega \qquad (3.31)$$

where Γ_q are the boundaries where a flux type boundary condition is imposed.

Substituting equation (3.31) into equation (3.30) results in the variational formulation of the heat conduction equation,

$$\int_{\Omega}(Re\,(\nabla\theta)\,\underline{u})\,.\,\theta'\;d\Omega + 1/Pr\int_{\Omega}\nabla\theta.\nabla\theta'\;d\Omega$$

$$= \int_{\Omega} Q.\theta' \, d\Omega + 1/Pr \int_{\Gamma_q} \theta' d\theta/dn \, d\Gamma \qquad (3.32)$$

In the following chapter, the variational formulations of the governing equations of convective heat transfer derived above, will be used to develop their finite element formulations for use in the computer code.

CHAPTER 4

FINITE ELEMENT FORMULATION

4.1 INTRODUCTION

This chapter concerns the finite element modelling based on the variational formulation of the governing equations as derived previously. A large number of texts are available which deal with the theory and application of the finite element method. Those found to be most useful were written by Hinton and Owen [45,46], and Dhatt and Touzot [47].

The basic concepts, with specific reference to the convection heat transfer problem investigated in this analysis, are presented in a summarized form in the following section. Explanations regarding the finite element mesh, nodal points, basis functions, element mapping and isoparametric representations, and numerical integration are included therein.

The finite element formulations of the governing equations' weak formulations are developed and these are then implemented in the FORTRAN program to solve the various numerical examples.

4.2 BASIC CONCEPTS

4.2.1 The Finite Element Method Applied To Second Order Boundary-Value Problems

For a second order variational boundary-value problem of the form,

$$B(u,v) = l(v) \quad , \quad \text{for all } u,v \in V \tag{4.1}$$

the space of admissible functions V consists of all those functions which satisfy the essential boundary conditions.

The above equations may be solved, using a Galerkin approximation u_h , by constructing a finite-dimensional subspace V_h of V, which is spanned by a finite number of basis functions, Φ_i . The problem is then transformed into solving for $u_h \in V_h$ which satisfies,

$$B(u_h, v_h) = l(v_h) \quad , \quad \text{for all } u_h, v_h \in V \ . \tag{4.2}$$

4.2.2 The Finite Element Mesh

In order to represent a domain, Ω, using finite element techniques, a mesh of subdomains Ω^e is constructed. These subdomains, termed finite elements are non-overlapping and cover Ω. In the one-dimensional sense, this subdivision of the domain simply amounts to partitioning an interval into line elements, connected at nodal points located at their ends. However, for the two-dimensional (and three-dimensional) case, the discretization of Ω is less obvious

as the basic shape of the elements has first to be established. It is further assumed, in this case, that the domain is polygonal, and that every side of the boundary of an element is either part of the boundary Γ, or it is an entire side of another element.

The first concern in the two-dimensional case is to choose a discretization that will be general enough to model irregular domains but consist of elements simple enough to minimize computational effort. Simple triangles and/or quadrilaterals are commonly used for this purpose. If Ω is curved, there will obviously be some discretization error, since the finite element mesh, Ω° will not exactly coincide with the domain, Ω.

4.2.3 Nodal Points

At this stage, it is necessary to identify certain points called nodes or nodal points in the subdivided two-dimensional domain. (They have already been mentioned above in connection with the one-dimensional situation.) Nodes are allocated at least at the vertices of elements, but in order to improve the approximation, further nodes may be introduced, for example, at the midpoints of the sides of elements. The typical element used in this analysis is the eight-noded quadrilateral, with nodes at the corners and the midpoints of the sides.

4.2.4 Basis Functions

Another reason for considering elements of simple shapes is that there is a natural correspondence between the

number and location of nodal points in an element and the number of terms used in the local polynomial expression.

For example, for piecewise approximations in two dimensions, a bilinear function,

$$v_h(x,y) = a_1 + a_2 x + a_3 y + a_4 xy$$

has four constants, and thus four independent values of v_h must be specified to determine these constants. This implies that the element should have four nodes, suggesting a quadrilateral with a node at each corner.

Remembering that the Galerkin approximation of the second order boundary-value problem required solving equations (4.2) for u_h ,it should now be noted that both u_h and v_h must be linear combinations of the basis functions of V_h . They can thus be described by,

$$u_h(\underline{x}) = \sum_{1}^{N} a_i \Phi_i(\underline{x}) \quad ; \quad v_h(\underline{x}) = \sum_{1}^{N} b_j \Phi_j(\underline{x}), \text{ for } \underline{x} \in \Omega_h \qquad (4.3)$$

where $\phi_i(\underline{x})$ are basis functions defined over the domain and satisfying,

$$\Phi_i(x_j, y_j) = \begin{cases} 1 & \text{if } i = j \\ 0 & \text{otherwise} \end{cases} \qquad (4.4)$$

and (x_j, y_j) are the coordinates of nodal points in the finite element mesh. When equation (4.4) holds, equations (4.3) are,

$$u_h(x_j, y_j) = u_j \;;\; v_h(x_j, y_j) = v_j \quad , \quad j = 1,2,....N \qquad (4.5)$$

so that by setting $u_j = u(x_j, y_j)$ and $v_j = v(x_j, y_j)$, u_h and v_h will coincide with (and therefore interpolate) the given function at the nodes.

Since v_h in equation (4.3) is arbitrary, so are the coefficients b_k. The fact that $B(u_h, v_h)$ is bilinear and $l(v_h)$ is linear allows equations (4.2) to be rewritten as,

$$\sum_{i=1}^{N} \sum_{j=1}^{N} B(\Phi_i, \Phi_j)\, a_i\, b_j = \sum_{j=1}^{N} l(\Phi_j)\, b_j \qquad (4.6)$$

or more concisely,

$$\sum_{j=1}^{N} b_j \left(\sum_{i=1}^{N} K_{ij}\, a_i - F_j \right) = 0 \qquad (4.7)$$

where $K_{ij} = B(\Phi_i, \Phi_j)$ and $F_j = l(\Phi_j)$.

It is assumed that $N_i^{\bullet}$ is the restriction of Φ_i to Ω. i.e.

$$\Phi_i \Big|_{\Omega^{\bullet}} = N_i^{\bullet} \qquad (4.8)$$

From equations (4.4), it is clear that this function $N_i^{\bullet}$ defined on an element e will have the property that,

$$N_i^{\bullet}(x_j, y_j) = \begin{cases} 1 & \text{if } i = j \\ 0 & \text{otherwise} \end{cases} \qquad (4.9)$$

The construction of local element shape functions $N_i^{\bullet}$, defined over each element $\Omega_{\bullet}$ in the mesh, must be such that when patched together as indicated previously, they produce basis functions satisfying equation (4.6).

From (4.7), the stiffness matrix, K_{ij} can thus be written as,

$$K_{ij} \equiv B(\Phi_i, \Phi_j) = \sum_{e=1}^{E} B^{\bullet}(\Phi_i, \Phi_j) = \sum_{e=1}^{E} \underbrace{B^{\bullet}(N_i^{\bullet}, N_j^{\bullet})}_{K_{ij}^{\bullet}} \qquad (4.10)$$

and the load vector, F_j can be expressed as,

$$F_j \equiv l(\Phi_j) = \sum_{1}^{E} l^{\bullet}(\Phi_j) = \sum_{1}^{E} \underbrace{l^{\bullet}(N_j^{\bullet})}_{F_j^{\bullet}} \qquad (4.11)$$

The fact that $B(\Phi_i, \Phi_j)$ is of the integral form enables the above two equalities to be written as a sum of integrals over each element. Thus the evaluation of K_{ij} and F_j reduces to the evaluation of a series of matrices $K_{ij}^{\bullet}$ and vectors $F_j^{\bullet}$ for each element, and then involves the summing of these contributions over all the elements in the domain.

4.2.5 Element Mapping And Isoparametric Representations

The key concept in the finite element approach of this text is the notion of a master element. It is clear that the calculation of element stiffness matrices and load vectors for a curvilinear element Ω_e, such as illustrated in fig. 4.1, would be awkward if performed directly in terms of the (x,y) coordinates shown. Also, the character of such calculations (e.g. the limits of integration) would change from element to element in the mesh.

However, if an invertible transformation is used between a master element Ω' of a simple shape and an arbitrary element Ω_e, it should be possible to transform the

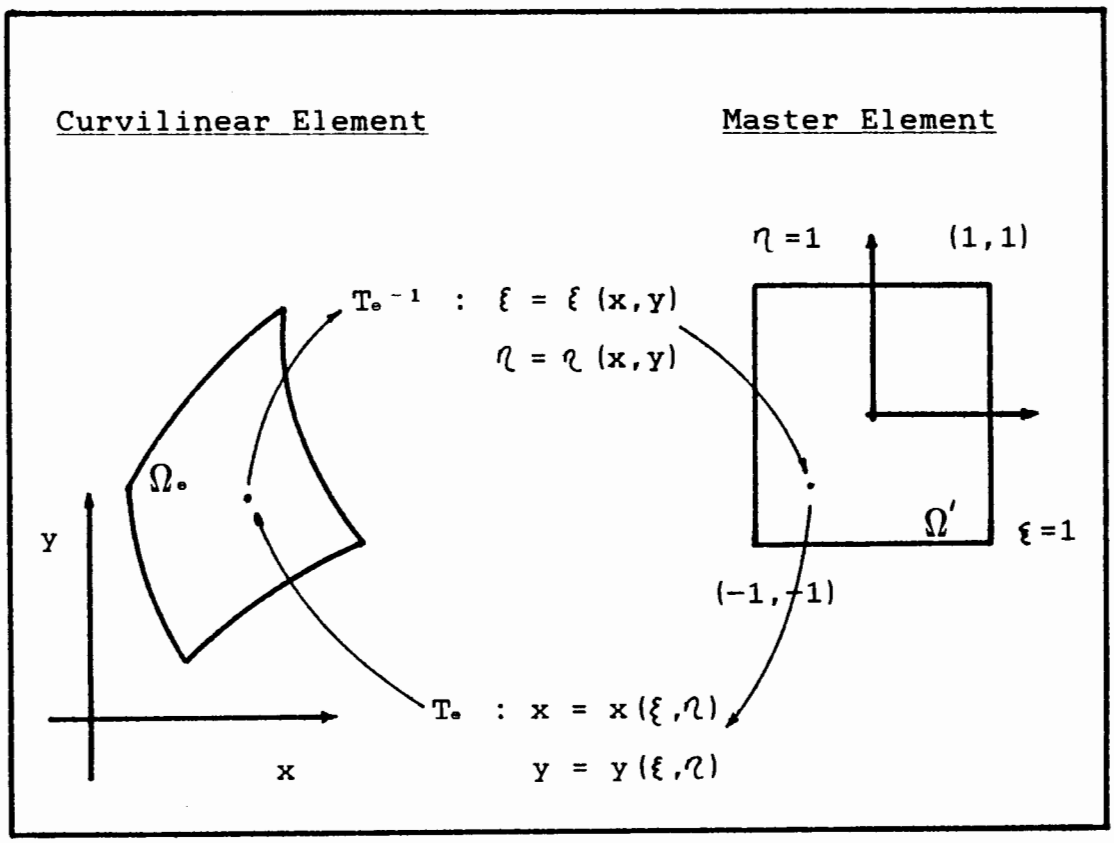

Fig. 4.1 CURVILINEAR ELEMENT MAPPED ONTO MASTER ELEMENT

operations on Ω_e so that they hold on Ω'. Then the calculations can be conveniently performed on the master element. This transformation is accomplished by a simple mapping of points into each element in the mesh.

The two-dimensional master element shown in fig. 4.1 has local coordinates ξ and η, where

$$-1 \leq \xi \leq 1 \quad \text{and,}$$
$$-1 \leq \eta \leq 1 \ .$$

The mapping T_e which maps Ω' onto Ω_e, is defined as being,

$$T_e : \quad x = x(\xi,\eta) \qquad (4.12)$$
$$y = y(\xi,\eta)$$

Using this mapping, all the properties of a given type of finite element can be prescribed for the master element and then carried to any element in the mesh.

The functions x and y are considered to be continuously differentiable with respect to ξ and η. Thus the infinitesimals $d\xi$ and $d\eta$ transform into dx and dy according to, in matrix form,

$$\begin{bmatrix} dx \\ dy \end{bmatrix} = \begin{bmatrix} dx/d\xi & dx/d\eta \\ dy/d\xi & dy/d\eta \end{bmatrix} \begin{bmatrix} d\xi \\ d\eta \end{bmatrix} = [J] \begin{bmatrix} d\xi \\ d\eta \end{bmatrix} \qquad (4.13)$$

The 2x2 matrix above is called the Jacobian matrix of the transformation and is denoted by [J].

If, at a point (ξ,η) in the master element, it is possible to solve equation (4.13) for $d\xi$ and $d\eta$ in terms of dx and dy, the inverse map T_e^{-1} of the (x,y) coordinates into the (ξ,η) coordinates can be constructed at this point. A necessary and sufficient condition for the invertibility of equation (4.13) is that the determinant $|J|$ be non-zero at (ξ,η) in R' i.e. whenever $|J| \neq 0$, the following can be written,

$$\begin{bmatrix} d\xi \\ d\eta \end{bmatrix} = 1/|J| \begin{bmatrix} dy/d\eta & -dx/d\eta \\ -dy/d\xi & dx/d\xi \end{bmatrix} \begin{bmatrix} dx \\ dy \end{bmatrix} \qquad (4.14)$$

and,

$$T_e^{-1} : \xi = \xi(x,y) \qquad (4.15)$$
$$\eta = \eta(x,y)$$

At this point, it is useful to introduce the concept of isoparametric finite element representations : the principal idea of isoparametric elements is to represent the element field variables at any point (in terms of the element nodal field variables) by using the same shape functions that are used to represent the geometry of the element.

Consider the master element and typical element in a mesh shown in fig. 4.2. Employing the isoparametric representation concept, the geometry and displacements for an eight-noded element can be expressed as,

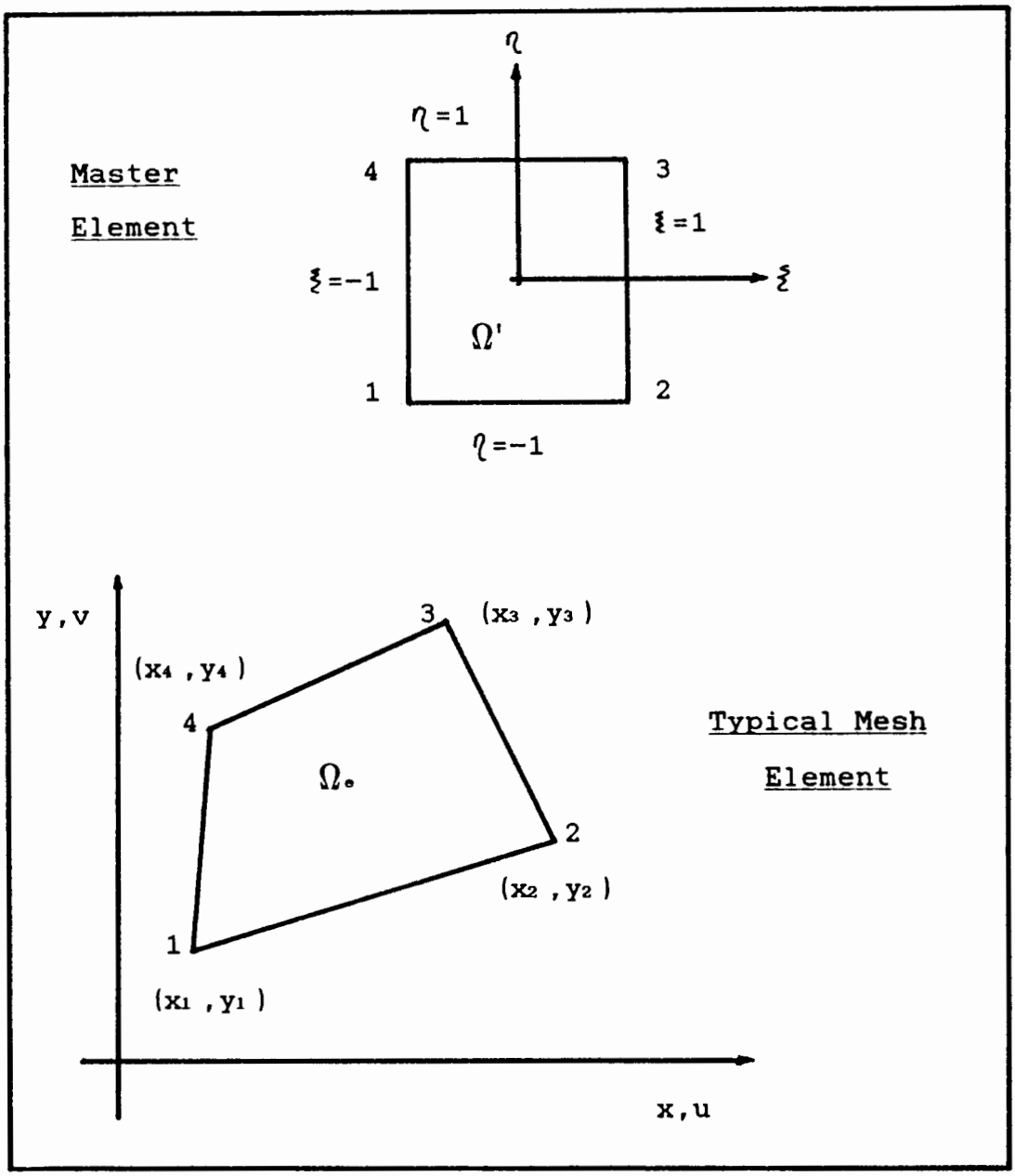

Fig. 4.2 MASTER ELEMENT AND TYPICAL ELEMENT IN A MESH

$$x = \sum_{1}^{8} N_i x_i \quad ; \quad y = \sum_{1}^{8} N_i y_i \quad ; \quad u = \sum_{1}^{8} N_i u_i \quad ; \quad v = \sum_{1}^{8} N_i v_i \qquad (4.16)$$

where,

$$N_1 = 1/4\,(1-\xi)\,(1-\eta)\,(-\xi-\eta-1) \quad ; \quad N_2 = 1/2\,(1-\xi^2)\,(1-\eta)$$
$$N_3 = 1/4\,(1+\xi)\,(1-\eta)\,(\xi-\eta-1) \quad ; \quad N_4 = 1/2\,(1-\eta^2)\,(1+\xi)$$
$$N_5 = 1/4\,(1+\xi)\,(1+\eta)\,(\xi+\eta-1) \quad ; \quad N_6 = 1/2\,(1-\xi^2)\,(1+\eta)$$
$$N_7 = 1/4\,(1-\xi)\,(1+\eta)\,(-\xi+\eta-1) \quad ; \quad N_8 = 1/2\,(1-\eta^2)\,(1-\xi)$$

The derivatives of these shape functions with respect to (x,y) can also be calculated where needed by using the determinant of the Jacobian and (4.17) above.

Equal order interpolation generally creates spurious zero eigenvalues of the system matrix, known as pressure modes, but they can occur in other elements as well. This situation results in a square mesh when an even number of those elements displaying a pressure mode, is used along each side. This 'checkerboard' mode has been effectively removed when mixed interpolation has been employed by previous authors, and thus the pressure variables in this analysis are defined by shape functions of one order lower than those used for defining the velocity variables.

Thus the element pressure variable can be written as follows,

$$P = \sum_{1}^{4} M_i P_i \quad , \text{ where } M_1 = 1/4\,(1-\xi)\,(1-\eta) \quad ; \quad M_2 = 1/4\,(1+\xi)\,(1-\eta)$$
$$M_3 = 1/4\,(1+\xi)\,(1+\eta) \quad ; \quad M_4 = 1/4\,(1-\xi)\,(1+\eta)$$

(4.18)

As with the velocities, the derivatives of the above shape functions can be evaluated via the Jacobian matrix and equations (4.18). The evaluation of the stiffness

matrices and load vectors in the previous section are thus greatly simplified using element mapping and the theory of isoparametry as described above.

4.2.6 Numerical Integration

It is obvious that the evaluation of the integrals necessary to compute the element matrices can become very difficult, especially when higher order elements are utilised. To overcome this problem, it is customary to employ a simple numerical integration procedure. There are many such algorithms, but they are all based on the idea that a typical integral,

$$I = \int_{-1}^{+1} f(\xi)\, d\xi \tag{4.19}$$

can be substituted by a summation of products of the form,

$$I_P = \sum_{1}^{P} w_i\, f(\xi_i) \tag{4.20}$$

where P is the total number of integration points at which the integrand $f(\xi)$ is evaluated, ξ_i are predetermined positions at which the integration points are located (within the domain of integration) and w_i are predetermined weighting factors associated with each of the integration points. Thus, for a 3-point integration rule (fig. 3.3),

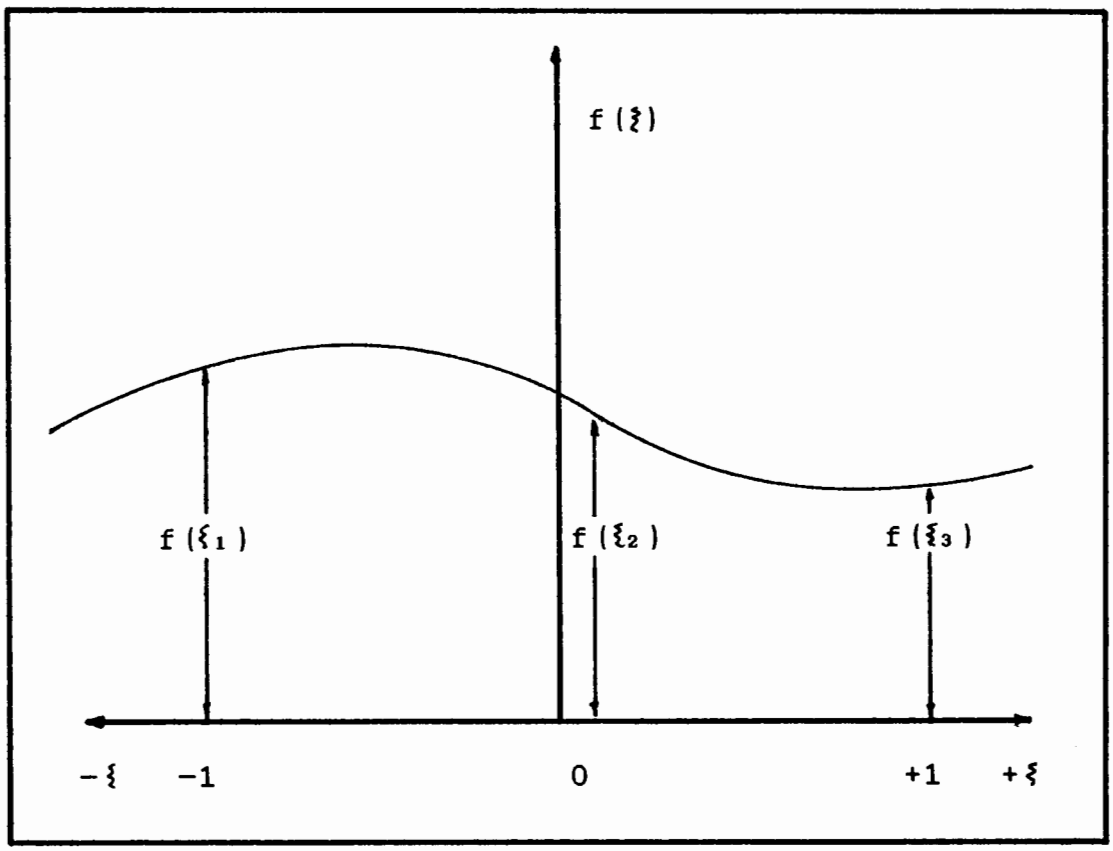

Fig. 4.3 TYPICAL INTEGRATION OVER $-1 \leq \xi \leq +1$

$$I_3 = w_1 f(\xi_1) + w_2 f(\xi_2) + w_3 f(\xi_3)$$

For certain values of ξ_i and w_i, the above equation becomes the well-known Simpson's rule. However, more efficient procedures do exist, and the Gauss-Legendre quadrature, which is used throughout this text, is particularly well suited to finite element analysis. For this numerical integration procedure, the sampling points are termed Gauss points. It is important to note that a p-point Gauss-Legendre rule will integrate exactly up to 2p-1 order.

Consider a general form of the governing equations

involving first order differentials, as derived in the previous chapter,

$$I = \int\int_{\Omega} F'(x,y)\ dxdy \qquad (4.21)$$

For an element, this can be written explicitly in terms of the master element coordinates as,

$$I = \int_{-1}^{+1}\int_{-1}^{+1} F(\xi,\eta)\ d\xi d\eta \qquad (4.22)$$

By using equation (4.20), this can be reduced to,

$$I = \sum_{j=1}^{m'} \sum_{i=1}^{m} (w_j w_i F(\xi_i, \eta_j)) \qquad (4.23)$$

resulting in a sequence of simple algebraic calculations.

The integration rule adopted in this analysis, for all the variables, is 3x3 Gaussian integration, although 2x2 Gaussian integration for the pressure variable would suffice. For 3x3 integration, m' = 3 and m = 3 in equation (4.23) above, and this results in nine integration or Gauss points. The weighting factors and sampling point positions for this type of integration are listed below in fig. 4.4.

m	i	a_i	ξ_i
	1	5/9	$-\sqrt{0.6}$
3	2	8/9	0.0
	3	5/9	$\sqrt{0.6}$

Fig. 4.4 3x3 GAUSS INTEGRATION FACTORS

4.3 FORMULATION OF MATRIX EQUATIONS

It can be deduced from equations (4.16) and (4.18) that, for an eight-noded element, the four variables of convection heat transfer can be approximated as follows,

$$u = \sum_{1}^{8} N_i u_i \; ; \; v = \sum_{1}^{8} N_i v_i \; ; \; \theta = \sum_{1}^{8} N_i \theta_i \; ; \; P = \sum_{1}^{4} M_l P_l \qquad (4.24)$$

where the variation in pressure is depicted by shape functions of one order lower than the others as explained previously. Obviously, the same method can be applied to the arbitrary functions, $\underline{u}'$ and θ'.

It is convenient at this stage to separate the Navier-Stokes equations into two equations with u, P and θ as the variables of the equation in the x-direction, and v, P and

θ as the variables of the equation in the y-equation. The x-direction equation will be considered first. Also, the individual terms will be considered seperately for clarity and ease of explanation.

The diffusion term of the x-direction momentum equation (see equation (3.28)) can be expressed as,

$$1/Re \int_{\Omega} \nabla u' . \nabla u \, d\Omega = 1/Re \sum_{1}^{ne} \int_{A^e} ([dN_i/dx] u_i' . [dN_j/dx] u_j + [dN_i/dy] u_i' . [dN_j/dy] u_j) \, dA^e \qquad (4.25)$$

As can be seen in the final form of the above term, the integral has been reduced to one performed over each elemental area, and these are then summed over the whole domain.

Similarly, the advection, or non-linear, term can be reduced to,

$$\int_{\Omega} (\nabla u) u . u' \, d\Omega \qquad (4.26)$$

$$= \sum_{1}^{ne} \int_{A^e} (N_i u_i' N_k \hat{u}_k [dN_j/dx] u_j + N_i u_i' N_k \hat{v}_k [dN_j/dy] u_j) \, dA^e$$

$\hat{u}$ is introduced in equation (4.26) to admit the non-linear procedure. It is evident that when dealing with a set of equations like the Navier-Stokes equations, more than one variable appears in the equations and some terms comprise the product of a variable and a derivative of the same, or of another, variable. In such instances, the method of solution becomes, of necessity, iterative.

Consider, for example, one component of the advection term, $(\hat{u}.du/dx)$ in which the variable associated with the differential is assumed to be the unknown. The procedure is then to assume a starting value or initial guess for u, namely $\hat{u}$, and solve the equations for u. A check is then made to ascertain whether $\hat{u}$ and u are sufficiently in agreement to state that the solution is complete.

Usually this is not the case, and a new estimate of $\hat{u}$ is made, utilizing the calculated, updated value of u as a guide to the required change in $\hat{u}$. This process is repeated until $(\hat{u}-u)/u$ is within a required tolerance.

The iteration procedures available for solving non-linear problems such as convection heat transfer are discussed in more detail in Chapter 5.

The pressure term can be written as,

$$\int_{\Omega} u' dP/dx \; d\Omega = \sum_{1}^{ne} \int_{A^e} (N_i \, u_i' \, [dM_i/dx] P_i) \, dA^e \qquad (4.27)$$

The right-hand side of the Navier-Stokes equations comprise the gravity term and the boundary term. The

former is treated in much the same manner as the above terms. However, since gravity does not act in the x-direction, this term in the x-direction momentum equation falls away. The boundary integrals can be expressed as,

$$1/Re \int_{\Gamma} u'.du/dn \; d\Gamma = 1/Re \int_{\Gamma} N_i u_i'.du/dn \; d\Gamma \qquad (4.28)$$

Thus the x-direction Navier-Stokes equation can be written as follows,

$$\sum_{1}^{ne} \int_{A^e} ((N_i u_i' N_k \hat{u}_k [dN_j/dx] u_j + N_i u_i' N_k \hat{v}_k [dN_j/dy] u_j) \qquad (4.29)$$

$$+ 1/Re ([dN_i/dx] u_i'.[dN_j/dx] u_j + [dN_i/dy] u_i'.[dN_j/dy] u_j)$$

$$+ (N_i u_i' [dM_l/dx] P_l)) \; dA^e = 1/Re \sum_{1}^{ne} \int_{\Gamma} N_i u_i' du/dn \; d\Gamma$$

Repeated subscripts are implied in the above equations such that,

$$l = 1.....4$$
$$i = 1.....8$$
$$j = 1.....8$$
$$k = 1.....8$$

The corresponding momentum equation in the y-direction is obtained by merely interchanging x,y and u,v in equation

(4.29). There is, however, an additional term, namely the gravity term, since the gravitational force acts in the y-direction. This term can be written as,

$$-Ra \int_{\Omega} \theta g.v' d\Omega = -Ra \sum_{1}^{ne} \int_{A^e} N_i v_i' N_k \hat{\theta}_k N_j g_j \delta_{j2} \, dA^e \qquad (4.30)$$

Thus the y-direction Navier-Stokes equation can be written as,

$$\sum_{1}^{ne} \int_{A^e} \left((N_i v_i' N_k \hat{u}_k [dN_j/dx] v_j + N_i v_i' N_k \hat{v}_k [dN_j/dx] v_j \right) \qquad (4.31)$$

$$+ 1/Re \left([dN_i/dx] v_i' . [dN_j/dx] v_j + [dN_i/dy] v_i' . [dN_j/dy] v_j \right)$$

$$+ \left(N_i v_i' [dM_l/dy] P_l \right) \right) dA^e$$

$$= -Ra \sum_{1}^{ne} \int_{A^e} (N_i v_i' N_k \hat{\theta}_k N_j g_j \delta_{j2}) \, dA^e + 1/Re \sum_{1}^{ne} \int_{\Gamma} N_i v_i' dv/dn \, d\Gamma$$

The variational formulation of the continuity equation (3.29) can be expressed as follows,

$$\sum_{1}^{ne} \int_{A^e} M_l u_l' ([dN_j/dx] u_j + [dN_j/dy] v_j) \, dA^e = 0 \qquad (4.32)$$

where the arbitrary function has a shape function M_l associated with the four noded quadrilateral element,

since the pressure, for which the lower order polynomial is used, is evaluated via the continuity equation.

The heat conduction equation is evaluated in a similar manner to the Navier-Stokes equations, and the variational formulation of the heat conduction equation (3.32) is thus readily transformed as follows,

$$\sum_{1}^{ne} \int_{A^e} \left(Re \left(N_i \theta_i' N_k \hat{u}_k [dN_j/dx] \theta_j + N_i \theta_i' N_k \hat{v}_k [dN_j/dy] \theta_j \right) + \right.$$

$$\left. 1/Pr \left([dN_i/dx] \theta_i' . [dN_j/dx] \theta_j + [dN_i/dy] \theta_i' . [dN_j/dy] \theta_j \right) \right) dA^e$$

$$= \sum_{1}^{ne} \int_{A^e} N_i \theta_i' N_j Q_j \, dA^e + 1/Pr \sum_{1}^{ne} \int_{\Gamma} N_i \theta_i' d\theta/dn \, d\Gamma \qquad (4.33)$$

Since the primed variables are arbitrary, they can be moved outside the integral formulation, and the equations can be written as :

$$[K_{pq}] (u_q) = (F_p) \qquad (4.34)$$

where $[K_{pq}]$ is the non-symmetric, semi-positive definite stiffness or conductivity matrix, (F_p) is the load vector, and (u_q) is the vector of nodal unknowns.

In expanded form, the contribution from one node to the element matrix can be written as :

$$K_{1\,1} = \int_{A^e} u_i' \left(N_i N_k \hat{u}_k \frac{dN_j}{dx} + N_i N_k \hat{v}_k \frac{dN_j}{dy} \right.$$

$$\left. + \frac{1}{Re} \left(\frac{dN_i}{dx} \cdot \frac{dN_j}{dx} + \frac{dN_i}{dy} \cdot \frac{dN_j}{dy} \right) \right) dA^e$$

$$K_{1\,3} = \int_{A^e} u_i' \left(N_i \left(\frac{dM_1}{dx} \right) \right) dA^e$$

$$K_{2\,2} = \int_{A^e} v_i' \left(N_i N_k \hat{u}_k \frac{dN_j}{dx} + N_i N_k \hat{v}_k \frac{dN_j}{dy} \right.$$

$$\left. + \frac{1}{Re} \left(\frac{dN_i}{dx} \cdot \frac{dN_j}{dx} + \frac{dN_i}{dy} \cdot \frac{dN_j}{dy} \right) \right) dA^e$$

$$K_{2\,3} = \int_{A^e} v_i' \left(N_i \left(\frac{dM_1}{dy} \right) \right) dA^e$$

$$K_{3\,1} = \int_{A^e} u_1' \left(M_1 \frac{dN_j}{dx} \right) dA^e$$

$$K_{3\,2} = \int_{A^e} u_1' \left(M_1 \frac{dN_j}{dy} \right) dA_e$$

$$K_{4\,4} = \int_{A^e} \theta_i' \left(Re \left(N_i N_k \hat{u}_k \frac{dN_j}{dx} + N_i N_k \hat{v}_k \frac{dN_j}{dy} \right. \right.$$

$$A^e$$

$$+ 1/Pr\,(dN_i/dx.dN_j/dx + dN_i/dy.dN_j/dy))\,dA^e$$

$$K_{12} = K_{14} = K_{21} = K_{24} = K_{33} = K_{34} = K_{41} = K_{42} = K_{43} = 0,$$

(since these terms when multiplied by the appropriate variables, are not involved in the final set of governing equations).

The load vector comprises the following :

$$(F_j) = \{\, 0 \quad \int_{A^e} N_i N_k \hat{\theta}_k N_j g_j \delta_{j2} \, dA^e \quad 0 \quad \int_{A^e} N_i N_j Q_j \, dA^e \,\}^T,$$

and the variable array is made up of :

$$(u_j) = \{\, u_j \quad v_j \quad P_1 \quad \theta_j \,\}^T.$$

It should be noted that the boundary integrals were not incorporated into the load vectors for boundary elements as, in all the problems considered, definite boundary conditions were assigned to the boundary elements.

The above finite element formulations of the convection heat transfer governing equations are directly implemented into the computer code in the subroutine which calculates the element matrices.

CHAPTER 5

SOLUTION OF STEADY-STATE NON-LINEAR PROBLEMS

5.1 INTRODUCTION

In physical problems, non-linearities can occur in one of two forms, namely (1) the material properties of the system may be dependent on the nodal variables, or (2) geometrical non-linearities may be present in the governing equation of the problem. In the case of natural convection, the non-linearity is of the latter type as it appears in the convective terms of the governing equations.

Non-linear problems can be written in the following manner (Dhatt and Touzot [47]) :

$$(R(U)) = (F) - [K(U)](U) \qquad (5.1)$$

where [K] is the global system matrix, (F) is the global right hand side load vector, (U) is the global vector of all nodal values of the unknown function, and (R(U)) is the global residual. Solution of equation (5.1) involves the search for a vector (U) that renders the residual (R(U)) as small as possible. For an exact solution, this term would be zero.

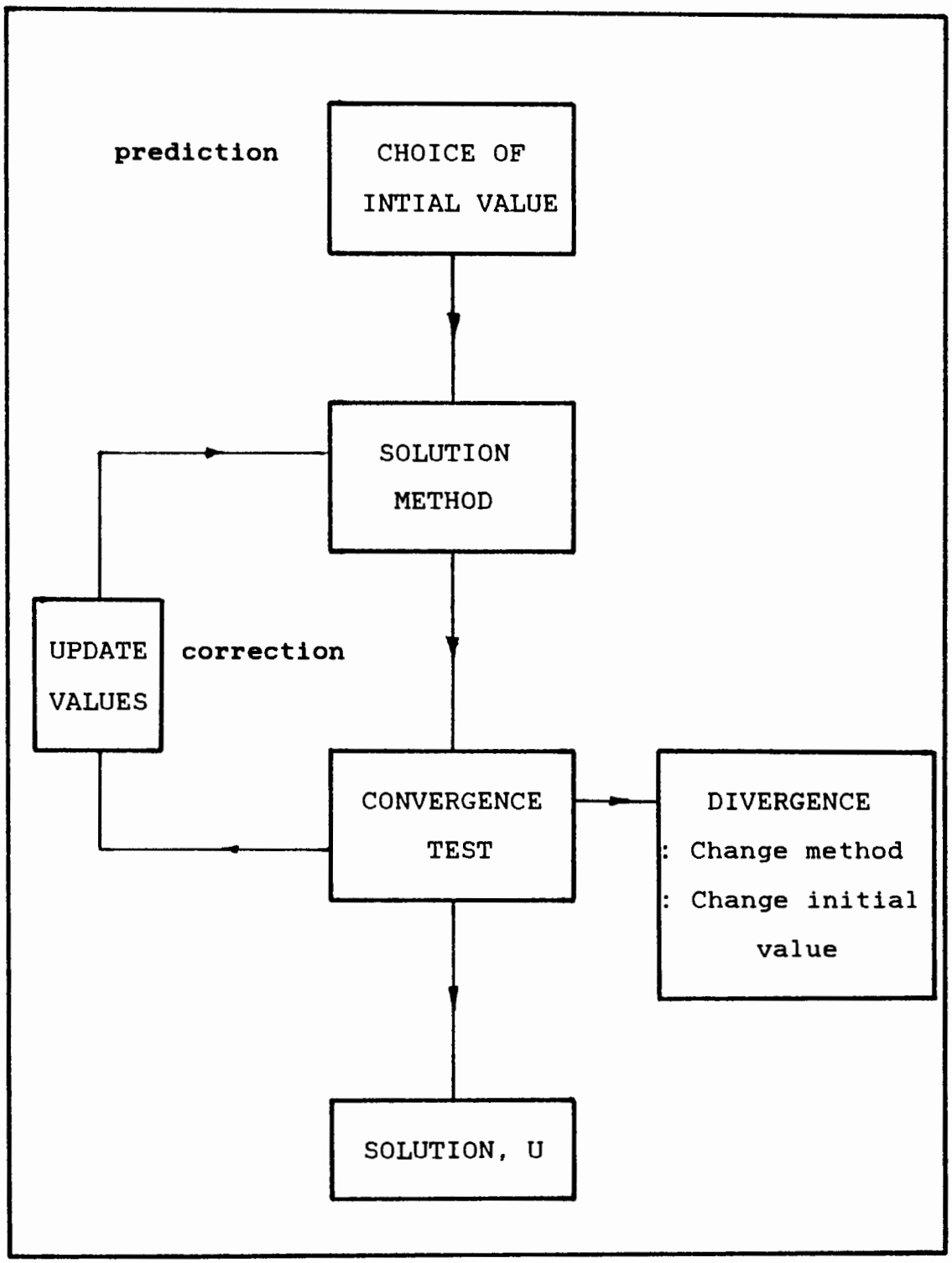

Fig. 5.1 NON-LINEAR SOLUTION ALGORITHM

Generally, non-linear solution algorithms are similar to the one shown in fig. 5.1 in that they involve the

solutions of systems of linear equations at each iteration step. Even though no single method available is general enough to solve all types of non-linear problems, most methods can be developed from the substitution method, the Newton-Raphson method, or the incremental method, or from combinations of these three strategies.

5.2 THE SUBSTITUTION METHOD

The substitution method necessitates the construction of a sequence of solutions $\{U^0\}$, $\{U^1\}, \ldots\ldots \{U^i\}$, where $\{U^i\}$ is calculated from the previous value $\{U^{i-1}\}$, and the solving of the linear system of equations :

$$\{R^i\} = \{R(U^{i-1})\} = \{F\} - [K(U^{i-1})]\{U^{i-1}\} \qquad (5.2)$$
$$[K(U^{i-1})]\{\Delta U^i\} = \{R^i\}$$
$$\{\Delta U^i\} = \{U^i\} - \{U^{i-1}\}$$

i.e. both $[K(U^{i-1})]$ and $\{R^i\}$ can be evaluated using a known vector $\{U^{i-1}\}$. The system of equations then essentially becomes linear, and can be solved using direct Gaussian elimination methods. In order to initiate this method, a starting value $\{U^0\}$ has to be assumed, but in a large number of problems it can be assumed to be zero. The convergence of the solution may be dependent upon the choice of these initial values, as well as the type of non-linearity and the loading amplitude.

The algorithm for the substitution method is illustrated in fig. 5.2. The iterative process in this algorithm is

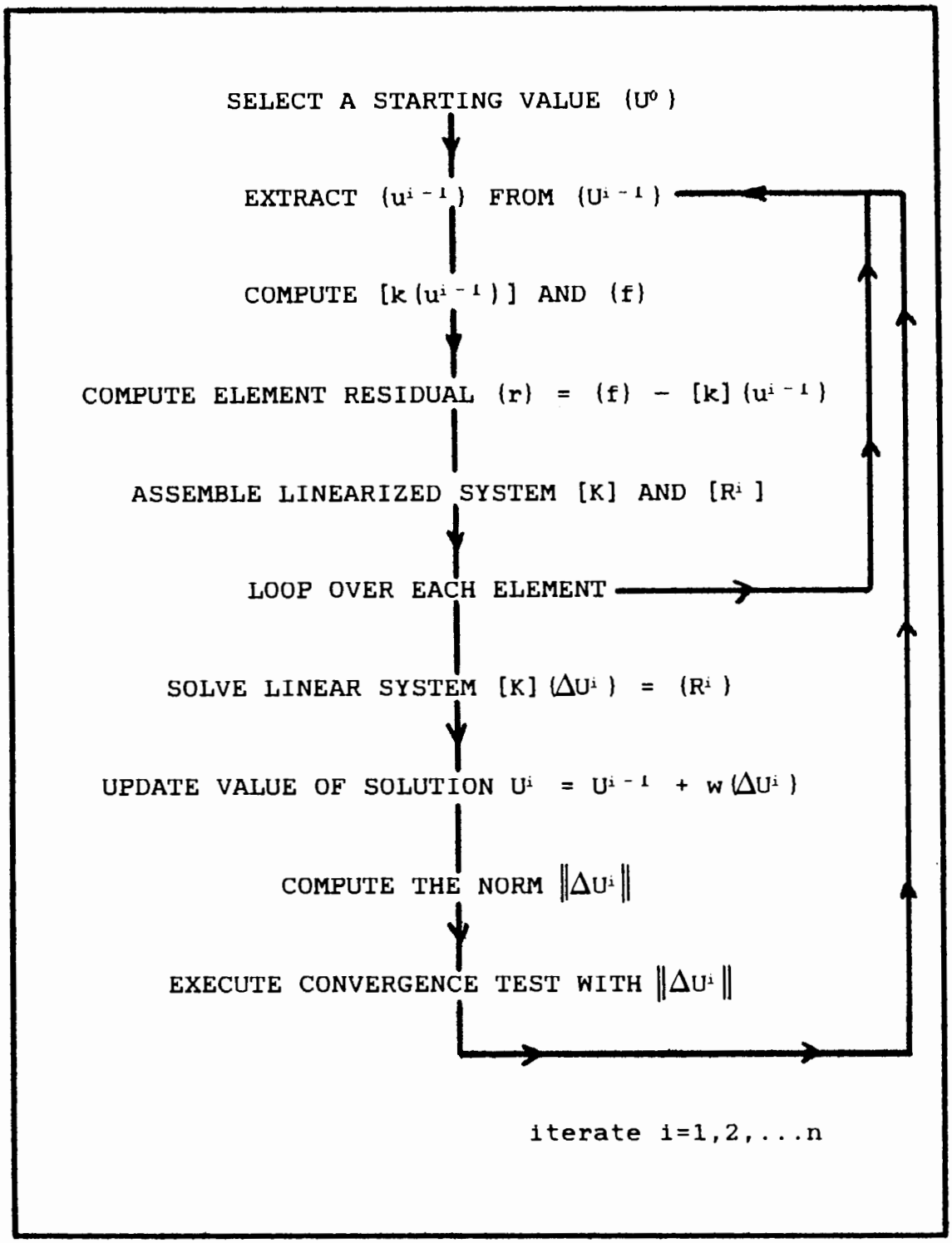

Fig. 5.2 SUBSTITUTION METHOD ALGORITHM

terminated when the norm $\|\Delta U^i\|$ becomes sufficiently small i.e.

$$\|\Delta U^i\| = \sqrt{<\Delta U^i>(\Delta U^i)/<U^i>(U^i)} < e$$

where e is an arbitrarily selected small number. An over-relaxation factor, w, can be used to improve the convergence rate. However, its value is problem dependent, and can usually only be determined by numerical experimentation.

5.3. THE NEWTON-RAPHSON METHOD

The Newton-Raphson algorithm involves developing the residual function in the neighbourhood of U^{i-1} (in the form of a Taylor series) to determine the residual for the following iteration, i :

$$\begin{aligned}(R(U^i)) &= (R(U^{i-1} + \Delta U^i)) \\ &= (R(U^{i-1})) + [dR/dU](\Delta U^i) = 0\end{aligned} \qquad (5.3)$$

(neglecting terms of order greater than one)

or,

$$-[dR/dU](\Delta U^i) = [K_t(U^{i-1})](\Delta U^i) = (R(U^{i-1})) \qquad (5.4)$$

The tangent matrix, $[K_t(U^{i-1})]$ can be obtained by differentiating equation (5.1) :

$$[K_t(U)] = -[dR/dU] = -[dF/dU] + [K(U)] + [dK/dU](U) \qquad (5.5)$$

In most physical problems, (F) is independent of U i.e.

$$[K_t(U)] = [K(U)] + [dK/dU](U) \qquad (5.6)$$

Equation (5.6) leads to an algorithm similar to that shown in fig. 5.2, except that [K] is replaced by the global tangent matrix, $[K_t]$. It is impracticable to assemble element tangent matrices to form $[K_t]$ since the derivation of $[k(u)]$ would require that its terms be defined explicitly. An easier approach is to derive the expression for $[k_t]$ starting from the integral form before discretization.

5.4 THE INCREMENTAL METHOD

One of the major difficulties encountered in the previous two methods, is that a poor choice of the initial value (U^0) can result in a divergent process. The incremental (step-by-step) method overcomes this problem by replacing the solution of :

$$[K(U)](U) = \lambda(F_0) = (F) \qquad (5.7)$$

with successive solutions of :

$$[K(U_j)](U_j) = \lambda_j(F_0) \qquad (5.8)$$

where $\lambda_j = \lambda_1, \lambda_2, \ldots\ldots, \lambda$ (λ_j is the load level parameter).

The starting value used in the calculation of U_j is the solution U_{j-1} obtained in the previous step. Each step is

a non-linear problem which can be solved by one or more iterations of the Newton-Raphson method i.e. for one iteration per step,

$$(R(U_{j-1})) = \lambda_{j-1}(F_0) - [K(U_{j-1})](U_{j-1}) \qquad (5.9)$$
$$[K_t(U_{j-1})](\Delta U_j) = (R(U_{j-1})) + (\lambda_j - \lambda_{j-1})(F_0)$$
$$(U_j) = (U_{j-1}) + (\Delta U_j)$$

and if more than one iteration is used, in each step,

$$[K_t(U_j^{i-1})](\Delta U_j^i) = (R(U_j^{i-1})) + (\lambda_j - \lambda_{j-1})(F_0) \qquad (5.10)$$
$$(U_j^i) = (U_j^{i-1}) + (\Delta U_j^i) \quad i = 2,3,....$$

5.5 CLOSURE

The choice of method is very much dependent on the problem to be solved. The type, severity and spread of the non-linearity, the possible existence of more than one solution, the ease of coding the algorithm, the desired precision of the results, and the speed of convergence and the risk of divergence, must all be considered when evaluating and comparing the methods available.

At each iteration, Taylor and Hughes [16] solved

$$[K(U^{i-1})](U^i) = (F),$$

and then used $(U^i)^*$ as a feedback value, where $(U^i)^* = 1/2((U^i) - (U^{i-1}))$. They successfully applied this solving technique to incompressible flow, and it was thus employed for this study to verify its capability in achieving satisfactory results for convection heat transfer.

CHAPTER 6

NUMERICAL EXAMPLES

Five example problems were chosen to illustrate the capability of the primitive variable mixed-interpolation finite element formulation in the field of convection heat transfer. The first four problems, namely thermally driven flow in a square window cavity, a vertical slot, a triangular cavity, and a liquid diode, are all examples of natural convection. The fifth example investigated, a power plant cooling pond, is a forced convection problem. All the problems were input into a FORTRAN computer program, developed by the author, which contained the finite element formulations of the governing equations as derived in the preceding chapters. The program was run on the SPERRY UNIVAC mainframe computer at the University of Cape Town.

In the case of the first example, both computational and experimental results have been previously published, enabling extensive correlation and verification of the data obtained using the current analysis. Where possible, comparisons with previously published material are also made for the other three examples of natural convection. However, for the last problem, available data from prior research is very limited, and thus only qualitative comparisons are possible.

6.1 SQUARE WINDOW CAVITY RESULTS

The thermally driven square cavity has been used as a benchmark problem in numerous computational and experimental studies. A paper presented by De Vahl Davis [65] was used as the basis for evaluation of the current analysis.

The geometry and solution domain for the thermally driven window cavity are shown in fig. 6.1 below. Results have

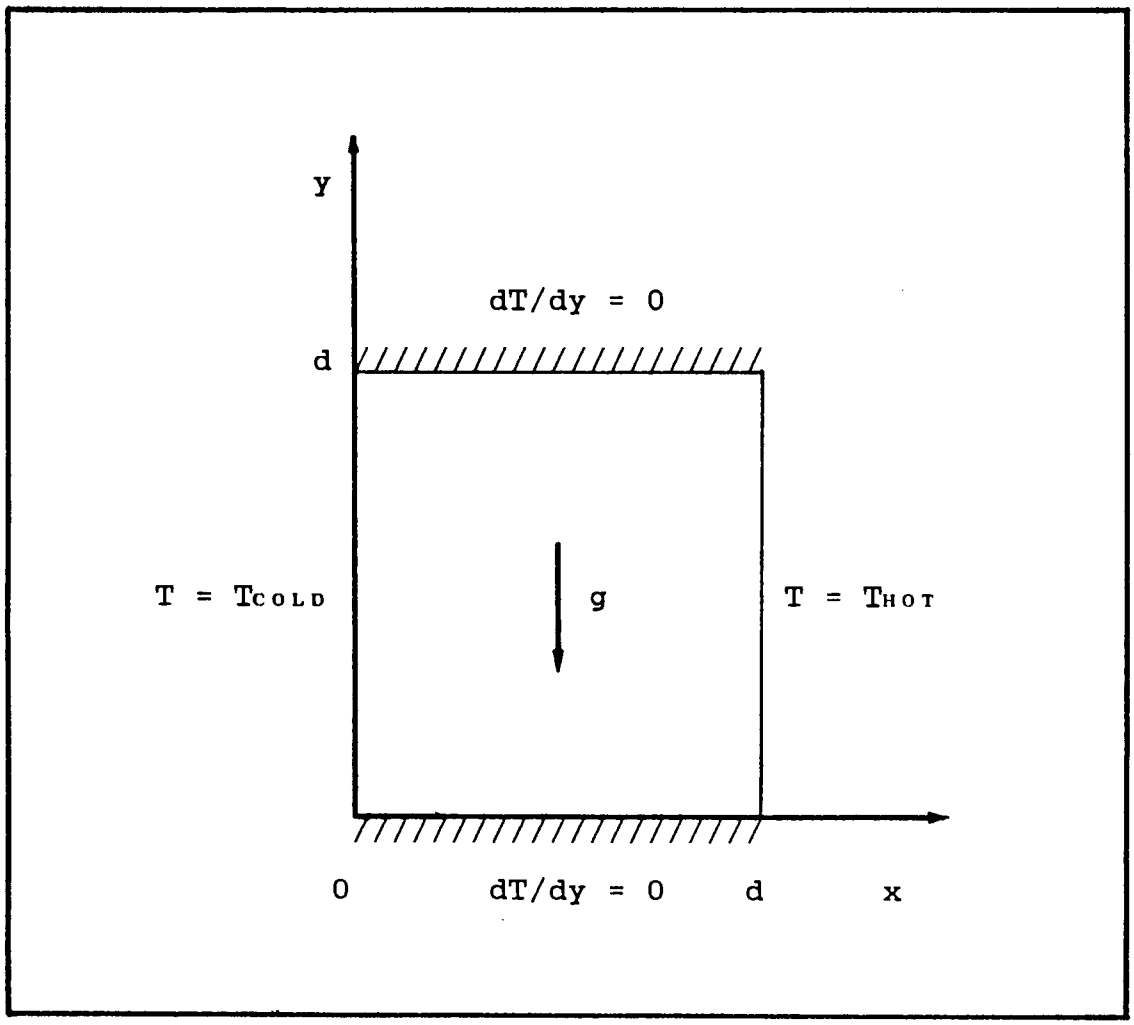

Fig. 6.1 GEOMETRY AND BOUNDARY CONDITIONS OF CAVITY

been computed for Rayleigh numbers in the range 10^3 to 10^5. For the Rayleigh numbers of 10^3 and 10^4, the Prandtl number was varied between 10^{-1} and 10. This was not possible for Ra=10^5 due to difficulties experienced with convergence. In all cases, the cooler wall is on the left side of the cavity. The only type of boundary condition considered in this example for the upper and lower walls, is the adiabatic or insulated boundary condition, although other types can be easily implemented. For this example, a 5x5 mesh of square elements is used.

6.1.1 Vertical Velocity Components

Plots of the vertical velocity component at the mid-height of the cavity (see figs. 6.2 - 6.4) were chosen to

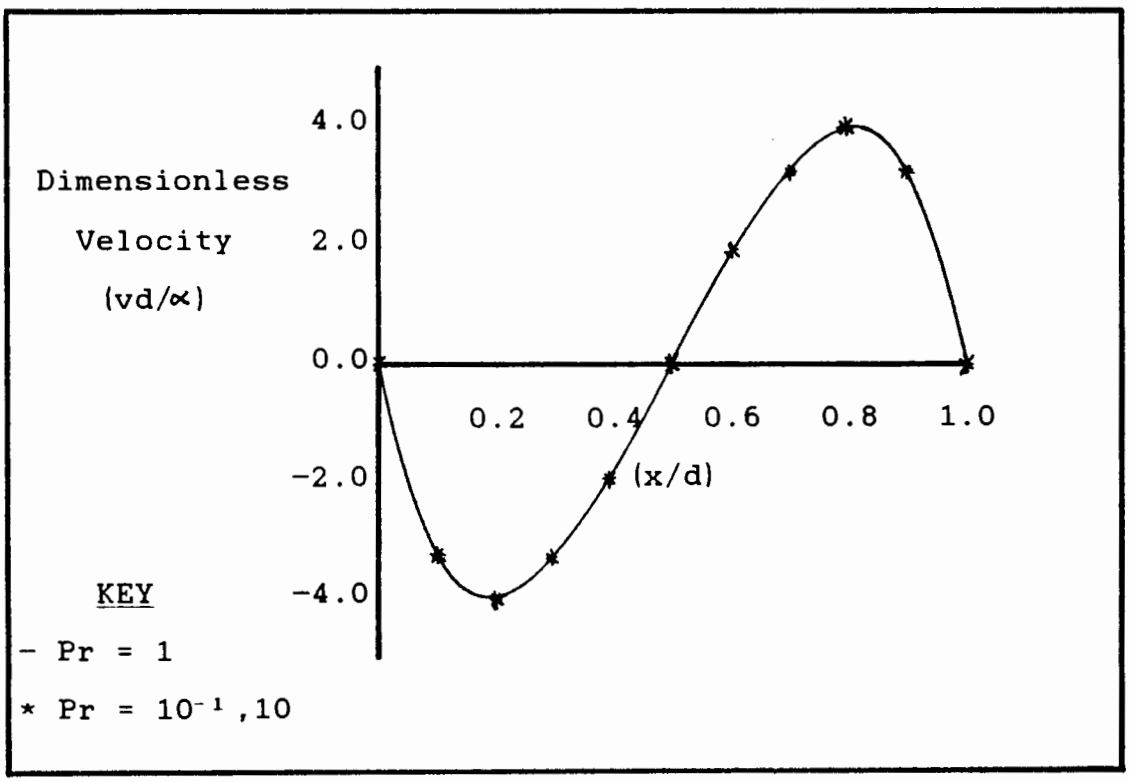

Fig. 6.2 VERTICAL VELOCITY COMPONENT : Ra = 10^3

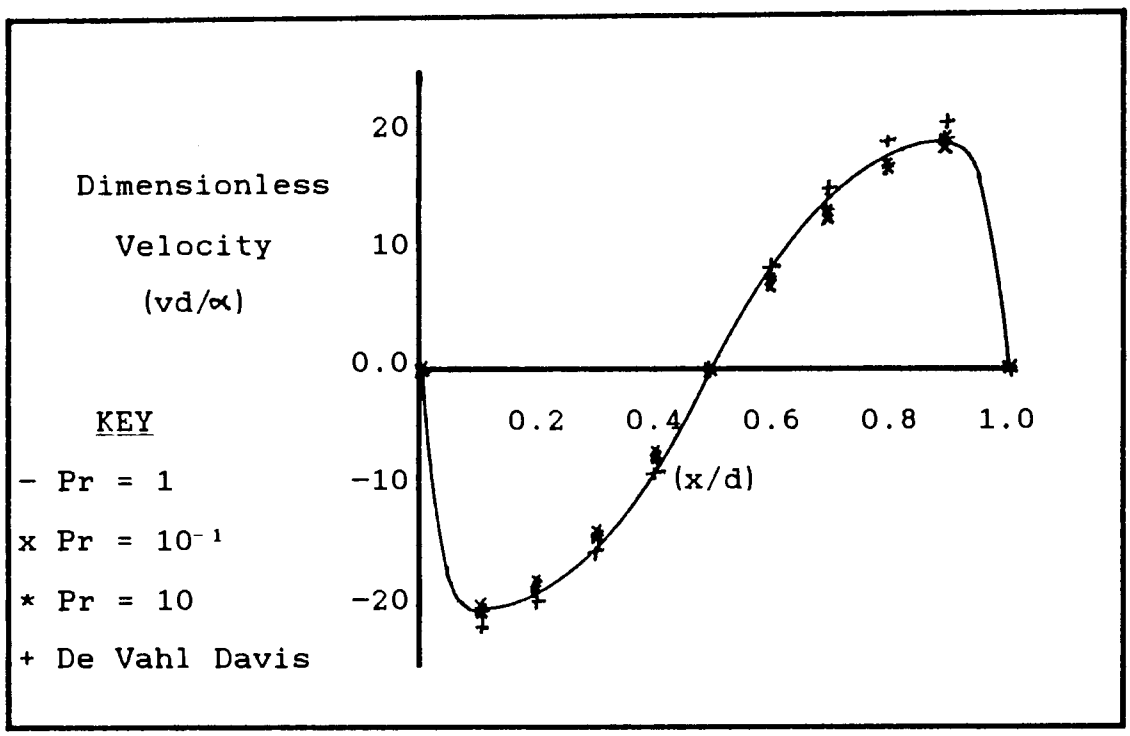

Fig. 6.3 VERTICAL VELOCITY COMPONENT : Ra = 10^4

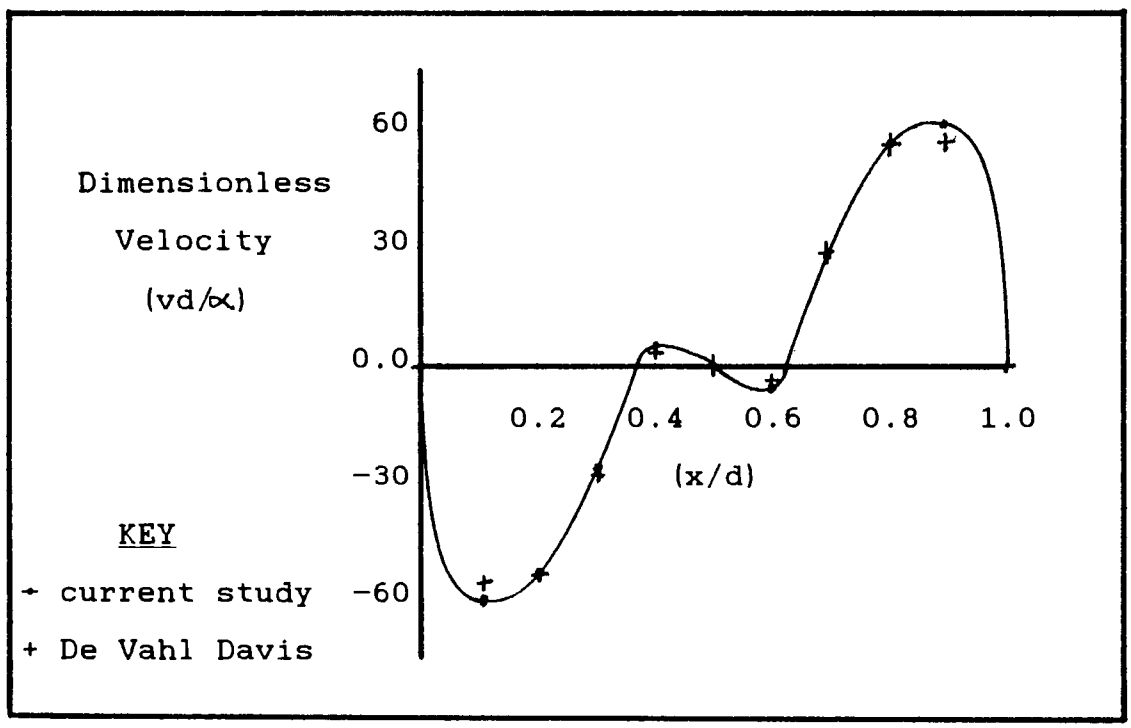

Fig. 6.4 VERTICAL VELOCITY COMPONENT : Ra = 10^5, Pr = 1

illustrate the fluid motion, since they give a detailed insight into the development of the motion, specifically the boundary layer, as the Rayleigh number increases. Where possible, the plot obtained using the current analysis is compared to the results quoted by De Vahl Davis [65]. As can be seen, the agreement is excellent.

Fig. 6.2 shows that, for $Ra=10^3$, the velocity of the fluid is low i.e. very little movement of the fluid occurs. However, it is clear from figs. 6.2 - 6.4 that, as the Rayleigh number increases, the fluid moves with greater velocity, and a distinct boundary layer develops. Of particular interest is the reverse flow which occurs near the centre of the cavity at $Ra=10^5$. This phenomenon was observed experimentally by Elder [62], and later verified by De Vahl Davis [65] in his numerical study.

A possible explanation for the double eddy occurring in fig. 6.4, is that for high Rayleigh numbers, the boundary layer flow is so well established that the strong vorticity near the walls is able to sustain a weak return motion in the outer part of the boundary layer, and that, in this region of the flow (near the mid-height of the cavity), the opposite boundary layer is less able to influence this flow.

6.1.2 Isotherms

Figs. 6.5 - 6.7 show the isotherm distributions for the cavity for the various Rayleigh numbers presently under consideration. Each isotherm line in the diagrams represents a 10% change in the temperature. At the low

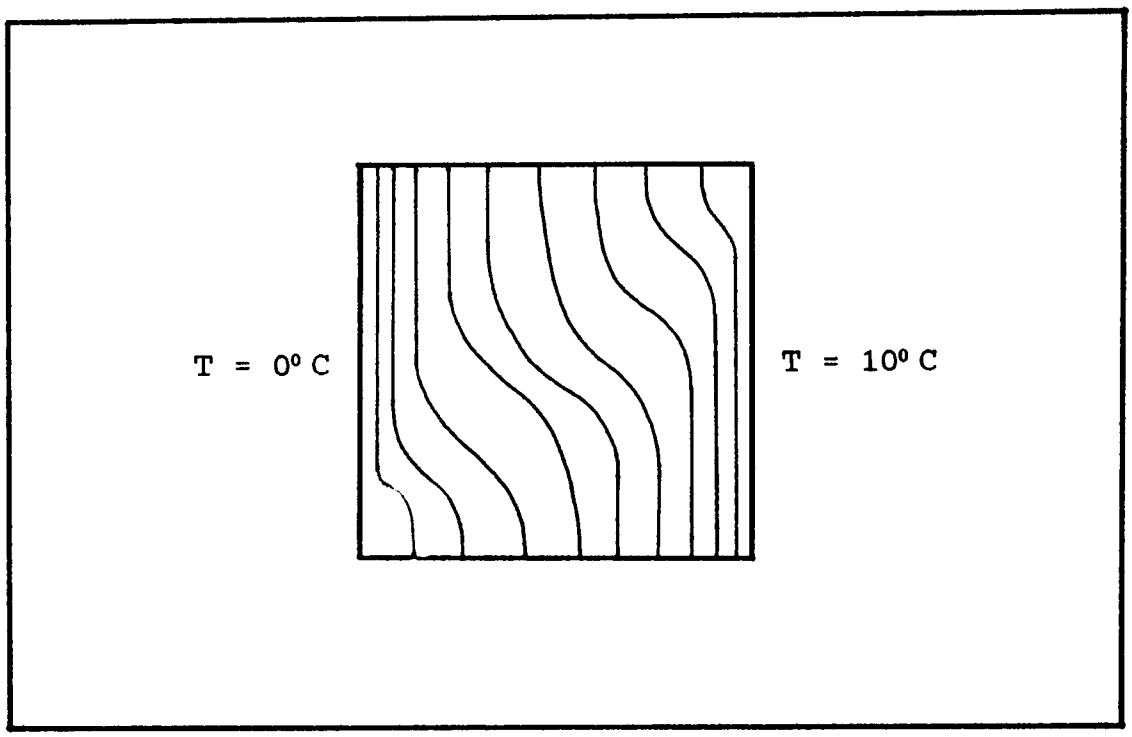

Fig. 6.5 ISOTHERMS : Ra = 10^3, Pr = 1

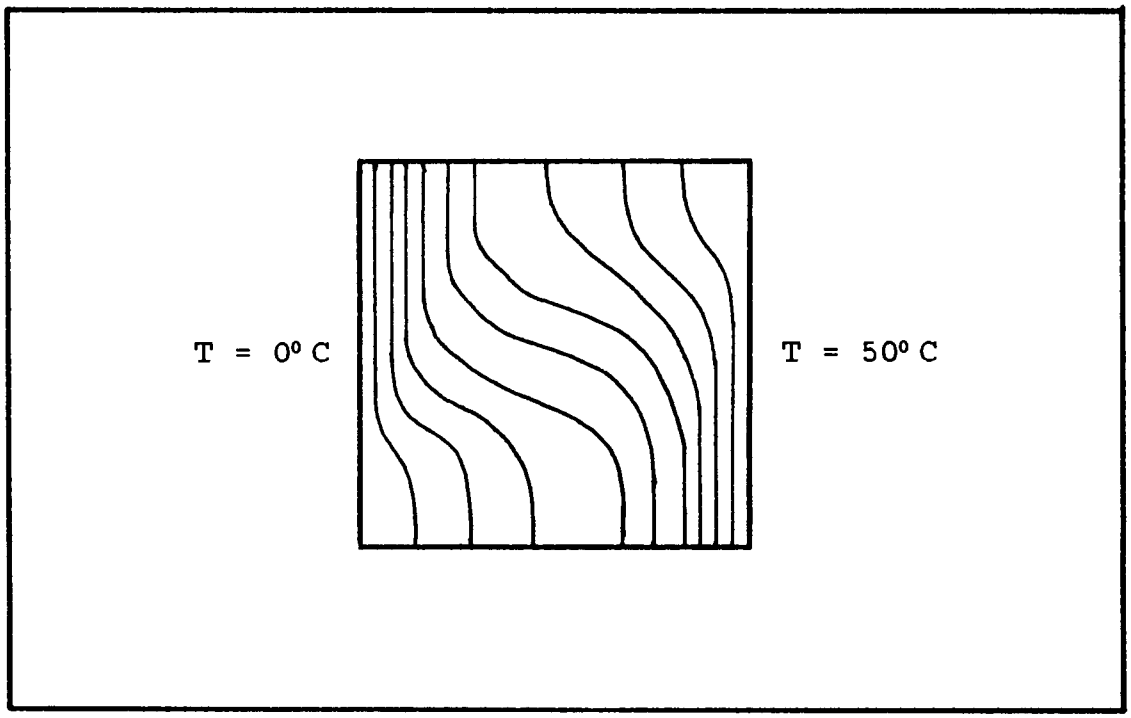

Fig. 6.6 ISOTHERMS : Ra = 10^4, Pr = 1

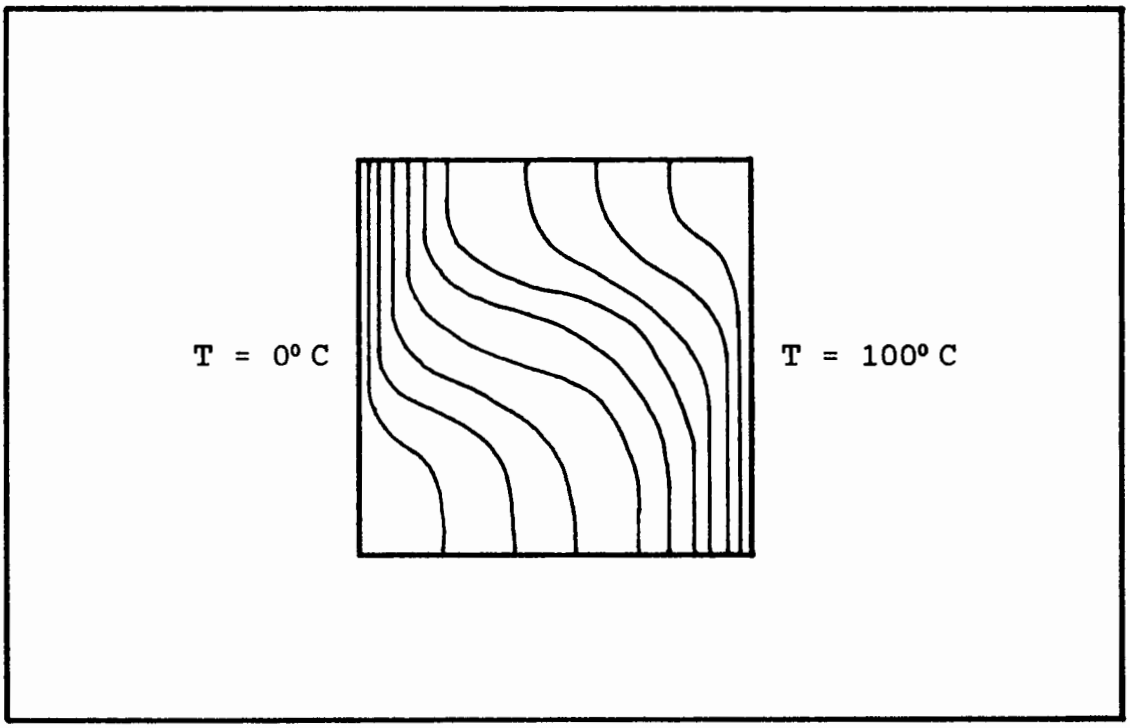

Fig. 6.7 ISOTHERMS : Ra = 10^5, Pr = 1

Rayleigh number, 10^3 (see fig. 6.5), there is virtually no distortion of the temperature distribution since minimal fluid motion takes place under these conditions. Thus it can be deduced that most of the heat transfer at low Rayleigh numbers ($Ra \leqslant 10^3$) is still in the form of conduction. Obviously, the limit of this situation is when no flow occurs and the heat transfer is by conduction alone.

The following two plots, fig. 6.6 and fig. 6.7, show that, as the Rayleigh number becomes larger, the consequent development of the motion causes the distribution of the temperature to progressively distort from that due to conduction alone i.e. the amount of heat transfer due to convection is directly proportional to the size of the

Rayleigh number. All these isotherm plots are in excellent correlation with those published by Schnipke and Rice [28], and De Vahl Davis [65].

6.1.3 Temperature Distributions

Both Eckert and Carlson [61], and De Vahl Davis [65] used the temperature distribution to distinguish between three regimes of flow. Using the same method adopted by the latter author, the temperature distribution at the mid-height of the cavity is plotted for the various Rayleigh numbers. Once again, these plots (see figs. 6.8 - 6.10) compare very well with those quoted by De Vahl Davis [65].

The temperature profile at the lowest Rayleigh number of

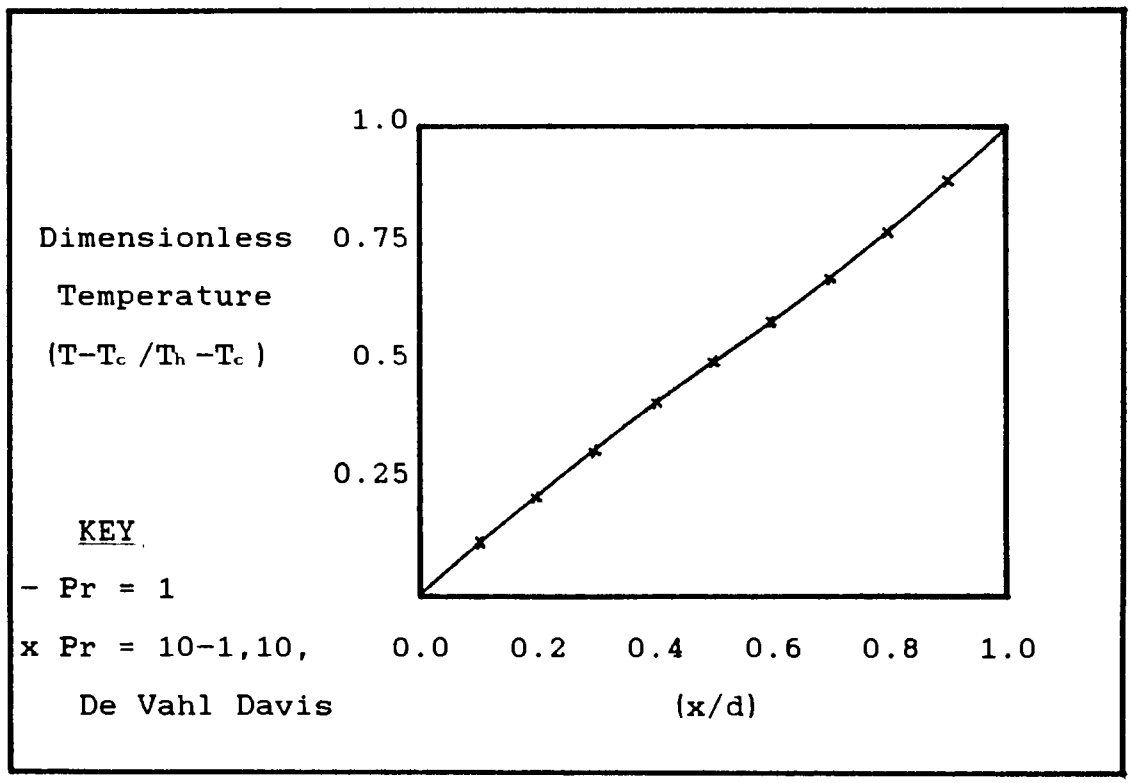

Fig. 6.8 TEMPERATURE DISTRIBUTION : Ra = 10^3

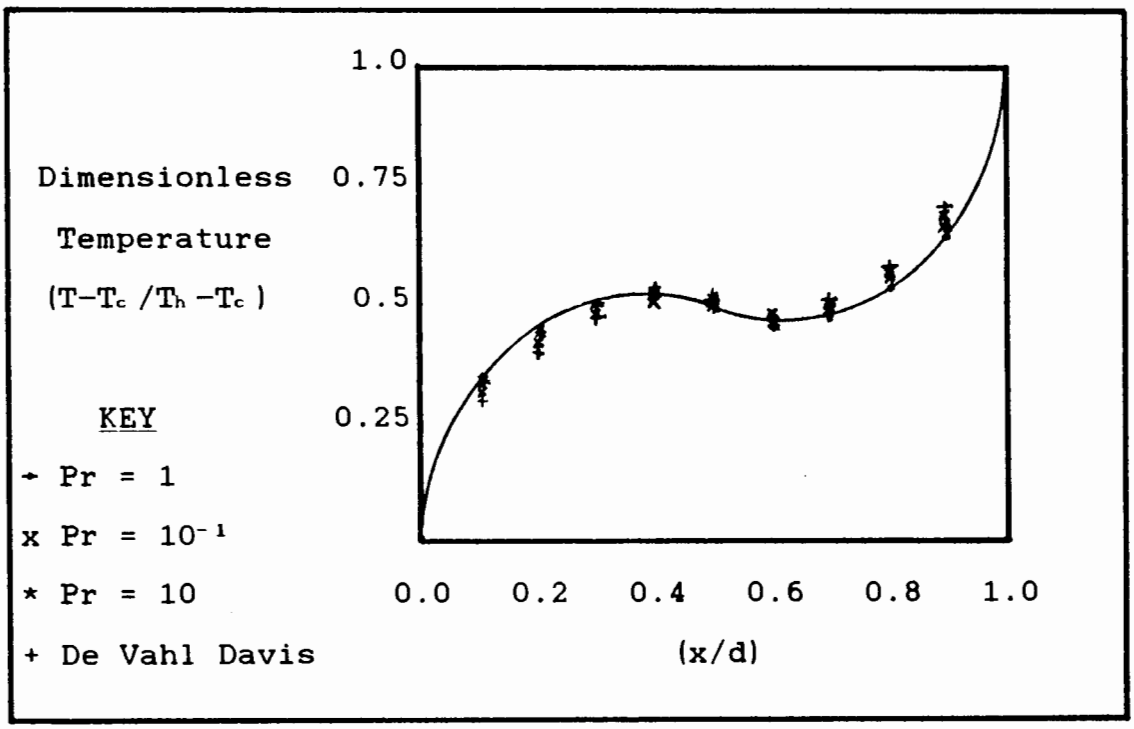

Fig. 6.9 TEMPERATURE DISTRIBUTION : Ra = 10^4

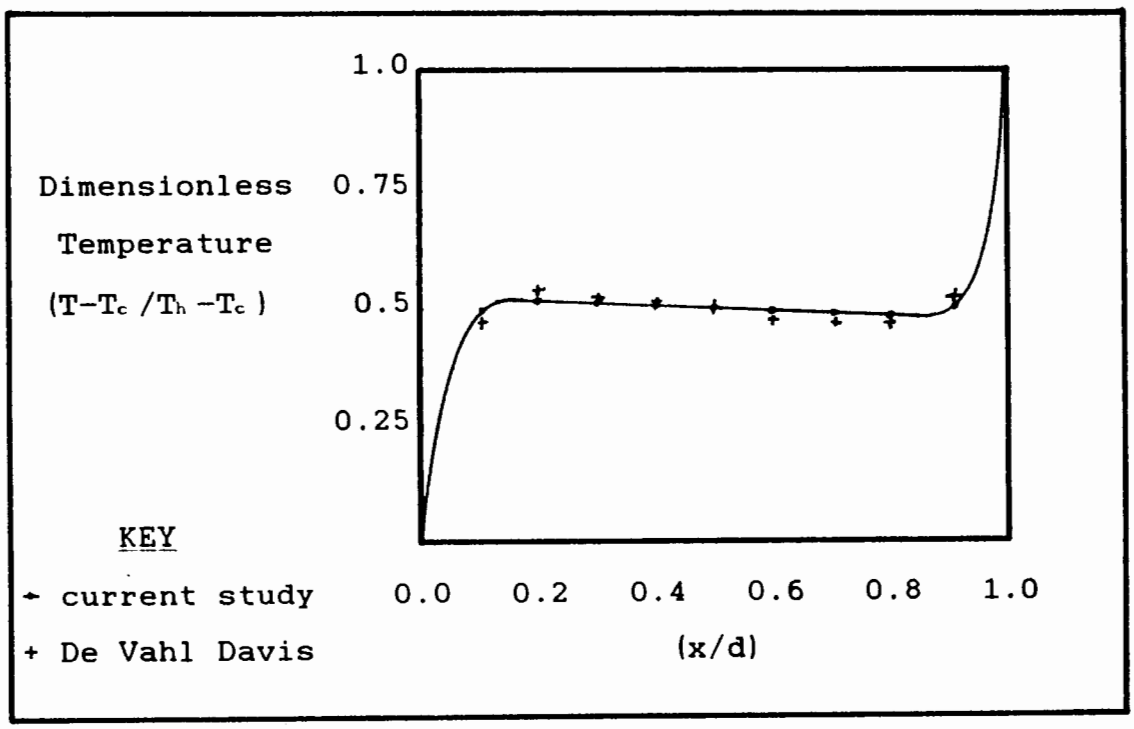

Fig. 6.10 TEMPERATURE DISTRIBUTION : Ra = 10^5, Pr = 1

10^3 is virtually linear which once again shows that the flow of heat across the cavity under these conditions is due almost entirely to conduction, as was deduced in the previous section. As the Rayleigh number increases however, convection becomes increasingly more significant, and the profiles show a progressive departure from linearity. The horizontal temperature gradient at the cavity midpoint becomes smaller, indicating that the amount of heat crossing the cavity directly by conduction is diminishing.

At $Ra=10^4$, the horizontal temperature gradient is, in fact, negative. This implies that the flow, now in the boundary layer regime, is so strong that the hot fluid has been carried over to the cold side of the cavity, and vice versa. Conduction in the central portion of the cavity is actually opposite to the overall direction of heat flow. Also, since the fluid flow is mainly in the vertical direction, very little convection occurs in this central region. At the largest Rayleigh number of 10^5, the horizontal gradient of temperature is almost zero, and this is consistent with the conclusion made by De Vahl Davis [65] that, as the Rayleigh number increases past $3.5x10^4$, the temperature gradient approaches zero.

6.1.4 Pressure Contours

The pressure contours for the various Rayleigh numbers are plotted in figs. 6.11 - 6.13. For the lower two Rayleigh numbers, these contours are nearly the hydrostatic distribution, although those for $Ra=10^4$ do show a distinct increase in the velocity from that experienced at $Ra=10^3$.

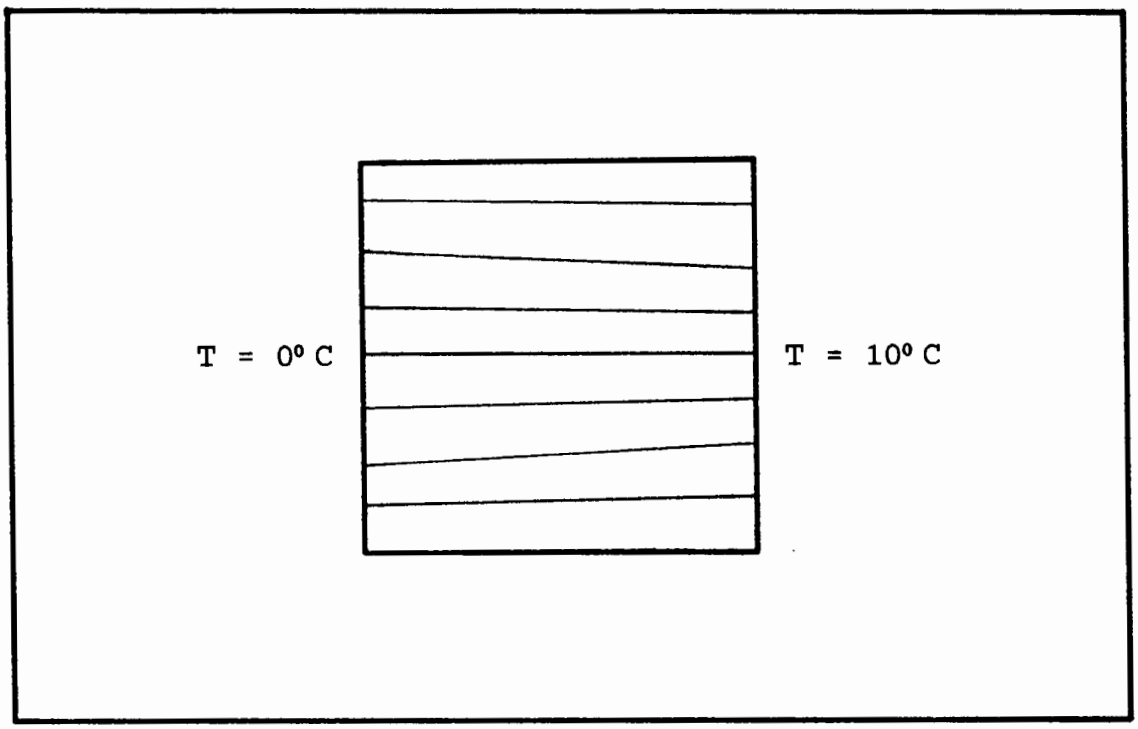

Fig. 6.11 PRESSURE CONTOURS : Ra = 10^3 , Pr = 1

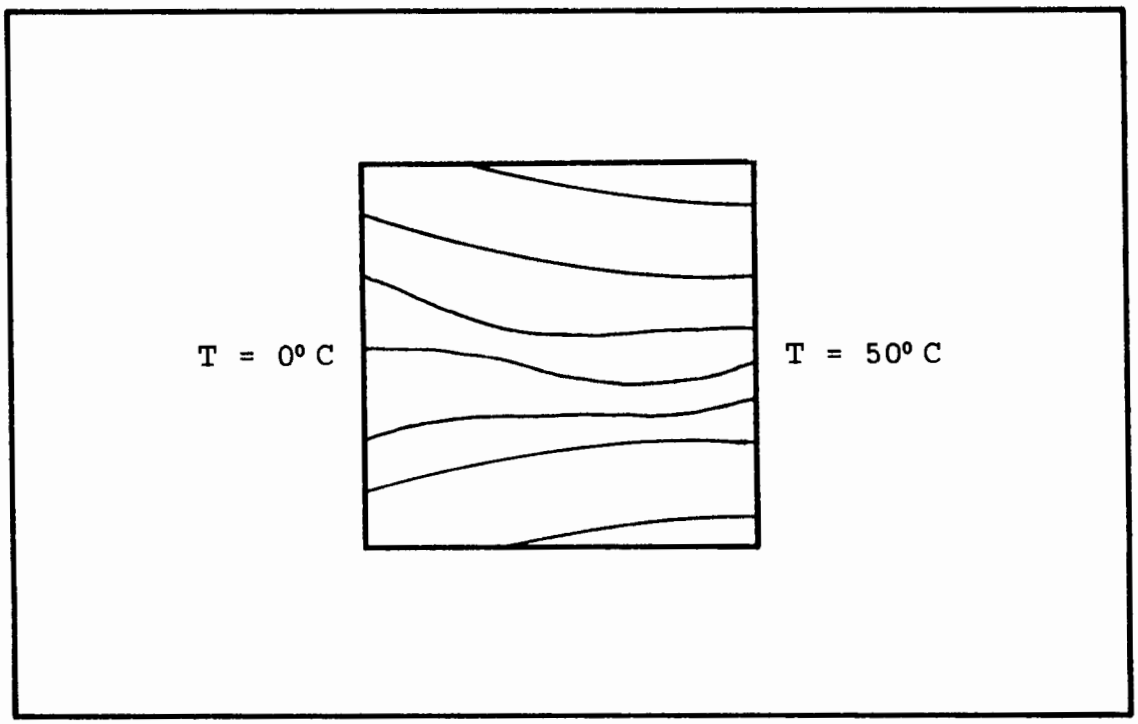

Fig. 6.12 PRESSURE CONTOURS : Ra = 10^4 , Pr = 1

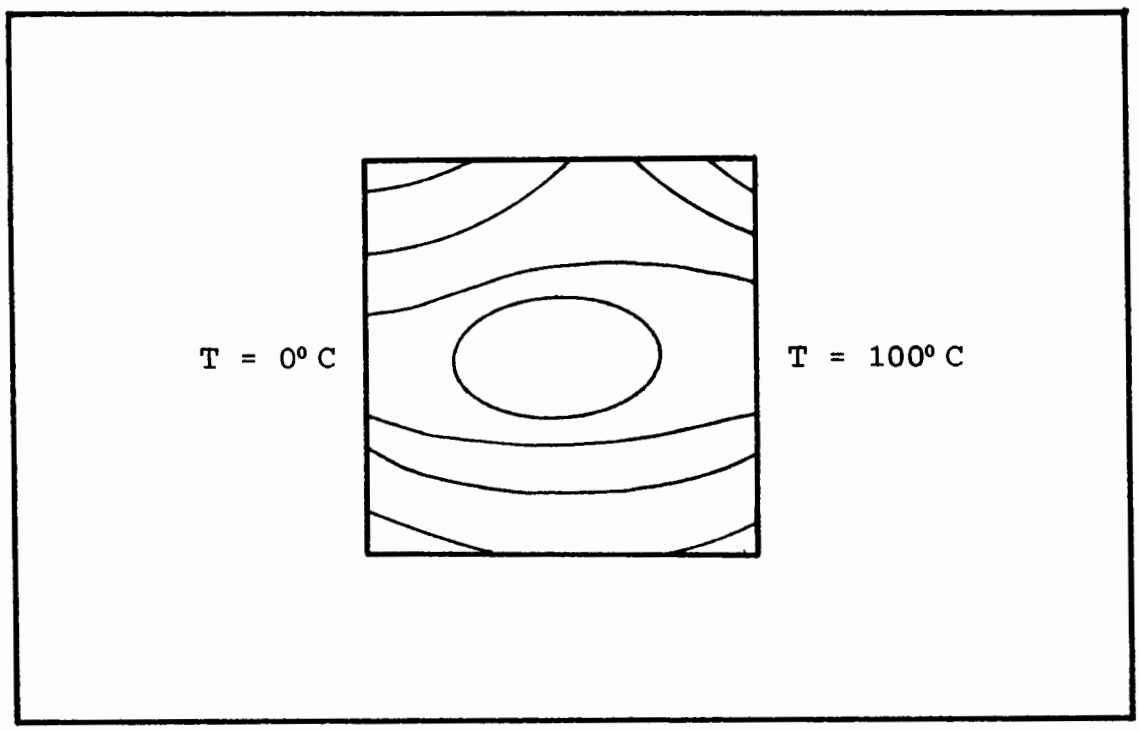

Fig. 6.13 PRESSURE CONTOURS : Ra = 10^5, Pr = 1

The increased fluid motion is more clearly demonstrated by the pressure contours at Ra=10^5 (see fig. 6.13), especially along the upper and lower walls of the cavity. The pressure contours plotted in these diagrams compare very well with those recently published by Schnipke and Rice [28].

6.1.5 Effect Of The Prandtl Number

As mentioned earlier, the Prandtl number was varied between 10^{-1} and 10 for Ra=10^3 and Ra=10^4. For Ra=10^3 (see fig. 6.2 and fig. 6.8), the results for the various Prandtl numbers were all within 1%-2% of each other for both the temperature and the velocity distributions. This lack of effect by the Prandtl number on the fluid motion

and temperature at low Rayleigh numbers was also observed by previous authors, who attributed it to the fact that the term containing the Prandtl number in the governing equations was neglible compared to the other terms, at these values of Rayleigh number.

As the Rayleigh number increased, so did the influence of the Prandtl number on the flow and the temperature, as can be seen in figs. 6.3 and 6.9. However, the results obtained for $Ra=10^4$ were still within 2%-8% of one another. Thus it can be deduced that the effect of the Prandtl number on the movement of the fluid and the temperature distribution is not neglible for $Ra>10^4$. This is consistent with the conclusions drawn by De Vahl Davis [65], as for higher Rayleigh numbers he found that the term containing the Prandtl number was no longer neglible.

6.1.6 Comparison With Previous Results

The slight variations between the results of the current analysis of the thermally driven window cavity, and those quoted by previous authors, can be ascribed to the comparatively coarse mesh used in this study. However, a coarse mesh does have advantages, in that computer execution times and storage requirements are reduced.

For the Rayleigh numbers less than 10^5 all the results were within 3% of those published by De Vahl Davis [65] and Schnipke and Rice [28]. At the highest Rayleigh number the results were found to agree to within 5% of the above authors. The reason for the decrease in accuracy as the Rayleigh number increased, is that the temperature

difference across the cavity was quite large, and thus steep temperature gradients existed in some of the elements.

6.2 VERTICAL SLOT RESULTS

An extension of the square cavity problem investigated in the previous section, is the thermally driven vertical slot, which has been studied experimentally by Elder [62], and numerically, using the finite element method, by Reddy and Satake [23].

The geometry and boundary conditions for the thermally driven vertical slot are shown in fig. 6.14. Results have been obtained for Rayleigh numbers (based on the width of the slot) between 10^3 to 10^5, and for height/base (h/b) ratios between 1.2 and 10. For ease of comparison with the results of Reddy and Satake [23], all the plots in this section are for an (h/b) ratio of 3. In each case, the cooler wall is on the left side of the slot, and the upper and lower walls are assumed to be adiabatic. Both square (sq) and irregularly-shaped (irr) 25 element meshes are used to determine the effect, if any, that the element shape has on the flow, and temperature and pressure distributions.

6.2.1 Vertical Velocity Components

Profiles of the vertical velocity components at the mid-height of the slot (see fig. 6.15) show the development of

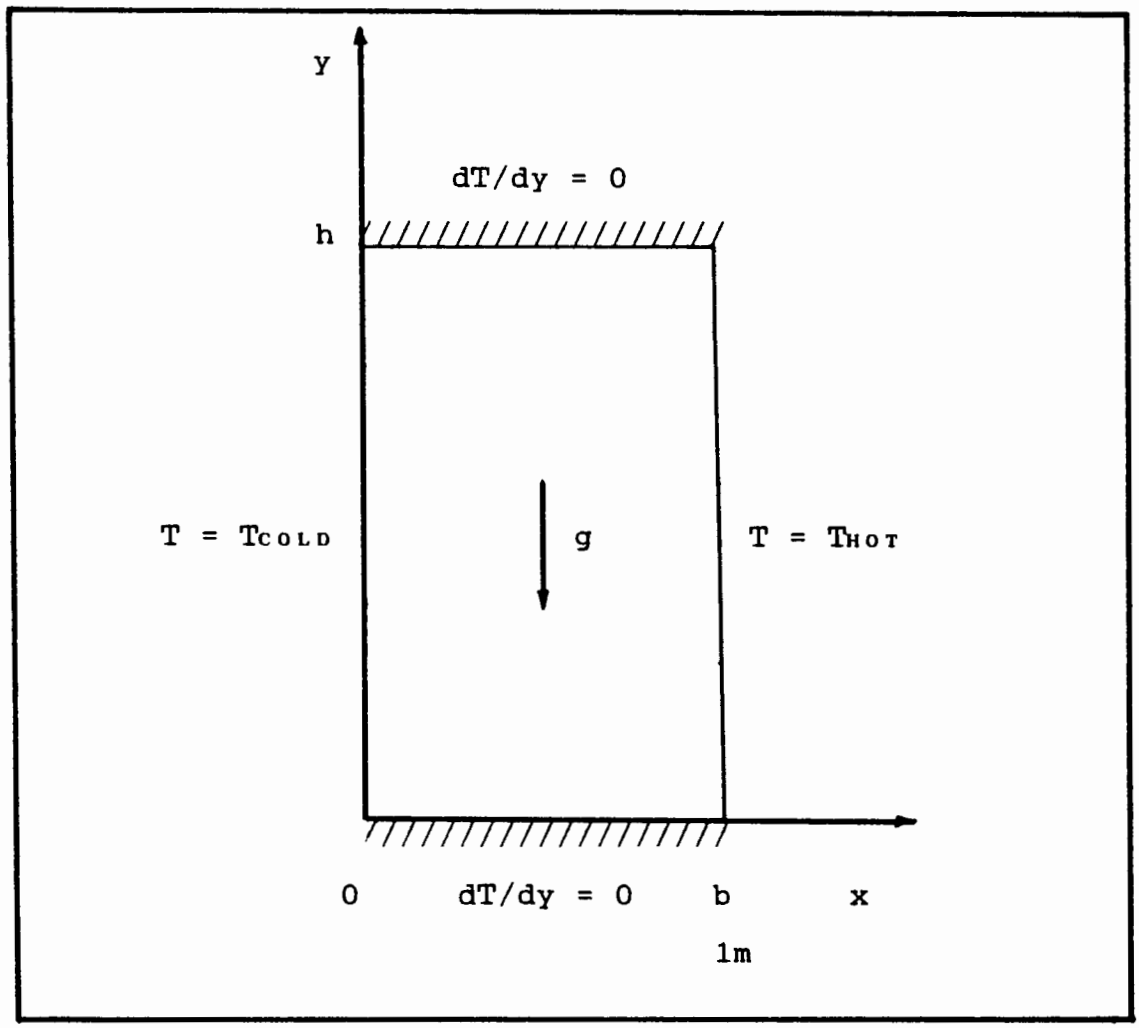

Fig. 6.14 GEOMETRY AND BOUNDARY CONDITIONS OF SLOT

the fluid motion as the Rayleigh number increases. At $Ra=10^3$, the velocity of the fluid is low, indicating that very little convection heat transfer takes place under these conditions. At $Ra=10^4$, the fluid motion has increased and a distinct boundary layer near the walls has become evident.

At the Rayleigh number of 10^5, a double eddy occurs near the centre of the slot. This implies that the boundary layer flow at this stage is so well established that the

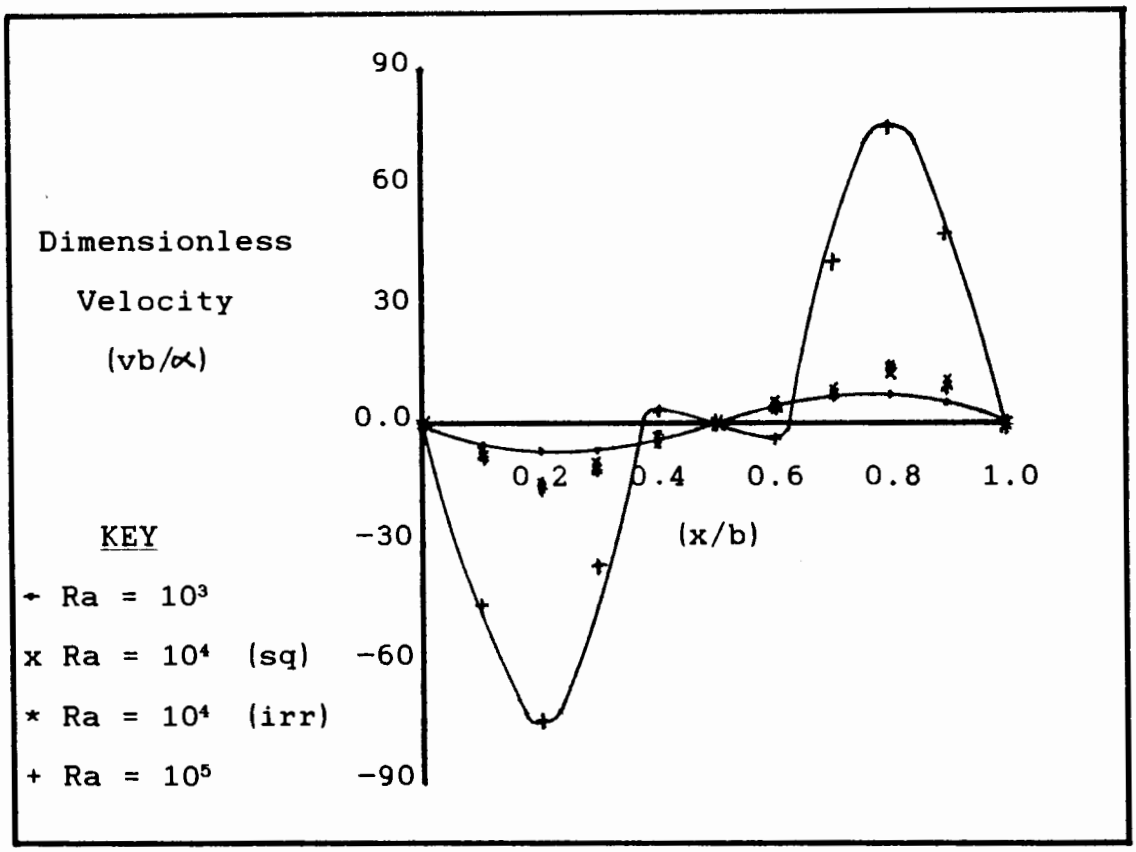

Fig. 6.15 VERTICAL VELOCITY COMPONENTS

strong vorticity near the walls is able to sustain a weaker reverse flow in the outer portion of the boundary layer is less able to influence.

6.2.2 Isotherms

The isotherm distributions for the vertical slot are shown in figs. 6.16 and 6.17. In these figures, each isotherm line represents a 10% variation in the temperature. For $Ra=10^3$, minimal distortion of the temperature distribution occurs, thus indicating that most heat transfer takes place by conduction at low Rayleigh numbers. For $Ra=10^4$ and 10^5, the isotherms become increasingly distorted,

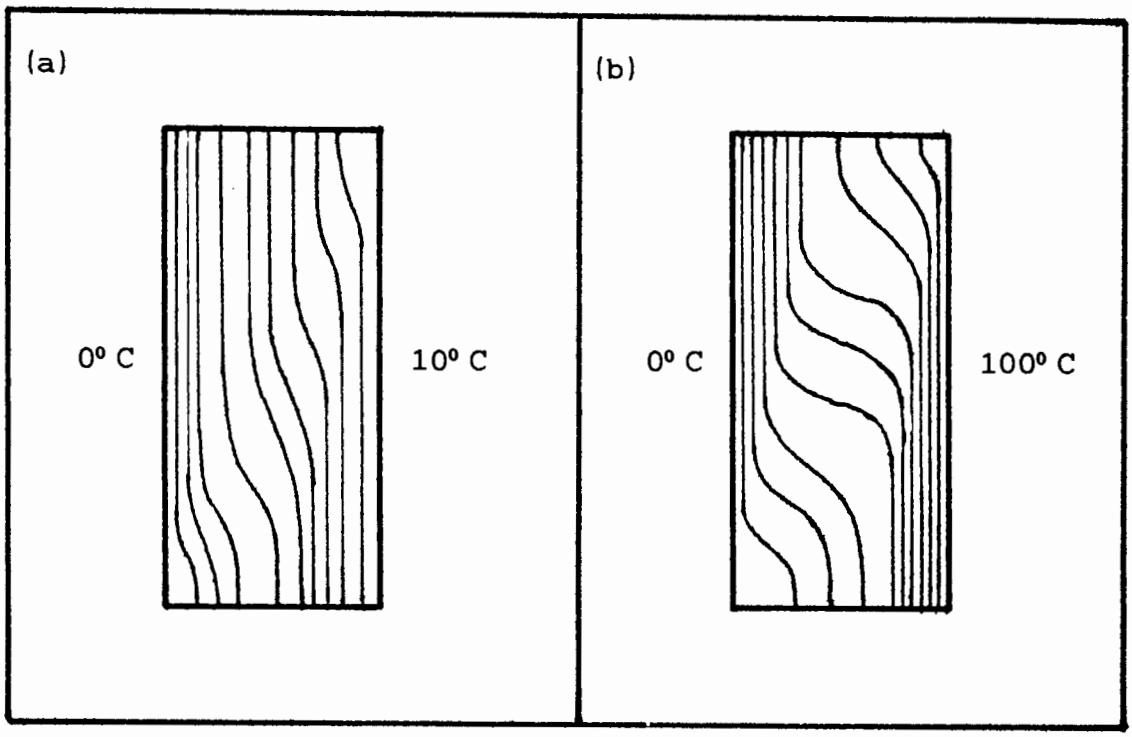

Fig. 6.16 ISOTHERMS : (a) Ra = 10^3, (b) Ra = 10^5

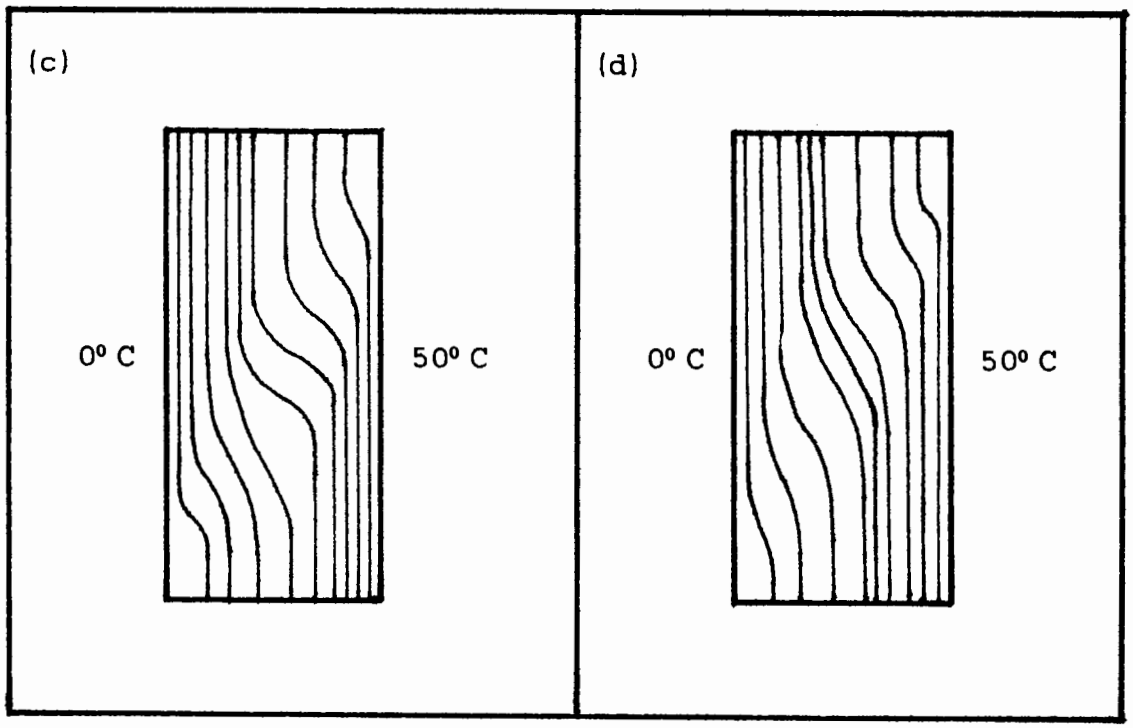

Fig. 6.17 ISOTHERMS : (c) Ra = 10^4 (Square Elements),
(d) Ra = 10^4 (Irregular Elements)

implying that more heat is being transferred by convection. These plots are in very good agreement with those published by Reddy and Satake [23], and are similar to those of the square cavity, except that the isotherm lines are more elongated.

6.2.3 Temperature Distributions

Profiles of the temperature distributions across the mid-height of the slot are displayed in fig. 6.20. The temperature increases in an approximately linear manner for $Ra=10^3$. This again implies that the heat transfer is largely due to conduction. Convection, however, becomes progressively more significant as the Rayleigh number increases in value, and the temperature profiles are

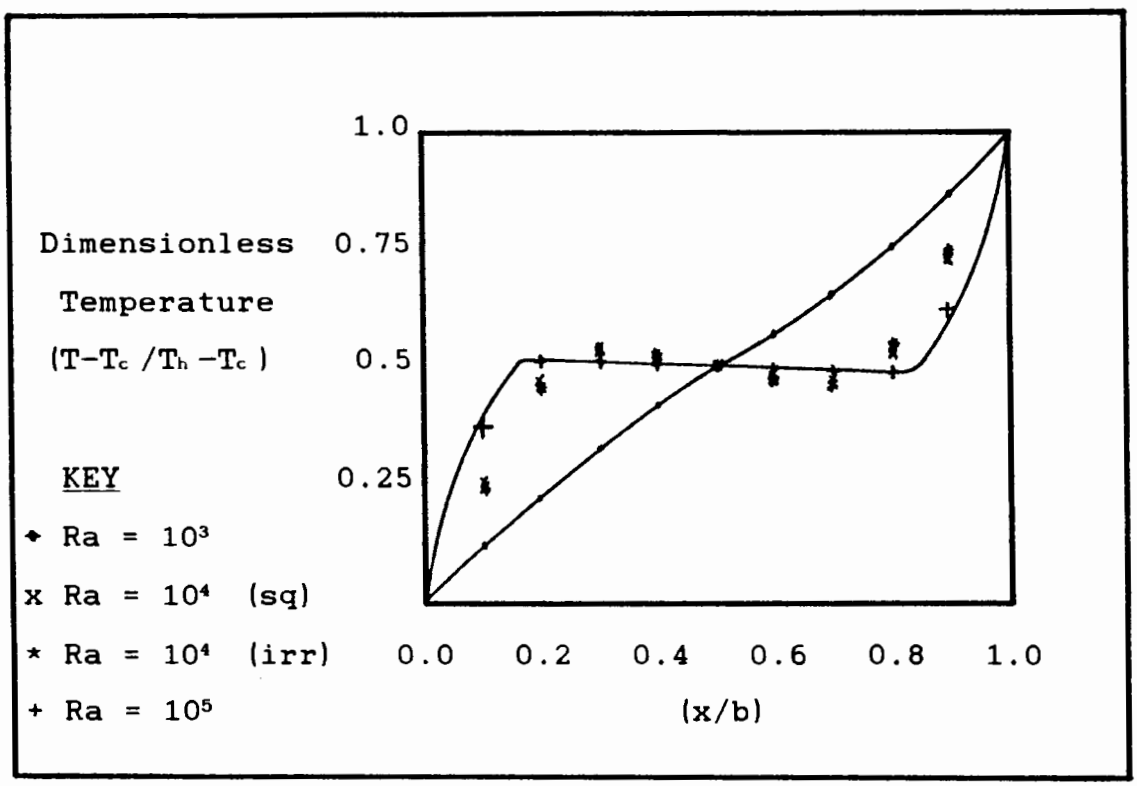

Fig. 6.18 TEMPERATURE DISTRIBUTIONS

consequently less linear. It should also be noted that, as Ra increases, the horizontal temperature gradient in the middle of the slot decreases, which shows that the heat transfer by pure conduction is diminishing.

As in the square cavity example, the horizontal temperature gradient for Ra greater than 10^4, is negative which suggests that the fluid motion is so strong that it carries the hot fluid to the cold side of the slot, and vice versa. This causes the conduction in the centre of the vertical slot to be opposite to the overall direction of the heat transfer. At $Ra=10^5$, the horizontal temperature gradient is almost zero, which is consistent with the results obtained for the square cavity.

6.2.4 Pressure Contours

The pressure contours for the vertical slot are shown in figs. 6.21-6.24. At the lowest Rayleigh number of 10^3, these contours almost exhibit a hydrostatic pressure distribution, which indicates a lack of fluid movement. At $Ra=10^4$, an increase in velocity is indicated by the departure of the pressure distribution from the hydrostatic case. This increased fluid motion is even more evident from the plot for $Ra=10^5$, especially along the upper and lower walls of the slot.

6.2.5 Effect Of The Irregular Elements

For $Ra=10^4$, both rectangular and irregular trapezoidal elements in a 6x4 mesh were considered to determine the effect of non-uniform elements on the results. For both

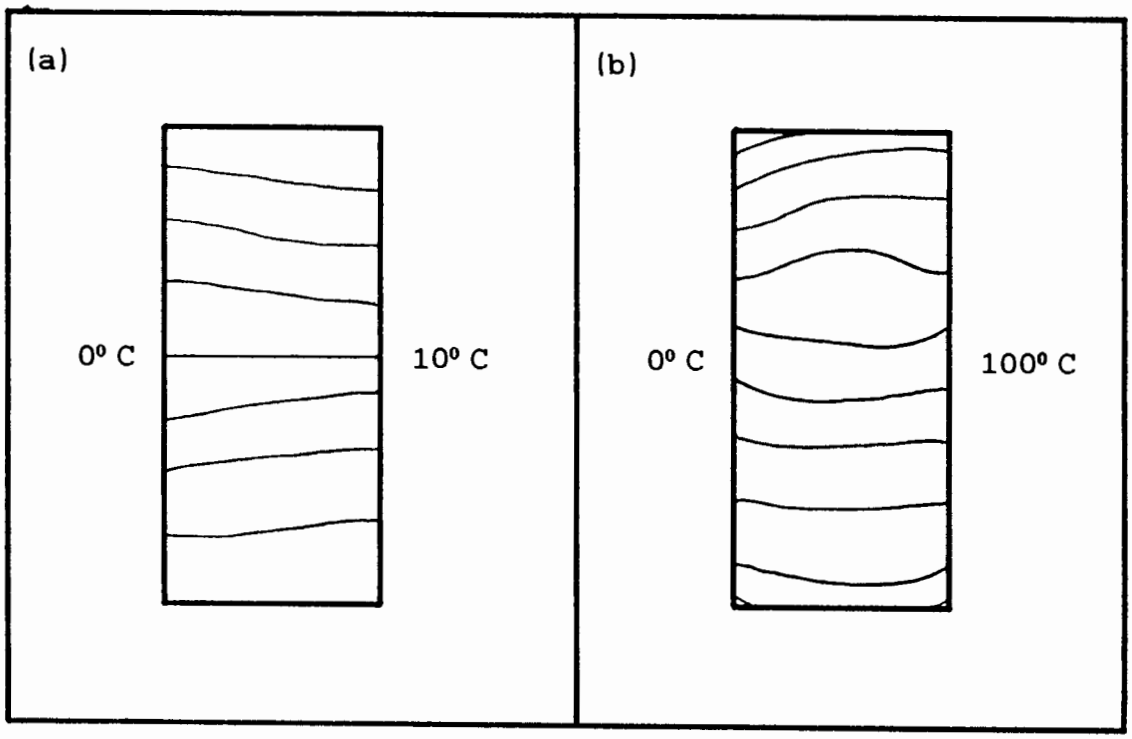

Fig. 6.19 PRESSURE CONTOURS : (a) Ra = 10^3 , (b) Ra = 10^5

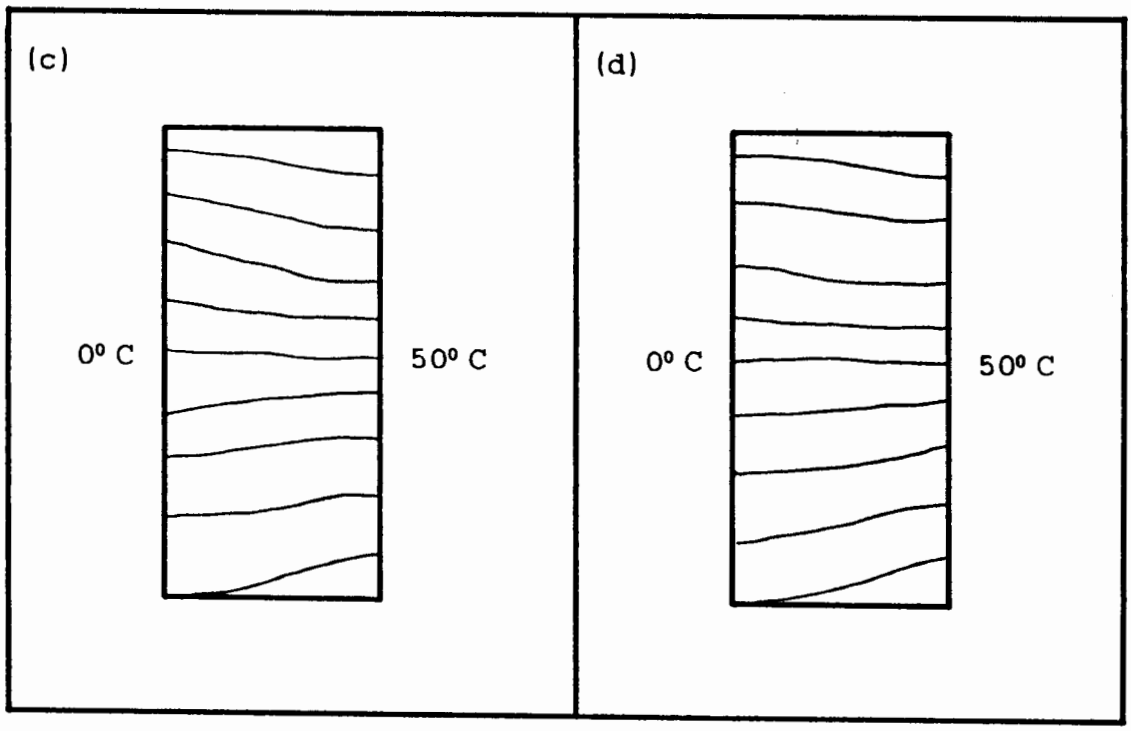

Fig. 6.20 PRESSURE CONTOURS : (c) Ra = 10^4 (Square Elements), (d) Ra = 10^4 (Irregular Elements)

the velocities and the temperatures, the results agreed to within 3%, and the results obtained for the pressure agreed to within 6%.

6.3 TRIANGULAR CAVITY RESULTS

The investigation of a triangular cavity is motivated by heat transfer problems such as pitched roofs with horizontal suspended ceilings and roof-type solar stills. For this study, it is assumed that the cavity is isosceles-triangular in section, so that the common boundary, the normal height of the cavity, can be taken as adiabatic, and only one half of the cavity need be considered.

The geometry and solution domain of the triangular cavity are shown below in fig. 6.21. Results have been computed for Rayleigh numbers between $4x10^3$ and $6.4x10^4$, and for height/base ratios between 0.25 and 1.0. These particular parameters were chosen to facilitate comparison with a paper presented by Akinsete and Coleman [82], who used finite difference techniques to analyse the same problem. In all cases, the hypotenuse is the hot wall, the base is the cold wall, and the wall normal to the base is adiabatic or insulated. The temperature singularity where the base and the hypotenuse intersect is assumed to be cold. For this example, a mesh of 20 square and triangular elements was used.

6.3.1 Vertical And Horizontal Velocity Components

In a similar manner to the previous examples, the vertical

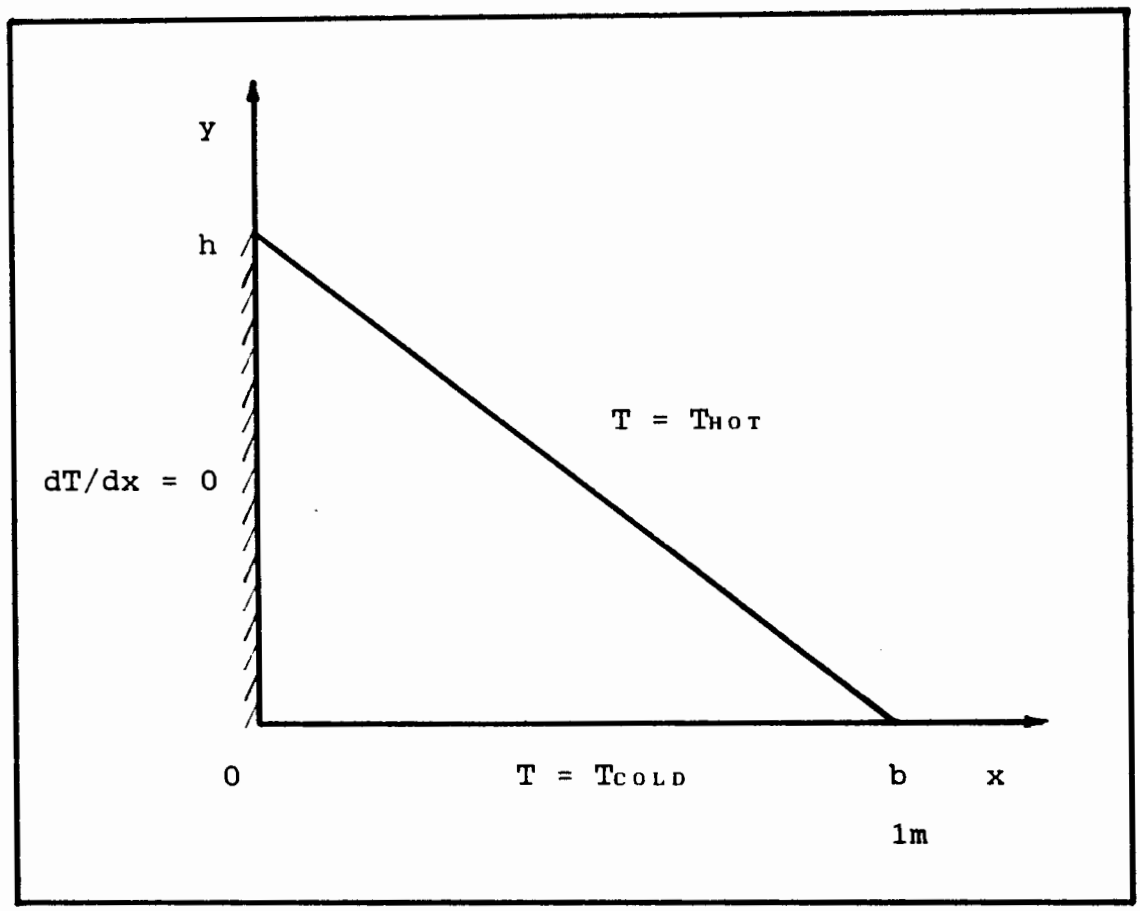

Fig. 6.21 GEOMETRY AND BOUNDARY CONDITIONS OF CAVITY

velocity components at the mid-height of the cavity are plotted in fig. 6.22. However, in order to obtain an overall view of the velocity distribution in the cavity, the horizontal velocity components midway along the base of the cavity are also plotted (see fig. 6.23). For $Ra=4x10^3$, very little fluid motion takes place. However, as the Rayleigh number increases, so the fluid moves with greater velocity, and a boundary layer begins to develop along the walls of the cavity. This phenomenon was also encountered by Akinsete and Coleman [82] in their research.

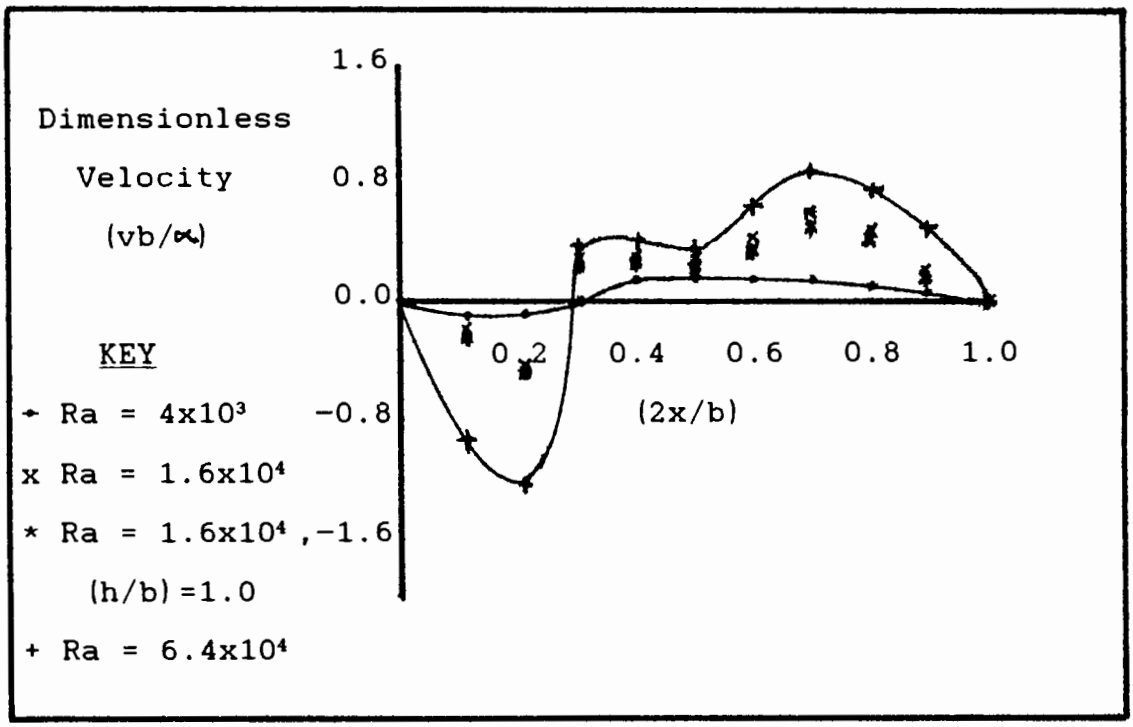

Fig. 6.22 VERTICAL VELOCITY COMPONENTS AT MID-HEIGHT

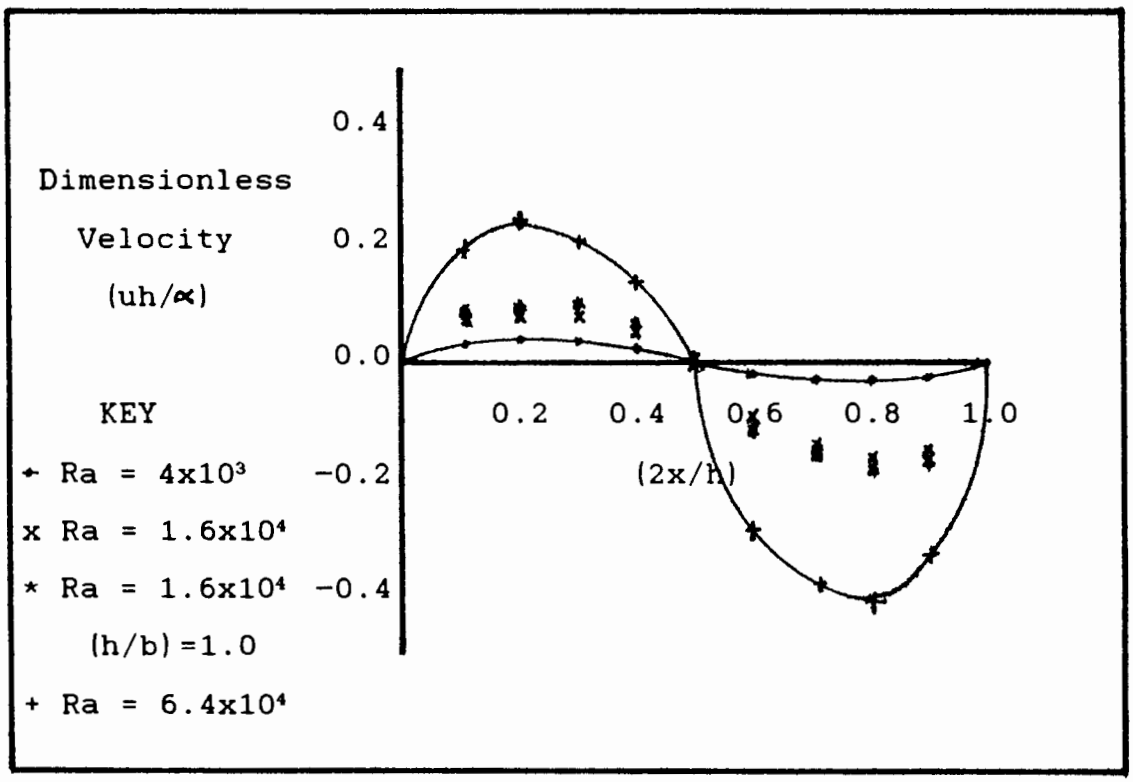

Fig. 6.23 HORIZONTAL VELOCITY COMPONENTS AT MID-WIDTH

6.3.2 Isotherms

Figs. 6.24-6.27 show the isotherm distributions for the triangular cavity for the Rayleigh numbers and (h/b) ratios under consideration. Each isotherm line represents a 10% change in the temperature. At both $Ra=4x10^3$ and $1.6x10^4$, the effect of convection on the isotherms is small, which implies that most of the heat transfer is occurring by means of conduction.

From fig. 6.27, it can be seen that a change in the isotherms distribution only occurs for relatively large Rayleigh numbers. For $Ra=6.4x10^4$, the effect of the adiabatic wall extends into the region of the cavity near the centre. The isotherms are pushed towards the hot wall for approximately the first quarter of the width of the

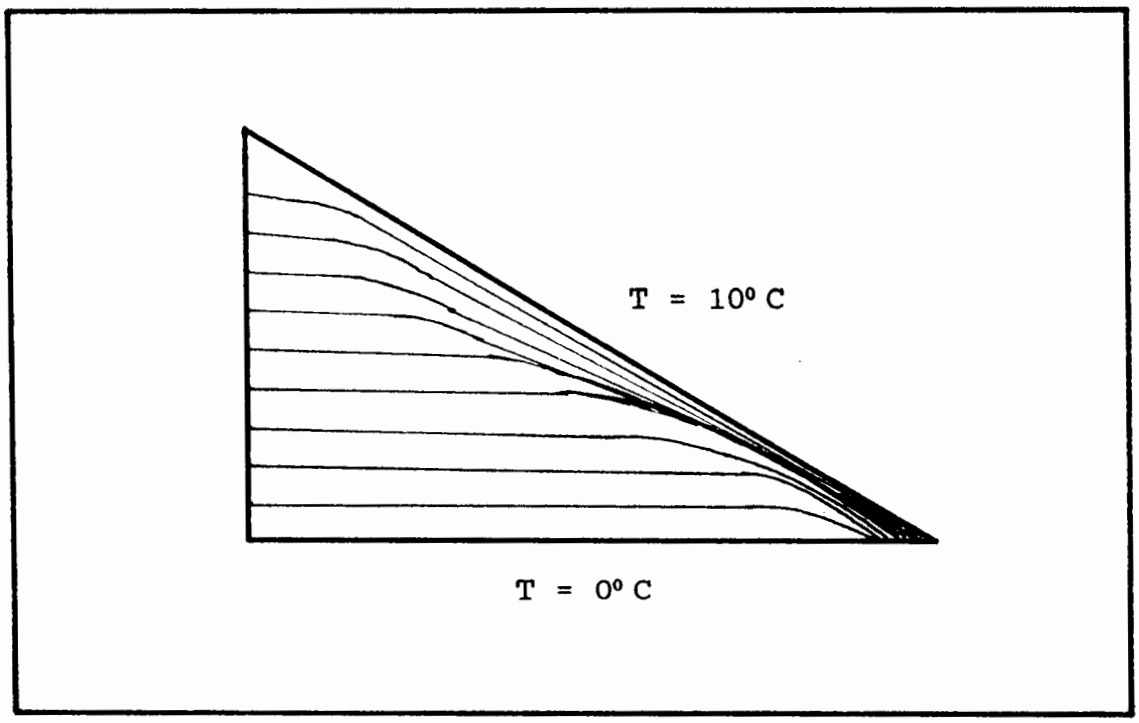

Fig. 6.24 ISOTHERMS : $Ra = 4x10^3$, $h/b = 0.25$

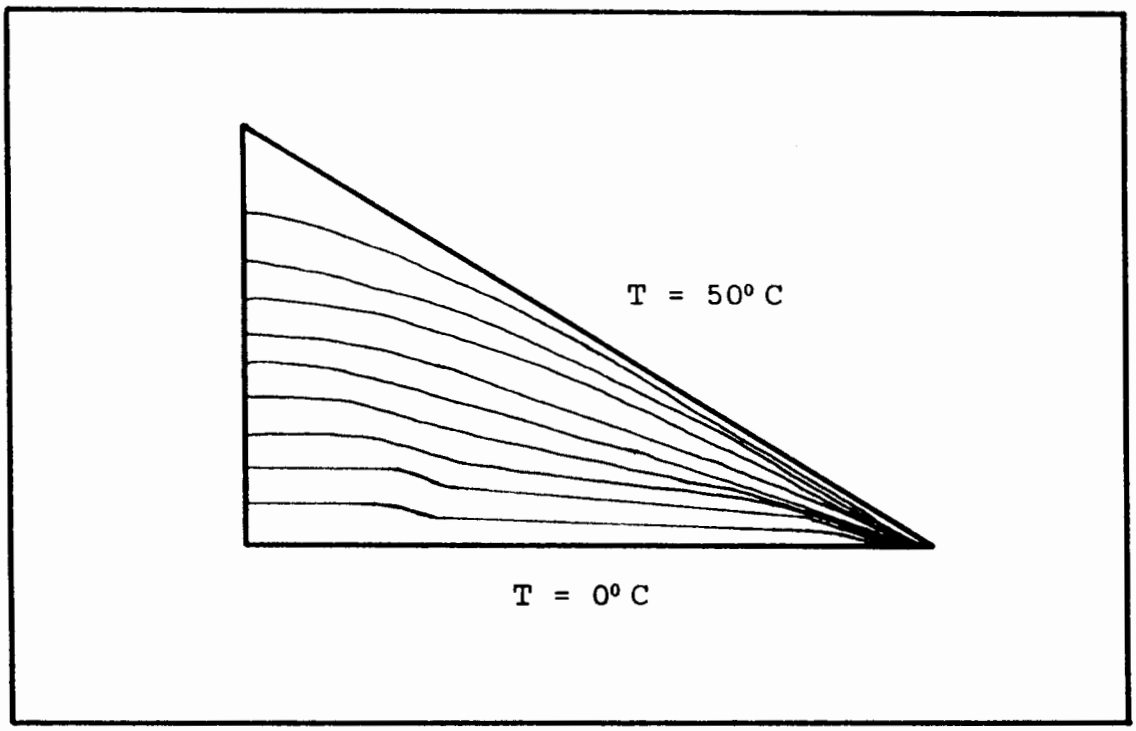

Fig. 6.25 ISOTHERMS : Ra = 1.6×10^4 , h/b = 0.25

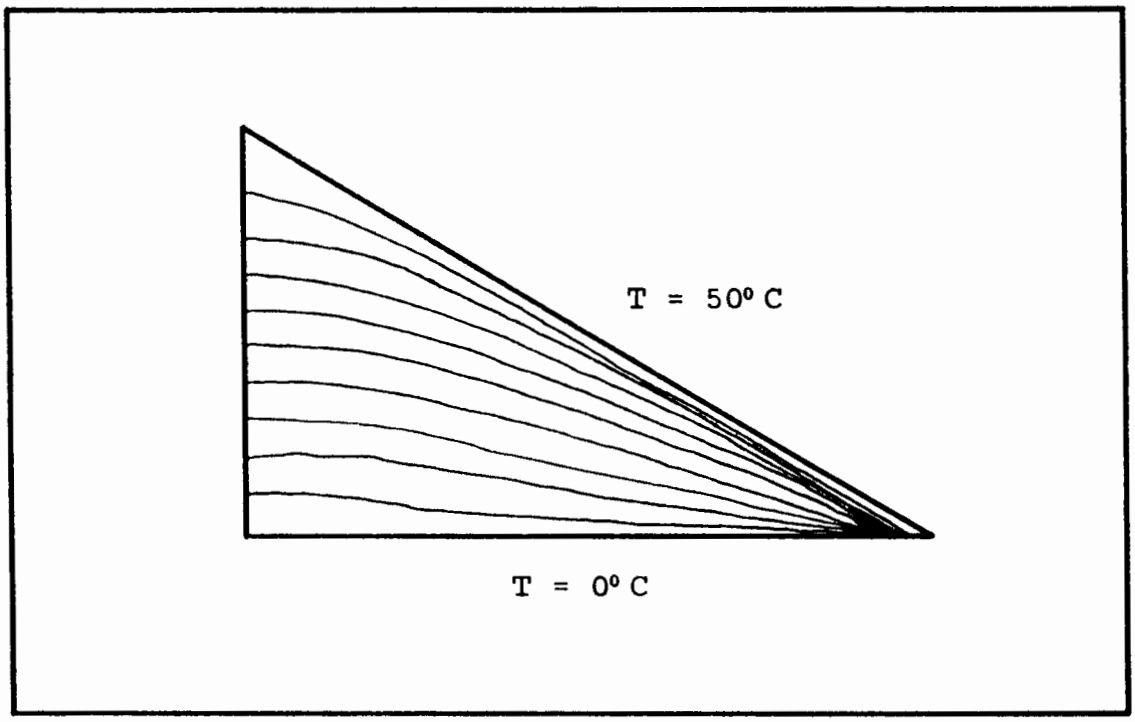

Fig. 6.26 ISOTHERMS : Ra = 1.6×10^4 , h/b = 1.0

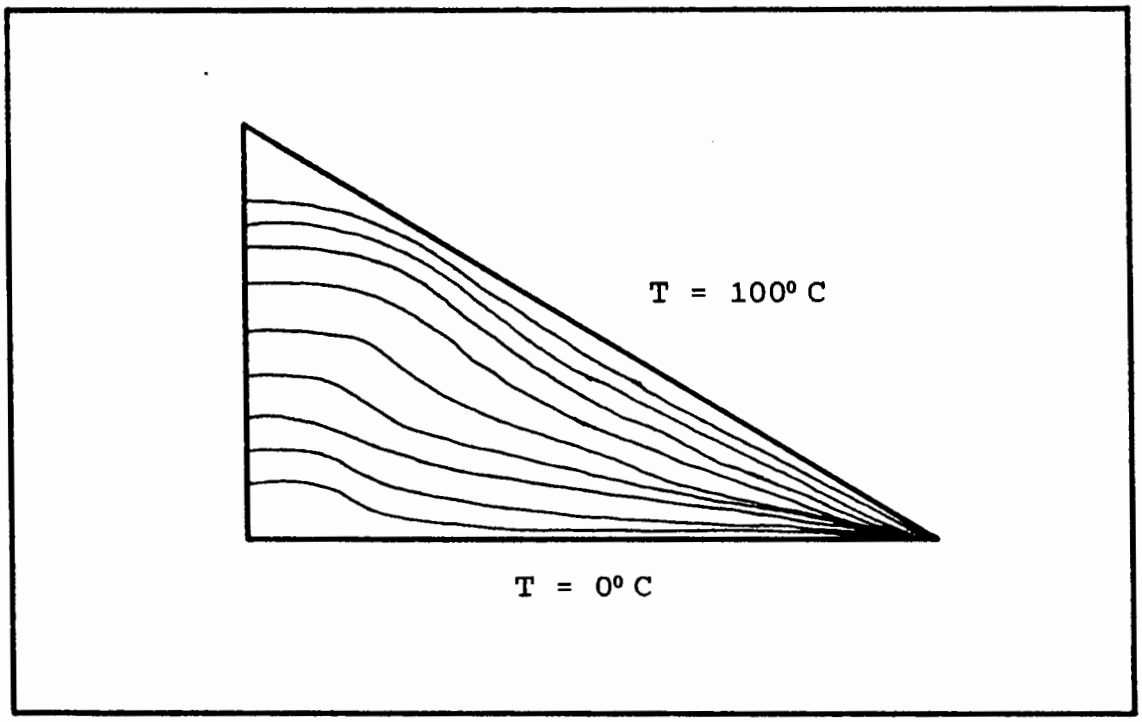

Fig. 6.27 ISOTHERMS : Ra = 6.4×10^4 , h/b = 0.25

cavity nearest the adiabatic wall. Thereafter, the isotherms are pushed downward toward the cold wall. This type of isotherm distribution implies that two boundary layers are being formed, one growing downward along the hot wall, and the other growing along the base towards the insulated wall. The sudden depression of the near-middle sections of the isotherms indicates the possibility of seperation occurring in the flow around these sections. The isotherm plots were all in excellent agreement with those published by Akinsete and Coleman [82].

6.3.3 Pressure Contours

The pressure contours for the triangular cavity are shown in figs. 6.28-6.31. For the lower Rayleigh number, 4×10^3 ,

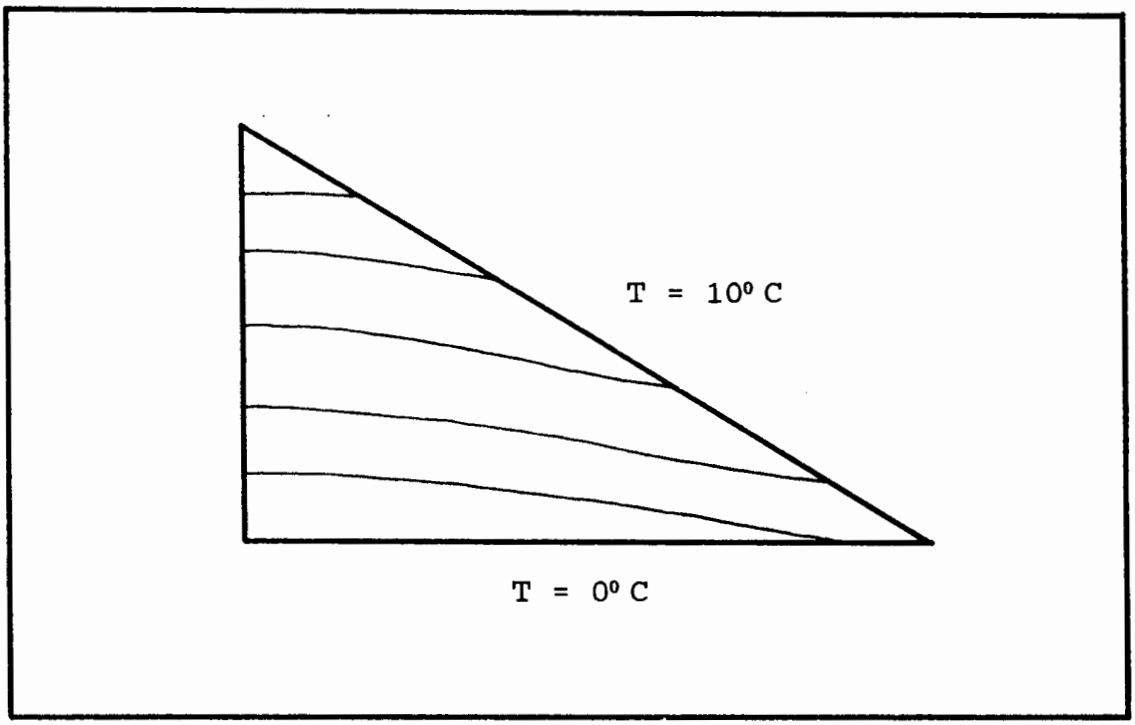

Fig. 6.28 PRESSURE CONTOURS : Ra = 4×10^3 , h/b = 0.25

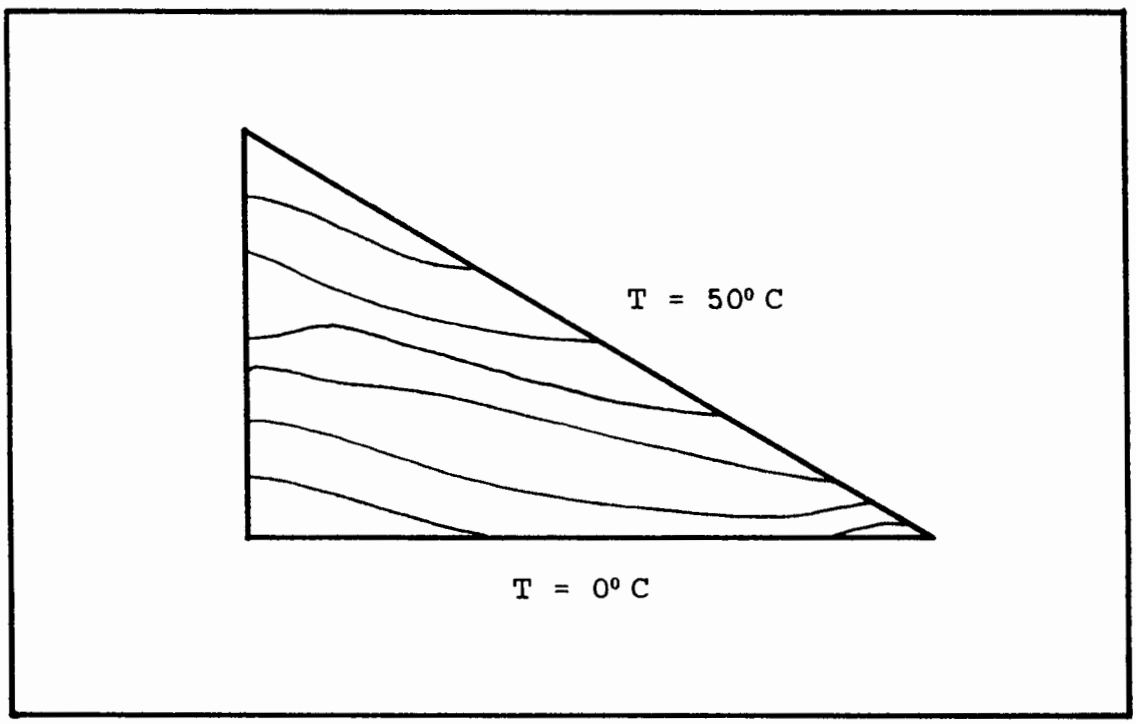

Fig. 6.29 PRESSURE CONTOURS : Ra = 1.6×10^4 , h/b = 0.25

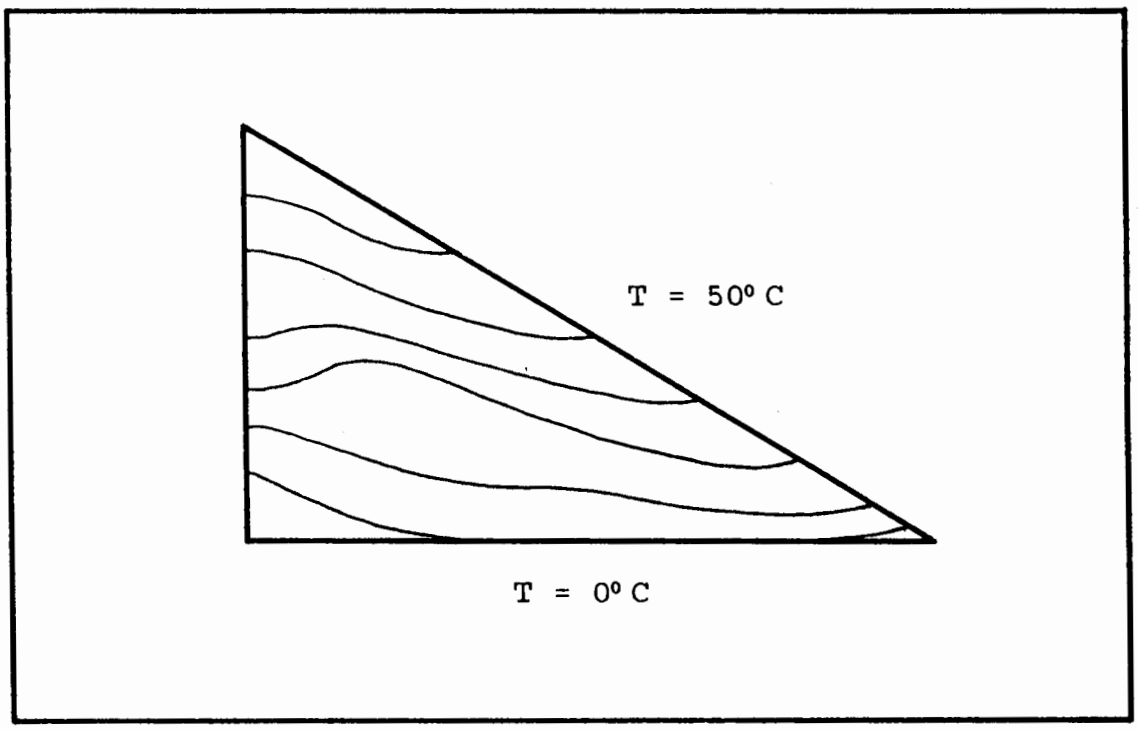

Fig. 6.30 PRESSURE CONTOURS : Ra = 1.6×10^4 , h/b = 1.0

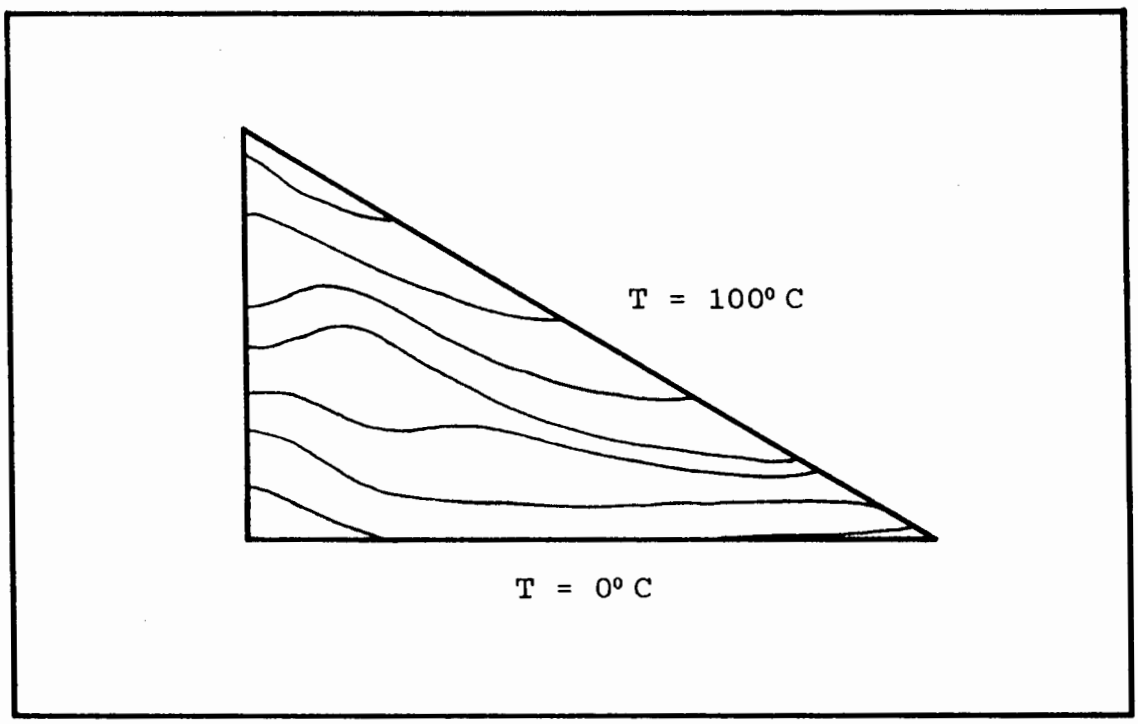

Fig. 6.31 PRESSURE CONTOURS : Ra = 6.4×10^4 , h/b = 0.25

these contours are approximately the hydrostatic distribution, indicating very little fluid motion and thus minimal heat transfer by convection. The fluid motion increases with an increase in Rayleigh number, as evidenced by the distortion of the pressure contours from the hydrostatic distribution. The increase in velocity is especially noticeable along the hypotenuse and base walls.

6.3.5 Effect Of The (h/b) Ratio

Figs. 6.22-6.31 show that, for $Ra=1.6x10^4$, an increase in the (h/b) ratio from 0.25 to 1.0 has the effect of increasing the temperature by as much as 60%, the velocities by approximately 100%, and the pressure by approximately 50%.

6.4 LIQUID CONVECTIVE DIODE RESULTS

A liquid convective diode is a passive solar heated device which transports heat preferentially in one direction i.e. heat that is collected at the surface of a building is transported to the inside by the diode, but cannot readily escape from the building along the same path. Representative dimensions and boundary conditions of the liquid convective diode are shown in fig. 6.32. The diode consists of a liquid-filled rectangular reservoir connected to a vertical slot or tongue. Insulation separates the reservoir from the outer wall of the building, which reduces the heat loss to the outside when the tongue is not sunlit.

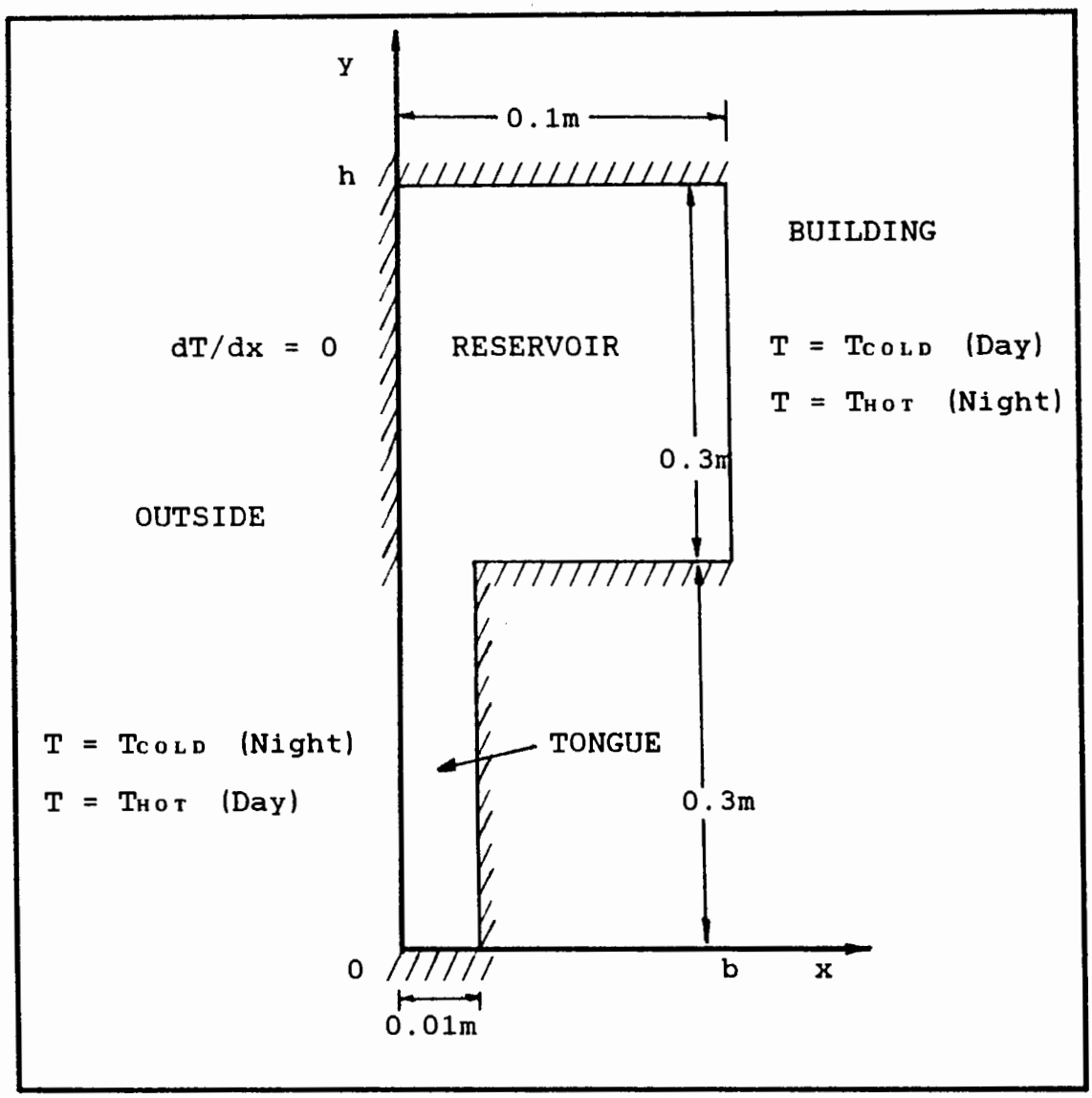

Fig. 6.32 GEOMETRY AND BOUNDARY CONDITIONS OF DIODE

During the day, when the tongue is irradiated, heat is transferred within the diode from the hot diode to the cooler reservoir, and from there to the inside of the building. This is termed the warm-up phase. During sunless periods, the tongue cools from exposure to the outside, and heat is transferred from the warm reservoir to the cooler tongue. This is known as the cool-down phase. In this study, a Rayleigh number (based on the width of the

reservoir) of 600 is used for the warm-up phase, whereas for the cool-down phase, the Rayleigh number is 300. These figures are based on average temperatures during these periods quoted by Jones [83], who studied this example using the finite difference method. For the finite element modelling of this problem, a mesh of 24 elements is used.

6.4.1 Vertical Velocity Components

Plots of the vertical velocity components at the mid-height of the reservoir of the diode for both the warm-up phase and the cool-down phase are shown in fig. 6.33.

During the warm-up phase, the fluid flows upwards along the outer wall of the diode, since the tongue is being

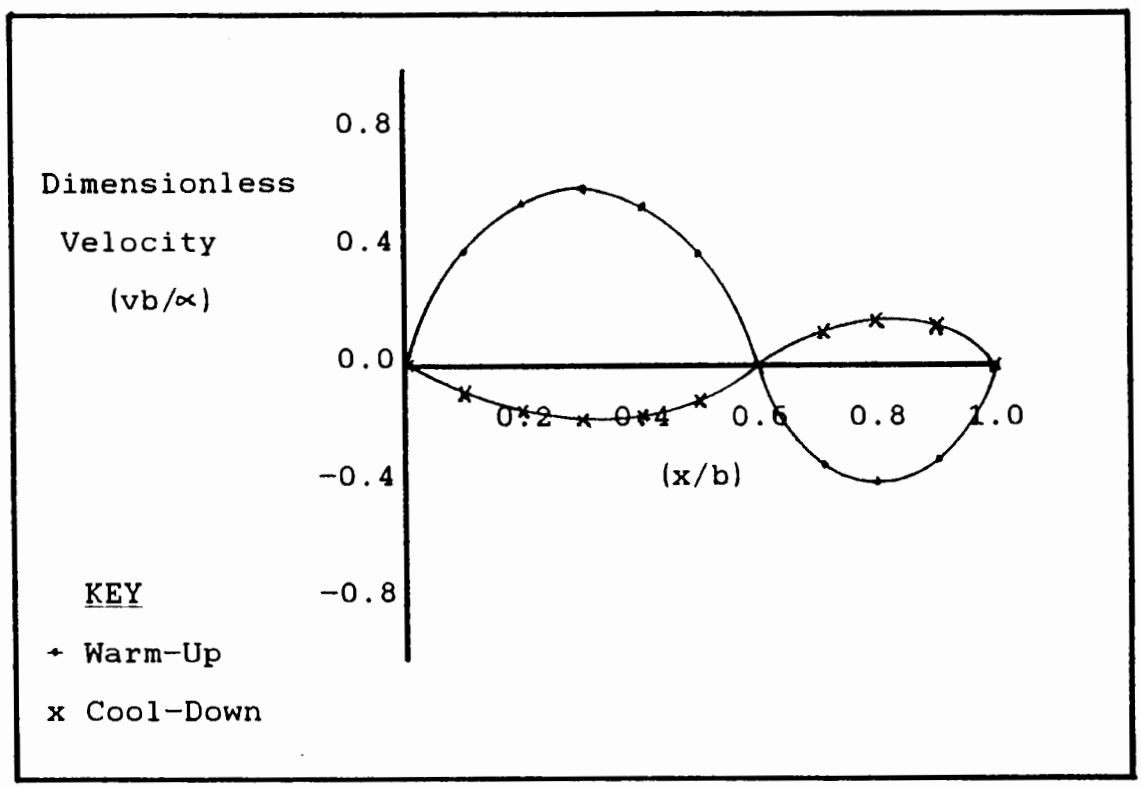

Fig. 6.33 VERTICAL VELOCITY COMPONENTS

irradiated by the sun, and downwards near the cool wall of the reservoir on the inside of the building. The velocity of the fluid is greater near the outside of the building than at the inside, with very little flow occurring at the centre of the reservoir. During the cool-down phase, the direction of the flow is reversed since the overall temperature difference is in the opposite direction to that of the warm-up phase. Also, during the cool-down phase, the fluid velocities are much lower, which can be ascribed to the smaller temperature gradient that exists across the diode. The velocity profiles are not symmetrical (a) due to the presence of the tongue, and (b) due to the fact that three of the walls of the reservoir are insulated.

6.4.2 Isotherms

Figs. 6.34 and 6.35 show the isotherm distributions for the liquid diode during the warm-up and cool-down phases. Each isotherm line represents a 10% change in temperature. During the warm-up phase, the isotherms are pushed upward on the outside wall of the reservoir and downward nearer the inner side. This indicates that convection occurs from the warm tongue to the higher-placed, cooler reservoir.

During the sunless periods, the tongue cools from exposure to the outside and the temperature distribution in most of the diode attempts to stabilize the fluid, and convection nearly ceases. This is evident from the lack of distortion of the isotherm distribution. During this phase, the dominant heat loss mechanism from the reservoir to the outside is by conduction through the tongue.

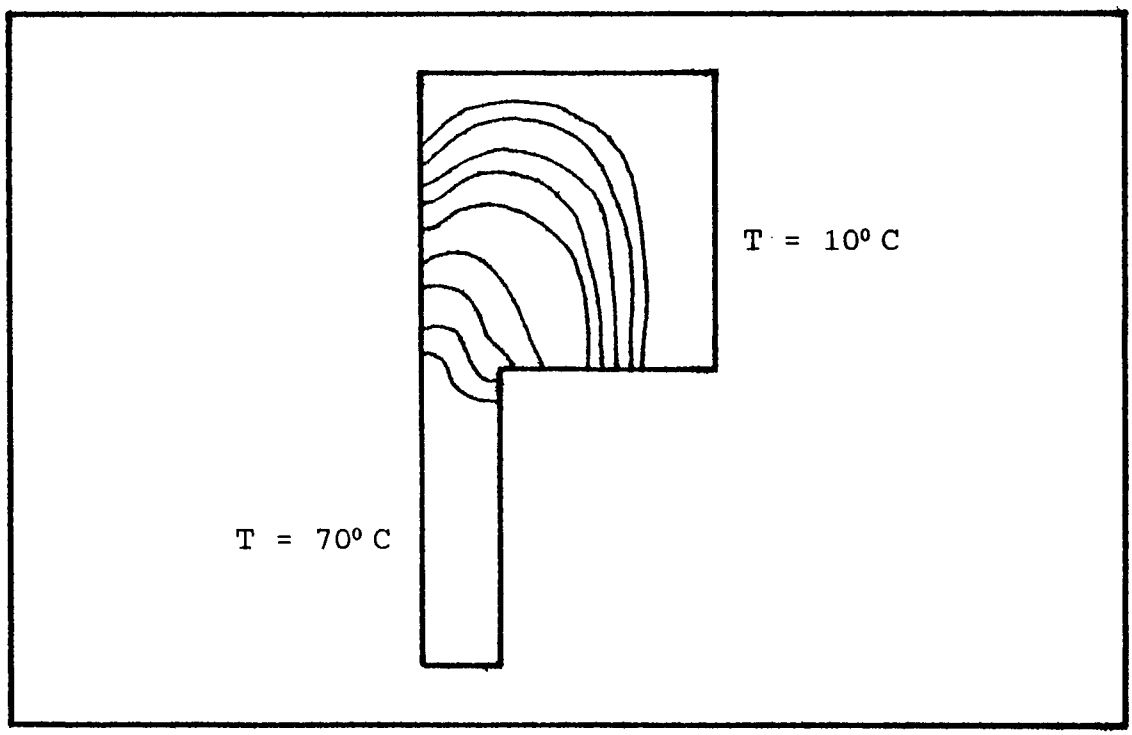

Fig. 6.34 ISOTHERMS : Ra = 600 (Warm-up Phase)

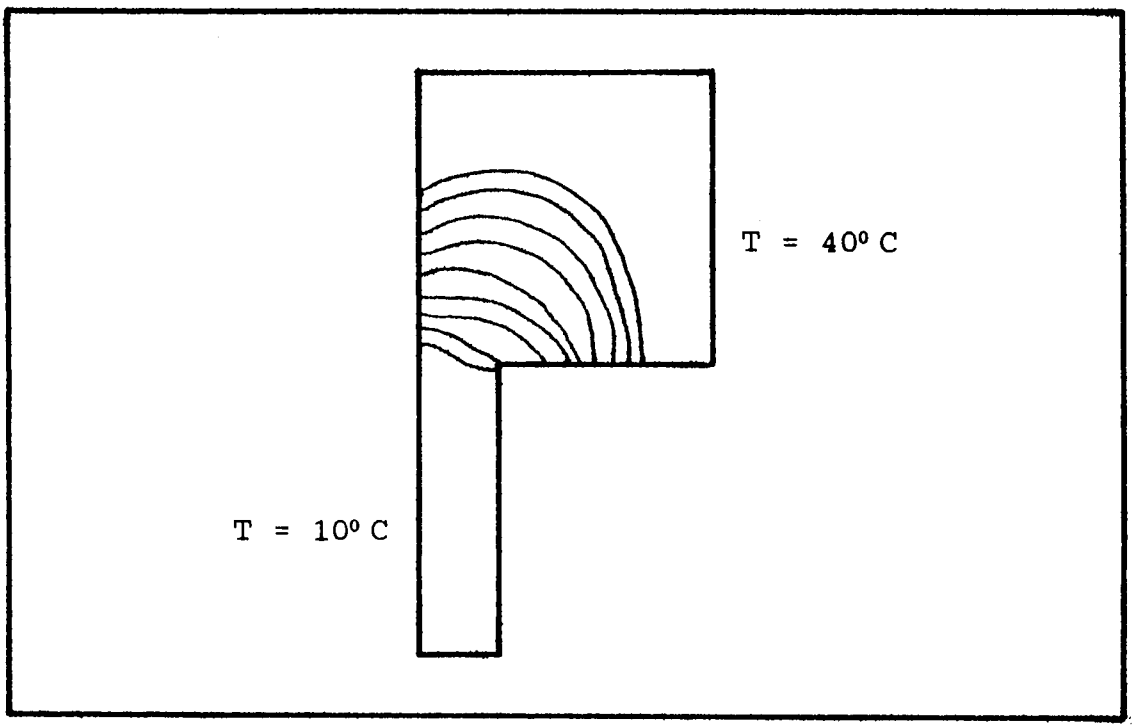

Fig. 6.35 ISOTHERMS : Ra = 300 (Cool-down Phase)

Thus a diode with a high efficiency can be obtained if a poorly conducting fluid is used in the diode.

6.4.3 Pressure Contours

The pressure contours during the warm-up phase (see fig. 6.36) show that fluid motion occurs in the reservoir, but that very little movement occurs in the lower portion of the tongue. During the cool-down phase, (see fig. 6.37) the pressure distribution is nearly hydrostatic in both reservoir and tongue, indicating that the fluid is moving with minimal velocity throughout the diode.

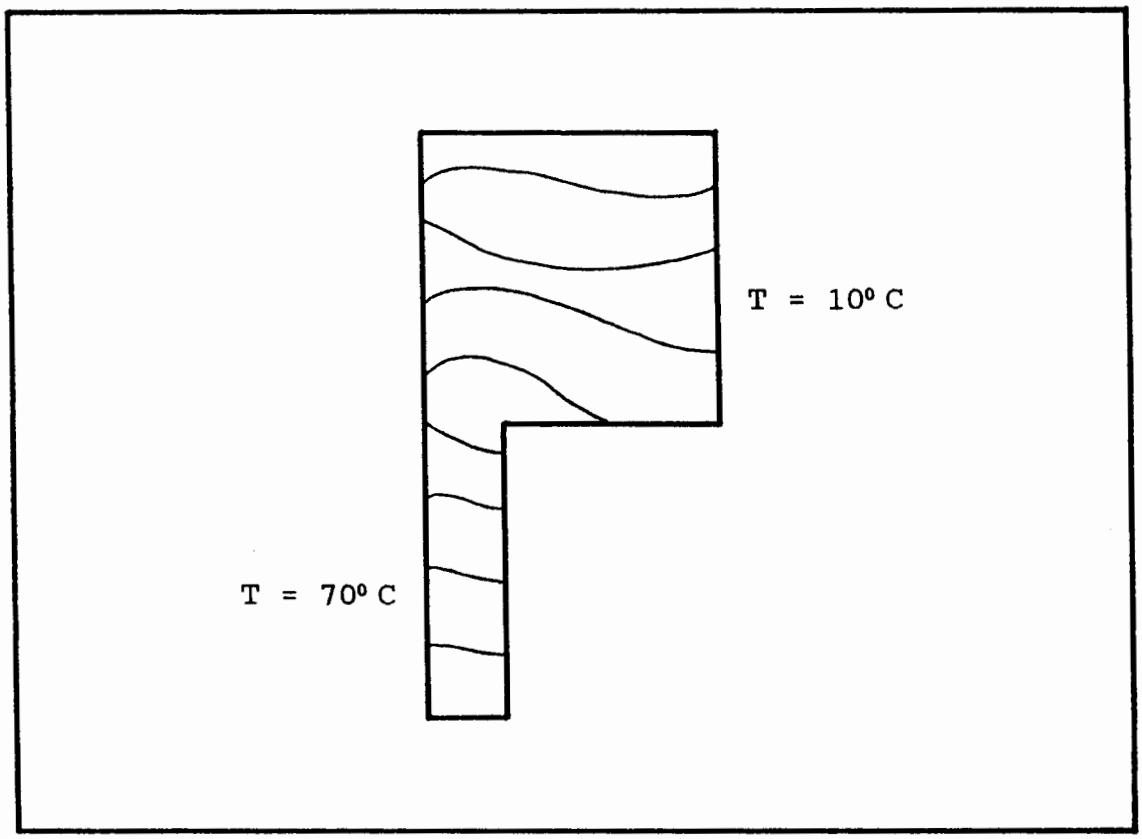

Fig. 6.36 PRESSURE CONTOURS : Ra = 600 (Warm-up Phase)

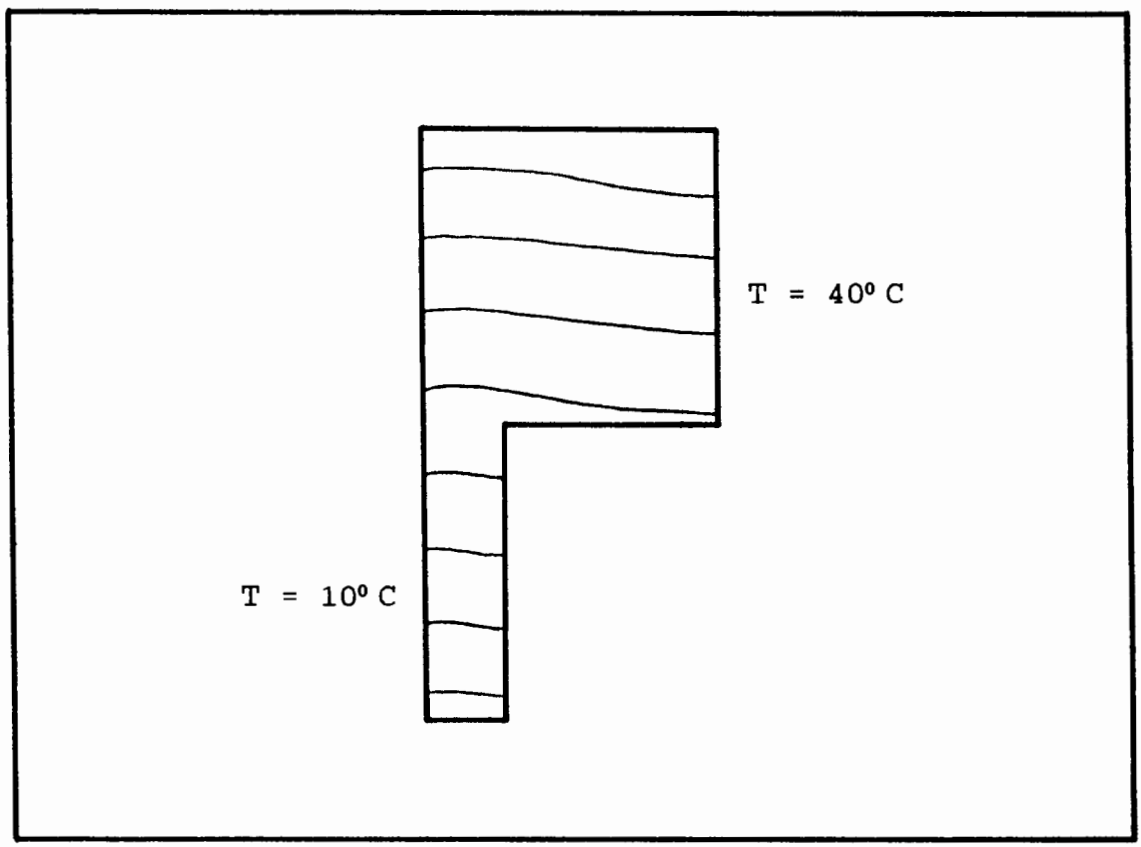

Fig. 6.37 PRESSURE CONTOURS : Ra = 300 (Cool-down Phase)

6.5 COOLING POND RESULTS

As stated at the beginning of this chapter, very little data is available for the comparison of the results of this example. However, the research that has been conducted has identified a definite need in this area, as increasing concern about heat pollution of streams, rivers and lakes has led government agencies to set more stringent regulations on the permissible temperature increase of bodies of water receiving heated discharges from power plants. At the same time, due to the ever-rising demand for power, the size of these plants has

steadily increased with a corresponding increase in the amount of waste heat.

Although the cooling water of a power plant usually contains no additives or impurities, it does alter the naturally-existing temperature balance in a body of water. The negative effect of heat addition, commonly referred to as thermal pollution, creates the need for any given project to be able to estimate the extent of this pollution both as to the area or volume encompassed and as to maximum temperature increase at any given point. The application of the current analysis to this type of problem enables estimates of this sort to be made quickly, efficiently and comparatively cheaply without having to resort to physical modelling of the problem. It is also advantageous in that changes to the parameters of a particular problem are easily implemented, and thus this technique greatly simplifies choosing the best possible design.

The geometry and solution domain for the plan view of a cooling pond containing a central dike are shown in fig. 6.38 below. This type of cooling pond was chosen as it corresponds to that of the nuclear power plant at Chernobyl, U.S.S.R., of which thermal photographs have recently been published by Edwards [84]. All the boundaries are insulated, except at the inlet and the outlet to the pond. As this example models the plan view, the gravity force is not applicable. The pond is assumed to be shallow, and heat losses by convection and conduction to the surrounding air are assumed to be negligible. A number of Reynolds numbers (based on the

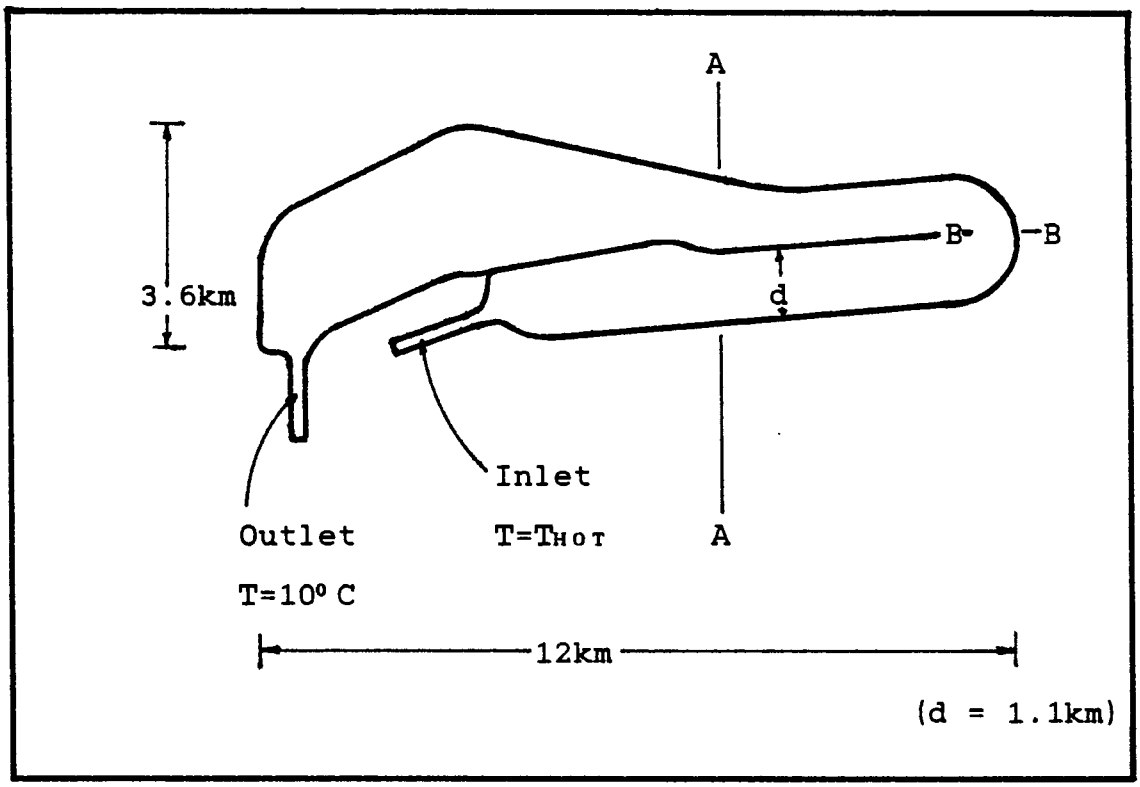

Fig. 6.38 GEOMETRY AND BOUNDARY CONDITIONS OF POND

input velocity) between 25 and $5x10^2$ were considered but, as the variations of the velocity temperature and pressure plots were negligible, only those obtained for $Re=10^2$ are included below.

6.5.1 Velocity Components

As with the thermally driven window cavity, plots of the velocity components are used to illustrate the motion of the fluid. The geometric positions of these plots are indicated by sections A-A and B-B on fig. 6.38 above. From figs. 6.39 and 6.40, it can be seen that the larger temperature difference between inlet and outlet caused an increase in the velocity of the fluid in the cooling pond.

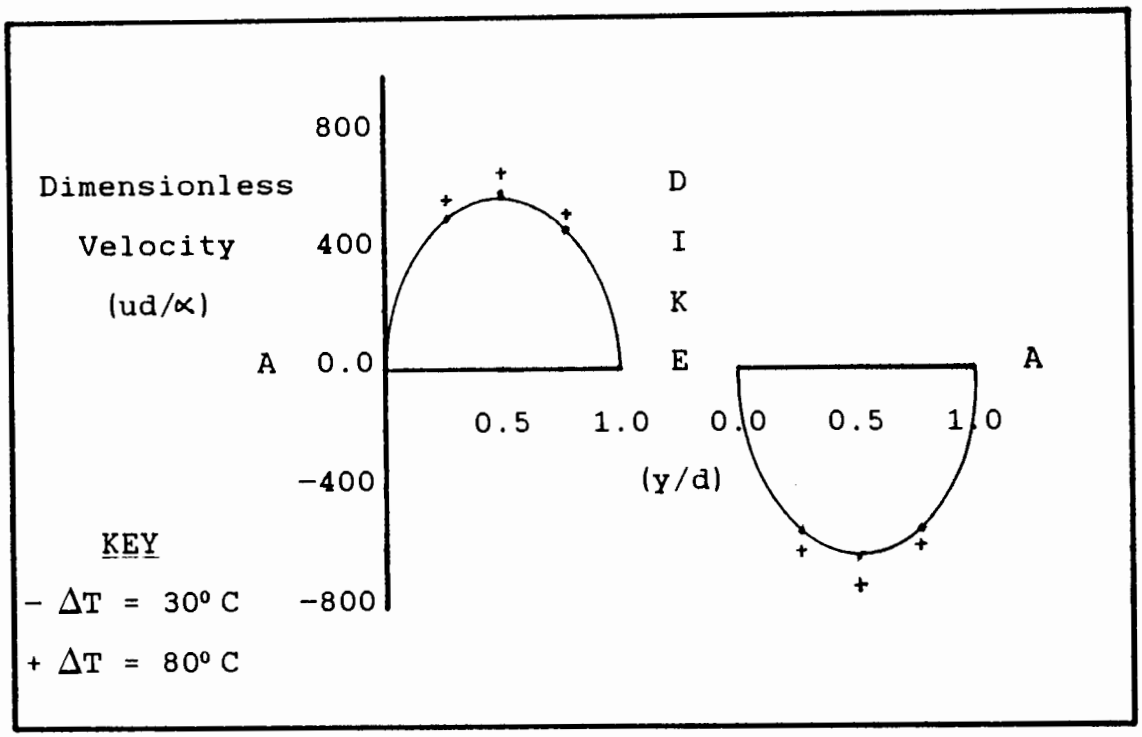

Fig. 6.39 VELOCITY COMPONENT (NORMAL TO A-A) AT A-A

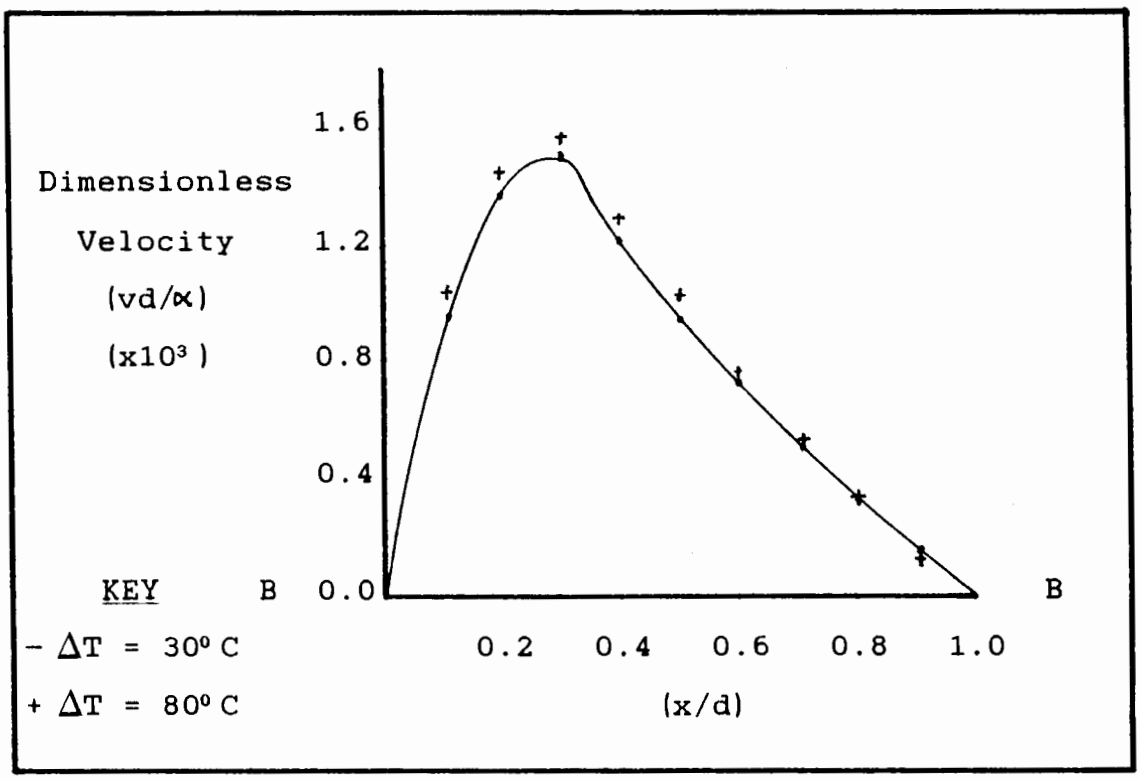

Fig. 6.40 VELOCITY COMPONENT (NORMAL TO B-B) AT B-B

However, due to the size of the pond, the temperature gradient is relatively small, and thus this comparatively large difference in temperature did not influence the velocity to increase to the same extent i.e. an increase of 170% in the temperature difference only caused an increase of approximately 5% in the maximum velocity.

It should be noted that the maximum velocity at B-B is significantly larger than the maximum velocity at A-A.

This is caused by the fluid flowing through a narrower section of the pond at section B-B than at section A-A. Another point of interest in fig. 6.40 is that the maximum horizontal velocity is not at the centre of section B-B. This can be attributed to the large drag effect of the lengthy outer boundaries of the pond in this region as opposed to the relatively small drag experienced by the fluid flowing round the edge of the dike.

6.5.2 Isotherms

Isotherms for both the large and the comparatively small temperature differences across the inlet and outlet of the cooling pond are plotted in figs. 6.41 and 6.42. Each isotherm line in the diagrams represents a 10% decrease in the temperature i.e. $3^{0}C$ in fig. 6.41, and $8^{0}C$ in fig. 6.42.

In fig. 6.42, the temperature decreases quite rapidly until it reaches the end of the dike, whereafter the decrease becomes more gradual and uniform. The isotherm plot of the larger temperature difference, fig. 6.43,

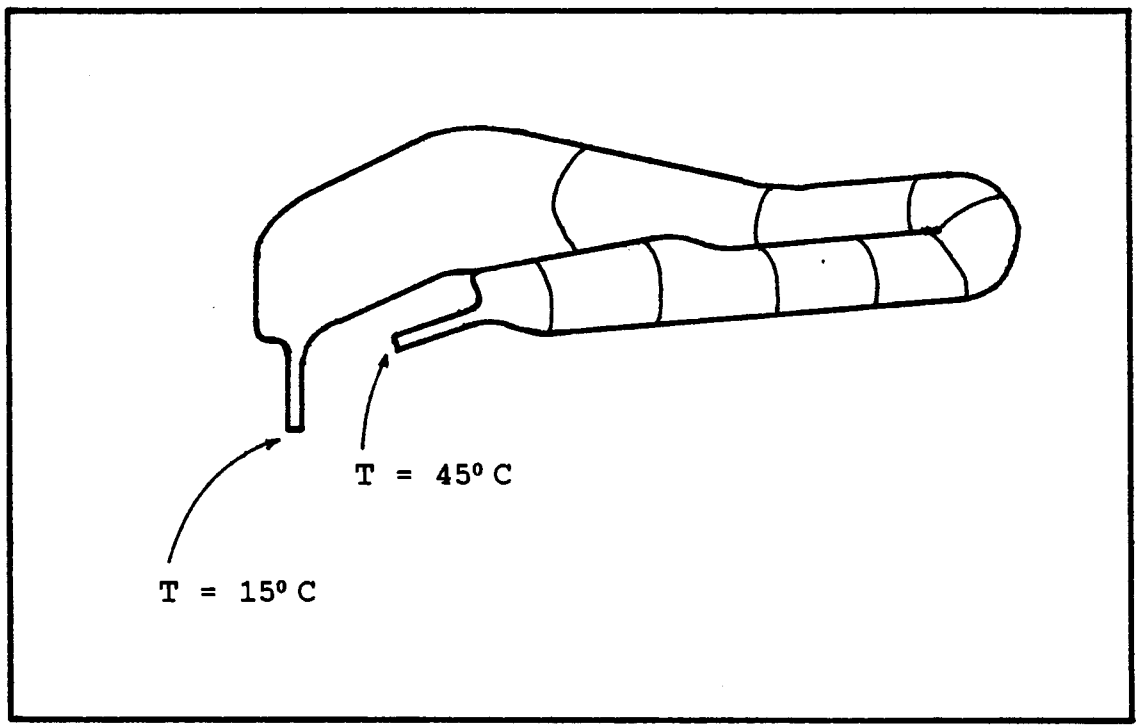

Fig. 6.41 ISOTHERMS : ΔT = 30° C

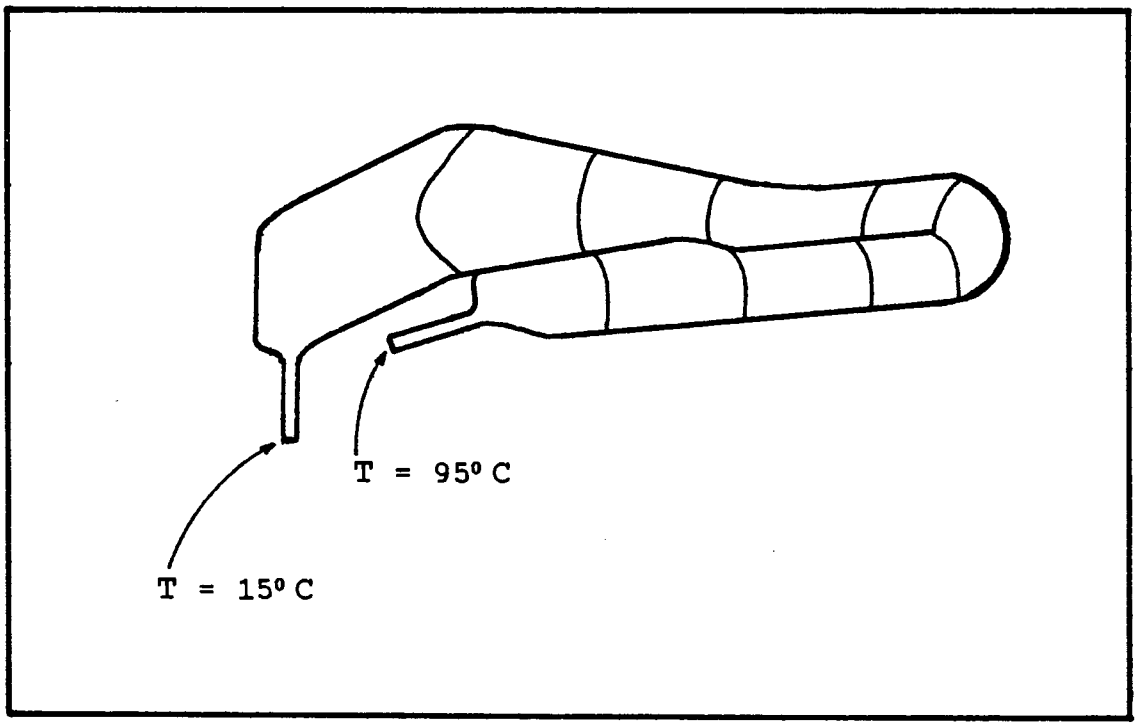

Fig. 6.42 ISOTHERMS : ΔT = 80° C

shows that the temperature decrease is more uniform over the entire length of the pond, although it also decreases more rapidly near the inlet. A notable feature of this plot is that the temperature remains fairly constant in the region of the bend, especially along the outer boundaries. This is probably due to the very low velocities which occur in this region (see fig. 6.41). These plots compare qualitatively with the thermal satellite images of the actual Chernobyl cooling pond published by Edwards [84].

6.5.3 Centre-Line Temperature Distribution

Using a similar method adopted for the window cavity results, the temperatures at various points along the centre-line of the cooling pond (for both temperature differences) are plotted in fig. 6.43, in order to determine a more detailed profile of the temperature distributions. Fig. 6.43 clearly corroborates the conclusions drawn from the isotherm plots that the greatest temperature drop occurs in the region of the inlet i.e. the profiles have the steepest slopes in this area. Thereafter, the slopes becomes more gradual as the temperatures drop towards their values at the outlet.

Comparing the profiles for the two temperature differences, it can be seen that the smaller temperature difference has a steeper slope in the region of the inlet. It can thus be concluded that the higher the temperature difference, the more gradual the decrease in temperature. Thus, apart from the higher temperatures involved, the heat transfer for large temperature differences occurs

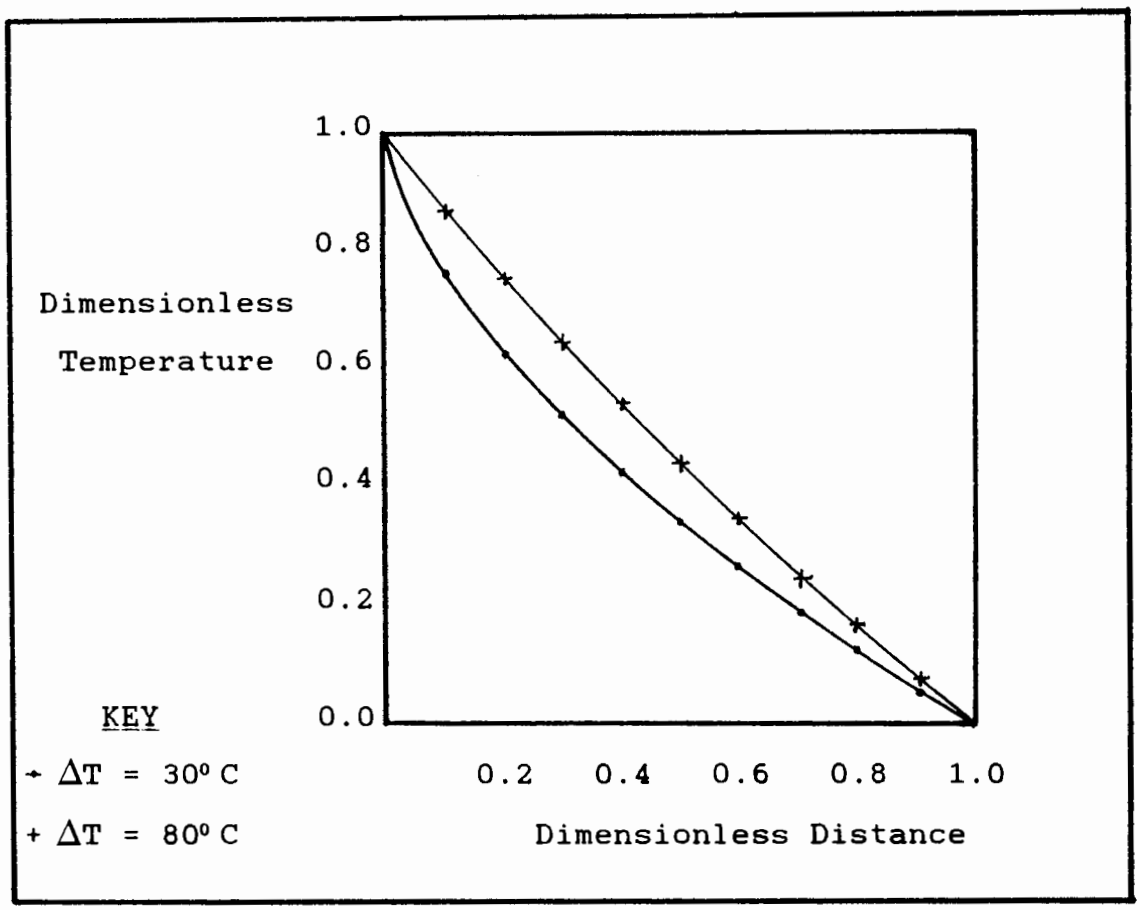

Fig. 6.43 CENTRE-LINE TEMPERATURE DISTRIBUTION

more slowly, implying an even greater impact of the thermal pollution on the surrounding environment.

6.5.4. Pressure Contours

The pressure contours for the two temperature differences considered are plotted in figs. 6.44 and 6.45. In both these cases, the pressure decreases at a relatively uniform rate from the inlet to the outlet. Of note is that the pressure remains reasonably constant as the fluid flows around the end of the dike, except at the outer corners of the bend. This constant pressure is, once

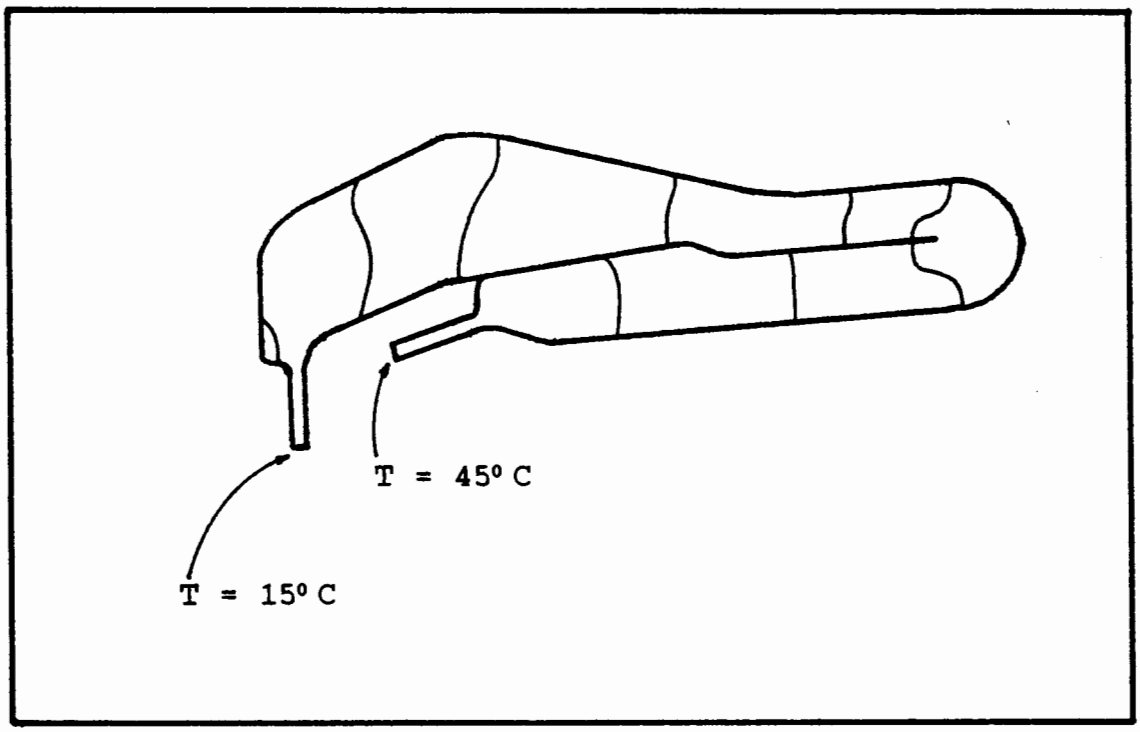

Fig. 6.44 PRESSURE CONTOURS : ΔT = 30° C

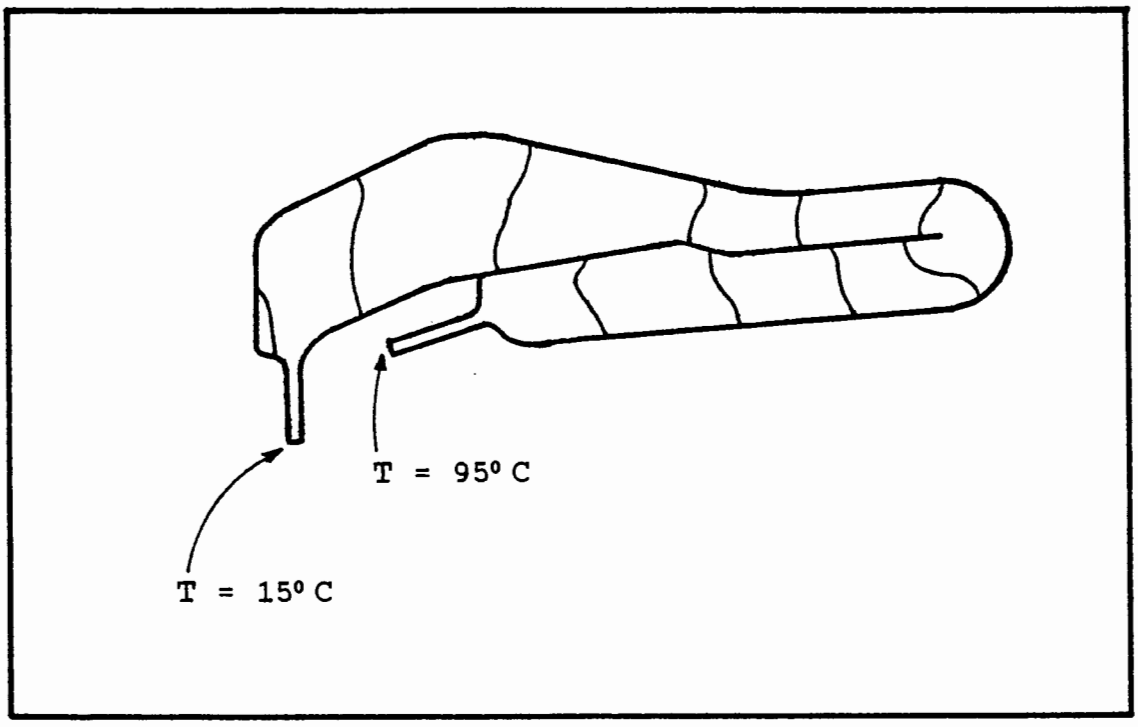

Fig. 6.45 PRESSURE CONTOURS : ΔT = 80° C

again, probably caused by the lower velocities occuring in this region.

6.5.5 Effect Of The Reynolds Number

As stated previously, only results obtained for the Reynolds number of 10^2 are presented above. This is due to the lack of effect of the Reynolds number on the overall flow and temperature distribution. This lack of influence can be ascribed to the fact that the Reynolds number was based on the input velocity of the fluid, which has very little effect on the overall flow in the cooling pond. Thus it can be deduced that the fluid motion was caused by the temperature and pressure differences which were present between the inlet and the outlet.

CHAPTER 7

CONCLUSIONS AND RECOMMENDATIONS

It has been shown that a stable finite element solution of the governing equations of convection heat transfer can be obtained for a variety of examples (for $Ra \leq 10^5$ and $Re \leq 5x10^2$) using the primitive variable formulation with mixed interpolation. Convergence of the solutions of these equations is obtained using the substitution method to update the appropriate variables in the non-linear terms.

Five examples are investigated in this study, namely the thermally driven square window cavity, the thermally driven vertical slot, the thermally driven triangular cavity, the liquid convective diode, and forced convection in a cooling pond.

Due to the similarity of the results obtained for the thermally driven square window cavity, vertical slot and triangular cavity, some conclusions, outlined below, are common to all these three examples.

For Rayleigh numbers less than $5x10^3$, very little flow of the fluid occurs, with the result that most of the heat transfer under these conditions is in the form of conduction. Also, the Prandtl number has a neglible effect on the results at this Rayleigh number. This behaviour is explicable when the relative magnitudes of the terms in

the governing equations are compared i.e. at large Prandtl numbers, the convective term of the heat conduction equation becomes neglible. Thus, it is only at very low values that the influence of the Prandtl number becomes significant.

For $5x10^3 < Ra < 2x10^4$, a distinct boundary layer develops, and the velocity of the fluid increases substantially. Thus more heat transfer takes place by means of convection, and less due to conduction, compared to that occurring at $Ra < 5x10^3$. The effect of the Prandtl number increases at this Rayleigh number, suggesting that above this value, the influence of Pr cannot be neglected.

For the square cavity and the vertical slot, the horizontal temperature gradient is actually negative (i.e. the little conduction which does occur at this value of Rayleigh number, is opposite to the overall direction of the heat flow), which implies that the flow under these conditions is so strong that the hotter fluid is being carried to the cold side of the cavity, and vice versa.

For the triangular cavity example, at $Ra=6.4x10^4$, the velocity of the fluid increases further, and the boundary layer becomes established. The effect of the adiabatic wall extends into the central region of the cavity. The sudden depression of the near-middle sections of the isotherms indicates that seperation of the flow occurs in this region.

For the square cavity and the vertical slot examples, at the highest Rayleigh number, 10^5, the fluid motion

increases from that existing at $Ra=10^4$, the boundary layer being very well established. Also, a double eddy develops in the central portion of the cavity or slot. A possible explanation for this behaviour is that, at sufficiently high Rayleigh numbers, the boundary layer regime is so strong that it is possible for the high vorticity near the walls to sustain a weak reversal of the flow in the outer part of the boundary layer. The horizontal temperature gradient is still negative although it is near zero, implying that very little conduction occurs for $Ra=10^5$ i.e. the heat transfer is primarily convective.

The liquid convective diode is studied in two different modes, namely the warm-up phase and the cool-down phase. During the warm-up phase, convection occurs from the warmer tongue to the higher and cooler reservoir, with the fluid flowing upwards along the outside wall of the reservoir and downwards along the inner wall. Along these walls of the reservoir, a distinct boundary layer forms. Very little flow takes place in the lower part of the tongue.

During the cool-down phase, the tongue is assumed to cool to below the inside temperature, with the overall temperature gradient in the opposite direction to that of the warm-up phase. Very little flow occurs during this phase, implying that virtually no convection takes place. Thus, most of the heat loss from the reservoir to the tongue is conductive. It can therefore be concluded that, in terms of thermal performance, the combination of a large amount of heat transfer due to the vigorous convection that occurring during warm-up, and the small

amount of heat transfer by conduction through a poorly conducting fluid during cool-down, results in a high diode efficiency.

The final problem investigated is the nuclear plant cooling pond currently in use at Chernobyl, U.S.S.R. The Reynolds number is found to have a neglible effect on the flow and the temperature distribution in the cooling pond. This is due to the fact that the Reynolds number is based on the input velocity, which has only a small influence on the overall motion of the fluid through the cooling pond. Thus it can be concluded that the overall flow is caused by the pressure difference existing between the inlet and the outlet.

A fairly substantial increase in the temperature difference between inlet and outlet, namely 50^{0} C, causes only a slight increase in the velocity of the fluid. This can be ascribed to the large dimensions of the pond, which ensure that the temperature gradient was relatively small.

The velocity at the bend in the pond is found to be substantially higher than the equivalent velocity of the fluid flowing along the length of the pond on either side of the dike. This is due to the smaller size of the pond in the region of the dike end. Also, the maximum velocity in this area is not in the centre of the bend, but nearer the end of the dike, which can be attributed to the large drag effect induced by the long outer boundaries of the bend as opposed to the short edge of the dike.

The temperature decreases more gradually and uniformly for

the larger temperature difference i.e. under these conditions, not only is the input temperature higher, but the temperature also decreases at a slower rate. From this, it can be concluded that the impact of the thermal pollution on the surrounding area will be much greater for large temperature differences. Another point of interest with regards the temperature, is that it remains reasonably constant in the region of the bend, especially along the outer boundaries. This is a result of the low velocities which occuring in this area, as mentioned previously.

It is recommended that further research of the finite element analysis of convection heat transfer be conducted in the following areas :-

(1) the governing equations should be extended to include the third dimension, in order to allow the analysis of more complex problems. This can be accomplished, without extension of the basic theory, by removing the relevant assumptions which produced the two-dimensional equation. It must be realised that three dimensional representations vastly increases the computational expense in comparison to the two-dimensional models, but, in order to investigate phenomena such as the response to the introduction of a thermal plume into a stratified lake, it should be justified.

(2) the time-dependent terms in the governing equations need to be included in the formulation, and stable algorithms sought that will accurately predict physical phenomena.

(3) the method should be used to investigate the instabilities at high Rayleigh numbers, especially in the turbulent region, as both theoretical and numerical results in this area of research appear limited.

(4) at the present time, confidence in the primitive variable formulation of the finite element method exists in certain problems, and this will be gained for other types of problems as real design projects are tackled.

CHAPTER 8

REFERENCES

1. **W.M. LAI, D. RUBIN and E. KREMPL**, 'Introduction To Continuum Mechanics', Pergamon Press, Oxford, pp 175-239 (1978)

2. **B.S. MASSEY**, 'Mechanics Of Fluids', 4th Edition, Van Nostrand Reinhold, pp 84-101, (1982)

3. **G. KINSMAN**, 'Power Plant Cooling Systems', ASCE J.Pow.Div., Vol. 98, pp 247-252 (1972)

4. **R.H. GALLAGHER, J.A. LIGGETT, and S.T.K. CHAN**, 'Finite Element Shallow Lake Circulation Analysis', ASCE J.Hyd. Div., Vol. 99, pp 1083-1096 (1973)

5. **J.P. HOLMAN**, 'Heat Transfer', 5th Edition, Mcgraw-Hill, Tokyo, pp 72-99 (1981)

6. **J.F. MILTHORPE and G.P. STEVEN**, 'On A Least Squares Approach To The Integration Of The Navier-Stokes Equations', Finite Elements In Fluids, Vol. 1, (Eds. R.H. Gallagher, O.C. Zienkiewicz, J.T. Oden, M. Morandi Cecchi, C. Taylor), John Wiley and Sons, pp 89-103, (1978)

7. **G.K. BATCHELOR**, 'Heat Transfer By Free Convection Across A Closed Cavity Between Vertical Boundaries At

Different Temperatures', Quart.J.App.Math., Vol. 12, pp 209-233 (1954)

8. **D.K. GARTLING and R.E.NICKELL**, 'Finite Element Analysis Of Free And Forced Convection', Finite Elements In Fluids, Vol.3, (Eds. R.H. Gallagher, O.C. Zienkiewicz, J.T. Oden, M. Morandi Cecchi, C. Taylor), John Wiley and Sons, pp 105-121, (1978)

9. **J.W. ELDER**, 'Numerical Experiments With Free Convection In A Vertical Slot', J. Fluid Mech., Vol. 24(4), pp 823-843 (1965)

10. **A.E. GILL**, 'The Boundary Layer Regime For Convection In A Rectangular Cavity', J. Fluid Mech., Vol. 26(3), pp 515-536 (1966)

11. **B.S. PETUKLOV**, 'Actual Problems Of Heat Transfer In Nuclear Power Engineering', Int. Seminar on Future Energy Production, Hemisphere Publishing Corporation, Washington D.C., pp 151-163 (1976)

12. **M. KAWAHARA**, 'Steady And Unsteady Finite element Analysis Of Incompressible Viscous Fluid', Finite Elements In Fluids, Vol. 3, (Eds. R.H. Gallagher, O.C. Zienkiewicz, J.T. Oden, M. Morandi Cecchi, C. Taylor), John Wiley and Sons, pp 23-53 (1978)

13. **J.C. CHATO and R.S. ABDULHADI**, 'Flow And Heat Transfer In Convectively Cooled Underground Electric Cable Systems: Part 1 - Velocity Distributions And Pressure Drop Correlations; Part 2 - Temperature Distributions And Heat

Transfer Correlations', J. Heat Trans., pp 30-40 (February 1978)

14. J.C. **HEINRICH** and R.S. **MARSHALL**, 'Viscous Incompressible Flow By A Penalty Function Finite Element Method', Computers And Fluids, Vol. 9, pp 73-83 (1981)

15. **P.E. ALLAIRE, M.C. ROSEN**, and **J.G. RICE**, 'Simplex Finite Element Analysis Of Viscous Incompressible Flow With Penalty Function Formulation', Finite Elements In Design, Vol. 1, pp 71-88 (1985)

16. C. **TAYLOR** and **T.G. HUGHES**, 'Finite Element Programming of the Navier-Stokes Equations', Pineridge Press, Swansea, (1981)

17. **P.S. HUYAKORN, C.TAYLOR, R.L. LEE**, and **P.M. GRESHO**, 'A Comparison Of Various Mixed Interpolation Finite Elements In The Velocity-Pressure Formulation Of The Navier-Stokes Equations', Computers And Fluids, Vol. 6, pp 25-35 (1978)

18. **J.N. REDDY**, 'Penalty-Finite-Element Analysis Of Three-Dimensional Navier-Stokes Equations', Comput.Meths.Appl. Mech. Eng., pp 88-106 (1982)

19. **Y. YOSHIDA** and **T. NOMURA**, 'A Transient Solution Method For The Finite Element Incompressible Navier-Stokes Equations', I.J.Num.Meth. Fluids, Vol. 5, pp 873-890 (1985)

20. **M. KAWAHARA, N. YOSHIMURA, K. NAKAGAWA**, and **H. OHSAKA**, 'Steady And Unsteady Finite Element Analysis Of

Incompressible Viscous Fluid', I.J.Num.Meth.Engng., Vol. 10, pp 437-456 (1976)

21. C. **CHEN, K.WONG, and J.W. CLEAVER**, 'Finite Element Solutions Of Laminar Flow And Heat Transfer Of Air In A Staggered And An In-Line Tube Bank', I.J. Heat Fluid Flow, Vol. 7, pp 291-300 (1986)

22. C. **CHEN, K. WONG, and S.LEE**, 'The Finite Element Solution Of Laminar Combined Convection From Two Spheres In Tandem Arrangement', Comp.Meth.Appl.Mech.Engng., Vol. 59, pp 73-84 (1986)

23. J.N. **REDDY and A. SATAKE**, 'A Comparison Of A Penalty Finite Element Model With The Stream Function-Vorticity Model Of Natural Convection In Enclosures', J. Heat Trans., Vol. 102, pp 659-666 (1980)

24. J.N. **REDDY**, 'Penalty-Finite Element Methods In Conduction And Convection Heat Transfer', Num. Meth. Heat Transfer, Vol. II, (Eds. R.W. Lewis, K. Morgan and B.A. Schreffler), John Wiley and Sons, pp 145-178 (1983)

25. H. **BERTIN and H. OZOE**, 'Technique For Rapid Convergence Of The Penalty Finite Element Method With A Modified Galerkin Scheme, And Its Application To Natural Convection', Num. Heat Trans., Vol. 10, pp 311-325 (1986)

26. C. **PRAKASH and S.V. PATANKAR**, 'A Control Volume-Based Finite Element Method For Solving The Navier-Stokes Equations Using Equal-Order Velocity-Pressure Interpolation', Num. Heat Trans., Vol. 8, pp 259-280

(1985)

27. **R.J. SCHNIPKE and J.G. RICE**, 'Examination Of A New Finite Element Method Applied To Convection Heat Transfer', Finite Elements In Analysis And Design, Vol. 1, pp 227-239 (1985)

28. **R.J. SCHNIPKE and J.G. RICE**, 'A Finite Element Method For Free And Forced Convection Heat Transfer', I.J.Num. Meth.Engng., Vol. 24, pp 117-128 (1987)

29. **M.T. DALMAN, J.H. MERKIN, and C. MCGREAVY**, 'Fluid Flow And Heat Transfer Past Two Spheres In A Cylindrical Tube', Computers And Fluids, Vol. 14(3), pp 267-281 (1986)

30. A. **CAMPION-RENSON and M.J. CROCHET**, 'On The Stream Function-Vorticity Finite Element Solutions Of Navier-Stokes Equations', I.J.Num.Meth.Engng., Vol. 12, pp 1809-1818 (1978)

31. **G. DHATT, B.K. FOMO, and C. BOURQUE**, 'A Stream Function-Vorticity Finite Element Formulation For The Navier-Stokes Equations', I.J.Num.Meth.Engng., Vol.17, pp 199-212 (1981)

32. **M.F. PEETERS, W.G. HABASHI, and E.G. DUECK**, 'Finite Element Stream Function-Vorticity Solutions Of The Incompressible Navier-Stokes Equations', I.J. Num. Meth. Fluids, Vol. 7, pp 17-27 (1987)

33. **M.D. OLSON**, 'Variational Finite Element Methods For Two-Dimensional And Axisymmetric Navier-Stokes Equations',

Finite Elements In Fluids, Vol. 1, (Eds. R.H. Gallagher, O.C. Zienkiewicz, J.T. Oden, M. Morandi Cecchi, C. Taylor), John Wiley and Sons, pp 57-72 (1978)

34. **B. TABARROK and R.C. LIN**, 'Finite Element Analysis Of Free Convection Flows', I.J. Heat Mass Trans., Vol. 20, p 945 (1977)

35. **H. OZOE, M. TAKEMOTO, and S.W. CHURCHILL**, 'Finite Element Analysis Of Laminar Natural Convection In Confined Rectangular Regimes - Extrapolation To Zero Element Size', Num. Heat Trans., Vol. 9, pp 323-333 (1986)

36. **Y. MIYAUCHI, M. MASUDA, and M. SHIMIZU**, 'A Transient Finite Element Analysis Of Natural Convection Around A Horizontal Hot Cylinder', I.J.Num.Meth. Fluids, Vol. 3, pp 429-443 (1983)

37. **M. KAWAHARA and T. OKAMATO**, 'Finite Element Analysis Of Steady Flow Of Viscous Fluid Using Stream Function', Proc. J.S.C.E., No. 247, pp 123-135 (1976)

38. **T. CEBECI and P. BRADSHAW**, 'Physical And Computational Aspects Of Convective Heat Transfer', Springer-Verlag, New York, pp. 385-455 (1984)

39. **S.C.R. DENNIS and G.Z. CHANG**, 'Numerical Solutions For Steady Flow Past A Circular Cylinder At Reynolds Numbers Up To 100', J. Fluid Mech., Vol. 42(3), pp 471-489 (1970)

40. **S.C.R. DENNIS and J.D.A. WALKER**, 'Calculation Of The Steady Flow Past A Sphere At Low And Moderate Reynolds

Numbers', J. Fluid Mech., Vol. 48, pp 771-789 (1971)

41. G.P. **WILLIAMS**, 'Numerical Integration Of The Three-Dimensional Navier-Stokes Equations For Incompressible Flows', J. Fluid Mech., Vol. 37, pp 727-750 (1969)

42. **K. AZIZ and J.D. HELLUMS**, 'Numerical Solution Of The Three-Dimensional Equations Of Motion For Laminar Natural Convection', The Physics of Fluids, Vol. 10(2), pp 314-324 (1967)

43. **A. GHOSH, C.W. MASTIN and J.F. THOMPSON**, 'Locally One-Dimensional Scheme For The Solution Of Three-Dimensional Navier-Stokes Equations', Computers in Flow Predictions and Fluid Dynamics Experiments, (ed. K.N. Ghia et al) American Society of Mechanical Engineers, New York, pp 3-10 (1981)

44. O.C. **ZIENKIEWICZ**, 'Finite Elements - The Background Story', The Mathematics Of Finite Elements And Applications (Ed. J.R. Whiteman), Vol. 1, pp 1-36 (1973)

45. **E. HINTON and D.R.J. OWEN**, 'Finite Element Programming', Academic Press (1977)

46. **E. HINTON and D.R.J. OWEN**, 'An Introduction To Finite Element Computations', Pineridge Press (1979)

47. **G. DHATT and G. TOUZOT**, 'The Finite Element Method Displayed', John Wiley, Chichester, pp 291-305 (1984)

48. **K.J. BATHE**, 'Finite Element Procedures In Engineering

Analysis', Prentice-Hall (1982)

49. **S. USUKI**, 'The Application Of A Variational Finite Element Method To Problems In Fluid Dynamics', I.J.Num. Meth.Engng., Vol. 11, pp 563-577 (1977)

50. **A. MOULT, D. BURLEY and H. RAWSON**, 'The Numerical Solution Of Two-Dimensional Steady Flow Problems By The Finite Element Method', I.J.Num.Meth.Engng., Vol. 14, pp 11-35 (1979)

51. **M. IKEGAWA**, 'A New Finite Element Technique For The Analysis Of Steady Viscous Flow Problems', I.J.Num.Meth. Engng., Vol. 14, pp 103-113 (1979)

52. **M.K. DENHAM and M.A. PATRICK**, 'Laminar Flow Over A Downstream Facing Step In A Two-Dimensional Flow Channel', Trans. Inst. Chem. Eng., Vol. 52, No. 4 (1974)

53. **D.J. ATKINS, S.J. MARSHALL and M.A. PATRICK**, 'Numerical Prediction Of Seperated Flows', Int. J. Num. Meth. Eng. (1980)

54. **H.H. BADR**, 'Laminar Combined Convection From A Horizontal Cylinder - Parallel And Contra Flow Regimes', I.J. Heat Mass Trans., Vol. 27(1), pp 15-27 (1984)

55. **P.F. HAMBLIN**, 'Finite Element Methods Applied To The Modelling Of The Circulation, Seiches, Tides And Storm Surges In Large Lakes', Finite Elements In Fluids, Vol. 3, (Eds. R.H. Gallagher, O.C. Zienkiewicz, J.T. Oden, M. Morandi Cecchi, C. Taylor), John Wiley and Sons, pp 269-

281 (1978)

56. **C. TAYLOR and J.M. DAVIS**, 'Tidal Propagation And Dispersion In Estuaries', Finite Elements In Fluids, Vol. 1, (Eds. R.H. Gallagher, O.C. Zienkiewicz, J.T. Oden, M. Morandi Cecchi, C. Taylor), John Wiley and Sons, pp 95-118 (1978)

57. **J.A. LIGGETT and C. HADJITHEODOROU**, 'Circulation In Shallow Homogenous Lakes', ASCE J.Hyd.Div., Vol. 95, pp 609-620 (1969)

58. **R.H. GALLAGHER**, 'Finite Element Lake Circulation And Thermal Analysis', Finite Elements In Fluids, Vol. 1, (Eds. R.H. Gallagher, O.C. Zienkiewicz, J.T. Oden, M. Morandi Cecchi, C. Taylor), John Wiley and Sons, pp 119-132 (1978)

59. **P.M. GRESHO, S.T. CHAN, R.L. LEE, and C.D. UPSON**, 'A Modified Finite Element Method For Solving The Time-Dependent Incompressible Navier-Stokes Equations. Part 1 : Theory', I.J.Num.Meth. Fluids, Vol. 4, pp 557-598 (1984)

60. **P.M. GRESHO, S.T. CHAN, R.L. LEE, and C.D. UPSON**, 'A Modified Finite Element Method For Solving The Time-Dependent Incompressible Navier-Stokes Equations. Part 2 : Applications', I.J.Num.Meth. Fluids, Vol. 4, pp 619-640 (1984)

61. **E.R.G. ECKERT and W.O. CARLSON**, 'Natural Convection In An Air Layer Enclosed Between Two Vertical Plates With Different Temperatures', I.J. Heat Mass Trans., Vol. 2, pp

106-120 (1961)

62. **J.W. ELDER**, 'Laminar Free Convection In A Vertical Slot', J. Fluid Mech., Vol. 23, pp 77-98 (1965)

63. **H. STEFAN**, 'Modelling Spread Of Heated Water Over A Lake', ASCE J.Pow.Div., Vol. 96, pp 469-482 (1970)

64. **J.C. TATINCLAUX, S.C. JAIN, and W.W. SAYRE**, 'Hydraulic Modelling Of Shallow Cooling Ponds', ASCE J.Pow.Div., Vol. 101, pp 43-55 (1975)

65. **G. DE VAHL DAVIS**, 'Laminar Natural Convection In An Enclosed Rectangular Cavity', I.J. Heat Mass Trans., Vol. 11, pp 1675-1693 (1968)

66. **G.D. MALLINSON and G. DE VAHL DAVIS**, 'Three-Dimensional Natural Convection In A Box : A Numerical Study', J. Fluid Mech., Vol. 83(1), pp 1-31 (1977)

67. **G.S. SHIRALKAR and C.L. TIEN**, 'A Numerical Study Of Laminar Natural Convection In Shallow Cavities', J. Heat Trans., Vol. 103, pp 226-231 (1981)

68. **W. SCHMIDT, P.W. GIEL, R.E. PHILLIPS, and D.F. WANG**, 'A Comparison Of Experimental And Predicted Results For Laminar Natural Convection In An Enclosure', I.J. Heat Fluid Flow, Vol. 7(3), pp 183-190 (1986)

69. **A.BHATTI and W. AUNG**, 'Finite Difference Analysis Of Laminar Seperated Forced Convection In Cavities', J. Heat Trans., Vol. 106, pp 49-54 (1984)

70. C.J. **CHEN and Y.H. YOON**, 'Finite Analytic Numerical Solution Of The Axisymmetric Navier-Stokes And Energy Equations', J. Heat Trans., Vol. 105, pp 639-645 (1983)

71. C.J. **CHEN and P. LI**, 'The Finite Analytic Method For Steady-State And Unsteady Heat Transfer Problems', 19th ASME/AICLE U.S. National Heat Transfer Conference, Orlando, Fla., ASME Paper No. 80-HT-86, July 27-30 (1980)

72. **H. OZOE, H. SAYAMA, and S.W. CHURCHILL**, 'Natural Convection In An Inclined Rectangular Channel At Various Aspect Ratios And Angles - Experimental Measurements', I.J. Heat Mass Trans., Vol. 18, pp 1425-1431 (1975)

73. **G. DE VAHL DAVIS**, 'Natural Convection Of Air In A Square Cavity : A Benchmark Numerical Solution', I.J.Num. Meth. Fluids, Vol. 3, pp 249-264 (1983)

74. **E.R.G. ECKERT and R.M. DRAKE**, 'Analysis Of Heat And Mass Transfer', Mcgraw-Hill, New York (1972)

75. **T.H. KUEHN and R.J. GOLDSTEIN**, 'An Experimental And Theoretical Study Of Natural Convection In The Annulus Between Horizontal Concentric Cylinders', J. Fluid Mech., Vol. 74(4), pp 695-719 (1976)

76. **K.T. YANG**, 'Laminar Forced Convection Of Liquids In Tubes With Variable Viscosity', J. Heat Trans., Vol. 84, pp 353-362 (1962)

77. **L.A. LOZIUK, J.C. ANDERSON, and T. BELYTSCHKO**, 'Hydrothermal Analysis By Finite Element Analysis', ASCE

J.Hyd.Div., Vol. 98, pp 1983-1998 (1972)

78. **K. WONG, S. LEE, and C. CHEN**, 'Finite Element Solution Of Laminar Combined Convection From A Sphere', J. Heat Trans., Vol. 108, pp 860-865 (1986)

79. **J. DONEA, S. GIULIANI, and H. LAVL**, 'Finite Element Solution Of The Unsteady Navier-Stokes Equations By A Fractional Step Method', Comp.Meth. In Appl.Mech.Engng., Vol. 30, pp 53-73 (1982)

80. **J.C. HEINRICH, P.S. HUYAKORN, O.C. ZIENKIEWICZ, and A.R. MITCHELL**, 'An 'Upwind' Finite Element Scheme For 2-Dimensional Convective Transport Equation', I.J. Num.Meth. Engng., Vol. 11, pp 131-143 (1977)

81. **S. CHANDRASEKHAR**, 'Hydrodynamic And Hydromagnetic Stability', Clarendon Press, Oxford, pp 17-18 (1961)

82. **V.A. AKINSETE and T.A. COLEMAN**, 'Heat Transfer By Steady Laminar Free Convection In Triangular Enclosures', I.J. Heat Mass Trans., Vol. 25(7), pp. 991-998 (1982)

83. **G.F. JONES**, 'Heat Transfer In A Liquid Convective Diode', J. Solar Energy Eng., Vol. 108, pp. 163-171 (1986)

84. **M. EDWARDS**, 'Chernobyl - One Year After', National Geographic Magazine, Vol. 171(5), pp 632-653 (1987)

CHAPTER 9

BIBLIOGRAPHY

1. **K.J. BATHE**, 'Finite Element Procedures in Engineering Analysis', Prentice-Hall (1982)

2. **G. DHATT and G. TOUZOT**, 'The Finite Element Method Displayed', John Wiley (1984)

3. **E. HINTON and D.R.J. OWEN**, 'Finite Element Programming', Academic Press (1977)

4. **J.P. HOLMAN**, 'Heat Transfer', 5th Edition, McGraw-Hill, Tokyo (1981)

5. **B.S. MASSEY**, 'Mechanics of Fluids', 4th Edition, Van Nostrand Reinhold (1982)

6. **C. TAYLOR and T.R.G. HUGHES**, 'Finite Element Programming of the Navier-Stokes Equations', Pineridge Press, Swansea (1981)